Modeling Charge Transport in Organic Semiconductors

Zur Erlangung des akademischen Grades einer

DOKTORIN DER NATURWISSENSCHAFTEN

(Dr. rer. nat.)

von der KIT-Fakultät für Chemie und Biowissenschaften
des Karlsruher Instituts für Technologie (KIT)

genehmigte
DISSERTATION
von

M. Sc. Sara Roostaei

Erster Gutachter: Prof. Marcus Elstner
Zweiter Gutachter: Prof. Wolfgang Wenzel
Tag der mündlichen Prüfung: 07.2023

Karlsruhe Institute of Technology
Institute of Physical Chemistry
Fritz-Haber-Weg 2
76131 Karlsruhe

I declare that I have developed and written the enclosed thesis completely by myself, and have not used sources or means without declaration in the text.

Karlsruhe, 2023

. . . . . .

(M. Sc. Sara Roostaei)

Abstract

In this thesis, we aimed to explore specific challenges in the field of organic semiconductors (OSCs) related to charge and energy transfer phenomena, employing efficient computational models. Consequently, the thesis is structured into five chapters. Chapter 1 functions as an introduction to organic semiconductors (OSCs). The second chapter provides a concise overview of the theoretical methods utilized in this study.
In chapter 3, we systematically examine the performance of two approximations in the fewest switched surface hopping (FSSH) simulations for charge transport (CT) in several representative OSCs. These approximations include (i) the substitution of the nuclear velocity scaling along the nonadiabatic coupling vector (NCV) by rescaling the hopping probability with the Boltzmann factor (Boltzmann correction (BC)) and (ii) a phenomenological approach to treat the quantum feedback from the electronic system to the nuclear system (implicit charge relaxation (IR)) in the OSCs. We find that charge mobilities computed by FSSH-BC-IR are in very good agreement with the mobilities obtained by standard FSSH simulations with explicit charge relaxation (FSSH-ER), however, at reduced computational cost. A key parameter determining the charge carrier mobility is the reorganization energy, which is sensitively dependent on DFT functionals applied. By employing the IR approximation, the FSSH method allows systematic investigation of the effect of the reorganization energies obtained by different DFT functionals like B3LYP or ωB97XD on CT in OSCs. In comparison to the experiments, FSSH-BC-IR using ωB97XD reorganization energy underestimates mobilities in the low-coupling regime, which may indicate the lack of nuclear quantum effects (e.g., zero point energy (ZPE)) in the simulations. The mobilities obtained by FSSH-BC-IR using the B3LYP reorganization energy agree well with experimental values in 3 orders of magnitude.
In chapter 4, we investigate the effects of halogen groups on the charge transport properties of n-type OSCs-halogenated tetraazapentacenes (TAPs). The charge mobilities are obtained from nonadiabatic molecular dynamics simulations and examined in comparison to the experimental values. The results show that for Cl and Br substituted TAPs, the molecular packing, reorganization energy and electron transfer integrals are very close to the TAP, which leads to the similar charge mobilities as TAPS. However, the mobility is significantly reduced for fluoride-substituted TAP. It is found that while the crystal packing of F-TAP is similar to Cl/Br-TAP, the strong electron-withdrawing effect of fluoride results in much lower electron transfer integrals and larger reorganization energy, which leads to a lower charge mobility.

Finally, in chapter 5, the investigation focused on electro-inductive effects on the charge mobilities. To gain insight into this effect, we conducted calculations on anthracene with varied electron donor and attractor substituents, evaluating their influence on molecular geometry, reorganization energy, transfer integrals and charge mobility to establish a correlation between structure and properties. We calculated the coupling with and without an entitled group for anthracene to observe the influence of geometrical and electronic properties. When considering dimethyl, dimethoxy, and dicyano anteracene as the MM part, and only anteracene as the QM part, the geometry plays a significant role as the coupling remains relatively unchanged. However, in the case of dibromo-anteracene, neglecting Br led to a significant alteration in the coupling, highlighting the importance of Electro-inductive by using the halogen atoms.

Zusammenfassung

In dieser Arbeit haben wir uns zum Ziel gesetzt, spezifische Herausforderungen im Bereich der organischen Halbleiter (OSCs) im Zusammenhang mit Ladungs- und Energietransferphänomenen mithilfe effizienter Rechenmodelle zu untersuchen. Daher ist die Arbeit in fünf Kapitel unterteilt. Kapitel 1 dient als Einführung in organische Halbleiter (OSCs). Das zweite Kapitel gibt einen kurzen Überblick über die in dieser Studie verwendeten theoretischen Methoden.

In Kapitel 3 untersuchen wir systematisch die Leistung von zwei Näherungen in den Simulationen des Ladungstransports (CT) in mehreren repräsentativen OSCs mit dem geringsten Switched Surface Hopping (FSSH). Diese Approximationen umfassen (i) die Ersetzung der Kerngeschwindigkeitsskalierung entlang des nichtadiabatischen Kopplungsvektors (NCV) durch Skalierung der Sprungwahrscheinlichkeit mit dem Boltzmann-Faktor (Boltzmann-Korrektur (BC)) und (ii) einen phänomenologischen Ansatz zur Behandlung der Quantenrückkopplung vom elektronischen System zum Kernsystem (implizite Ladungsrelaxation (IR)) in den OSCs. Wir finden dass die mit FSSH-BC-IR berechneten Ladungsmobilitäten sehr gut mit den Mobilitäten übereinstimmen, die mit Standard-FSSH Simulationen mit expliziter Ladungsrelaxation (FSSH-ER) erhaltenen Mobilitäten sehr gut übereinstimmen, allerdings bei geringeren Rechenkosten. Ein Schlüsselparameter, der die Ladungsträgermobilität ist die Reorganisationsenergie, die empfindlich von den verwendeten DFT-Funktionalen abhängt. Durch die Verwendung der IR Approximation ermöglicht die FSSH-Methode eine systematische Untersuchung der Auswirkungen der Reorganisationsenergien, die mit verschiedenen DFT-Funktionen wie B3LYP oder ωB97XD auf CT in OSCs. Im Vergleich zu den Experimenten unterschätzt FSSH-BC-IR mit ωB97XD Reorganisationsenergie unterschätzt die Mobilitäten im Niedrigkopplungsbereich, was auf das Fehlen von Kernquanteneffekten (z. B. Nullpunktenergie (ZPE)) in den Simulationen hinweist. Die Mobilitäten, die mit FSSH-BC-IR unter Verwendung der B3LYP-Reorganisationsenergie erhaltenen Mobilitäten stimmen gut mit experimentellen Werten in 3 Größenordnungen überein. In Kapitel 4 untersuchen wir die Auswirkungen von Halogengruppen auf die Ladungstransporteigenschaften Ladungstransporteigenschaften von OSCs des n-Typs mit halogenierten Tetraazapentacenen (TAPs). Die Ladungs Ladungsmobilitäten werden aus nicht-adiabatischen Molekulardynamiksimulationen gewonnen und im Vergleich mit den experimentellen Werten untersucht. Die Ergebnisse zeigen, dass für Cl- und Br-substituierte TAPs die Molekülpackung, die Reorganisationsenergie und die Elektronentransferintegrale sehr nahe an den TAPs liegen, was zu ähnlichen Ladungsmobilitäten wie bei TAPS führt. Bei fluorsubstituierten TAP ist die Mobilität jedoch deutlich geringer. Es wurde festgestellt, dass die Kristall-

packung von F-TAP zwar ähnlich ist wie die von Cl/Br-TAP, dass aber der starke elektronenziehende Effekt von Fluorid zu viel niedrigeren Elektronentransferintegralen und größerer Reorganisationsenergie führt, was wiederum eine geringere Ladungsmobilität zur Folge hat.
In Kapitel 5 schließlich konzentrierte sich die Untersuchung auf die elektroinduktiven Effekte auf die Ladungsmobilitäten. Um einen Einblick in diesen Effekt zu erhalten, führten wir Berechnungen an Anthracen mit verschiedenen Elektronendonor- und Attraktor-Substituenten durch und bewerteten deren Einfluss auf die Molekülgeometrie, die Reorganisationsenergie, die Transferintegrale und die Ladungsmobilität, um eine Korrelation zwischen Struktur und Eigenschaften herzustellen. Wir berechneten die Kopplung mit und ohne eine berechtigte Gruppe für Anthracen, um den Einfluss der geometrischen und elektronischen Eigenschaften zu beobachten. Wenn man Dimethyl-, Dimethoxy- und Dicyano-Anteracen als MM-Teil und nur Anteracen als QM-Teil betrachtet, spielt die Geometrie eine wichtige Rolle, da die Kopplung relativ unverändert bleibt. Im Falle des Dibrom-Anteracens führte die Vernachlässigung von Br jedoch zu einer signifikanten Änderung der Kopplung, was die Bedeutung der Elektroinduktion durch die Verwendung der Halogenatome unterstreicht.

Acknowledgements

I want to start by thanking my advisor, Prof. Marcus Elstner. His unwavering support and understanding during my challenging Ph.D. journey were priceless. His determination to help me grow as a researcher and person made a huge difference in my progress. I would also like to extend my heartfelt appreciation to Prof. Wolfgang Wenzel, my second supervisor.
I am deeply grateful to Dr. Weiwei Xie, who served as an exceptional mentor and a reliable source of support. Whenever I faced difficulties, he was there to provide valuable advice. Every interaction with him gave me profound insights, enriching my Ph.D. experience.
I appreciate all my collaborators for their valuable contributions to my research. Their expertise and perspectives enhanced my learning. My heartfelt thanks go to my committee members for their invaluable insights and thought-provoking questions. Their dedication to my Ph.D. committee was truly appreciated. I can't forget my colleagues and friends at KIT. Our friendship, engaging conversations, and shared experiences created some of the best memories during my Ph.D. years.
Lastly, I owe my deepest gratitude to my family. Their unwavering support and unconditional love were my constant motivation. Their encouragement and belief in me were the driving force behind my achievements.

Contents

List of Figures

List of Tables

1. Introduction

1.1. Organic Semi-conductors (OSCs)

Charge and energy transport phenomena in molecular materials are of great practical relevance, as electronic components made of amorphous or crystalline organic materials have continuously gained popularity over the last decades. Many are produced at the large industrial scale, and hold great promise in terms of material properties and process-ability over their inorganic counterparts, performance for many applications still lacks behind [1, 2, 3]. Organic semiconductor crystals are an important class of materials that have garnered significant attention in recent years due to their potential applications in various fields, including electronics, optoelectronics, and energy conversion. These materials are characterized by their unique electronic and optoelectronic properties, which arise from their molecular structure consisting of conjugated organic molecules or polymers[4, 5].

The electronic properties of these materials are highly dependent on the molecular structure and packing arrangement within the crystal lattice. For example, the degree of conjugation, the strength of intermolecular interactions, and the packing density can all significantly affect the electronic properties, such as the bandgap, charge carrier mobility, and exciton dynamics [7, 8]. In addition to these electronic properties, organic semiconductor crystals also exhibit interesting optical properties, including strong absorption and emission in the visible and near-infrared regions of the spectrum. These properties make them highly attractive for use in organic photovoltaics, light-emitting diodes, and other optoelectronic devices [9, 10]. The growth of high-quality organic semiconductor crystals is a challenging task due to their low solubility and tendency to form disordered or amorphous structures. However, recent advances in crystal growth techniques, such as solution and vapor-phase deposition methods, have enabled the growth of high-quality single crystals, which have provided deeper insights into the fundamental electronic and optoelectronic properties of these materials [11, 12]. Organic semiconductor crystals exhibit significant potential for the advancement of next generation electronic and optoelectronic devices, driving ongoing research in materials science and engineering [13, 14].
Mobility, a key property, plays a crucial role in determining the performance of organic electronic devices. Mobility represents the speed at which charge carriers, such as electrons or holes, can traverse a material [15, 16]. Higher mobility enables faster movement of these charge carriers, enhancing the efficiency of transport within a device. Consequently, mobility's importance in organic semiconductor

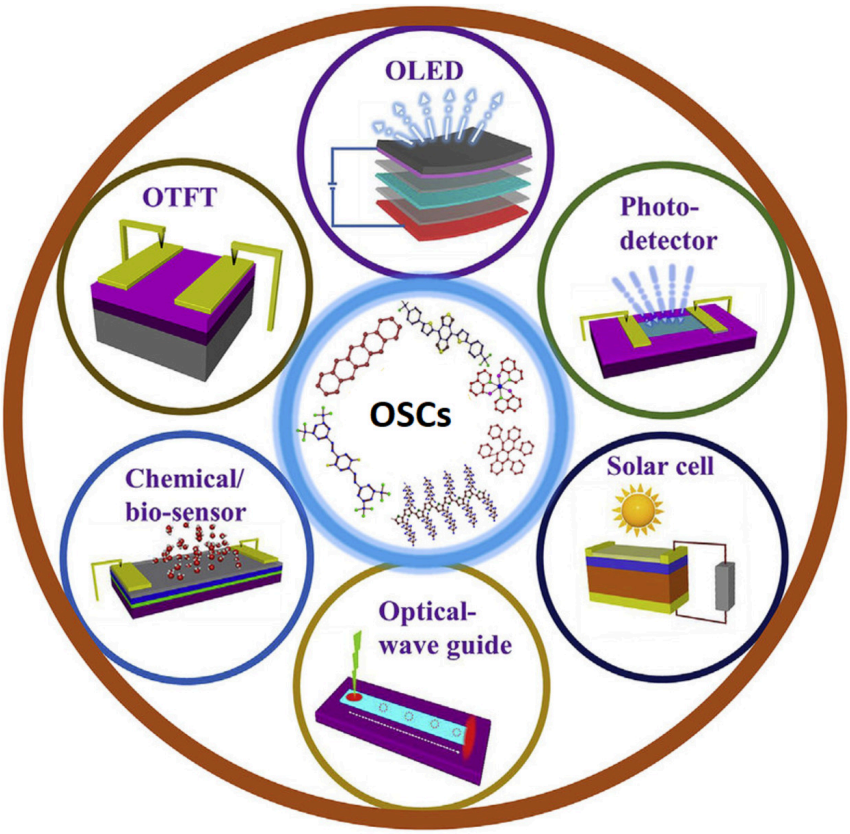

Figure 1.1.: The application of organic semiconductors[6]

crystals directly influences the overall performance of organic electronic devices [17, 18].

Organic semiconductor crystals are composed of organic molecules that possess semi-conductive properties. These materials have gained significant attention in recent years due to their advantages over traditional inorganic semiconductors, such as low cost, flexibility, and processability. However, one of the major limitations of organic semiconductor crystals is their relatively low mobility compared to inorganic materials. This is due to their amorphous structure and weak intermolecular interactions, which impede charge carrier mobility[19, 20, 21]. The mobility of organic semiconductor crystals is critical in a wide range of electronic devices, including solar cells, field-effect transistors, and organic light-emitting diodes. In organic solar cells, for example, the efficiency of the device is directly proportional to the mobility of the charge carriers. Higher mobility results in a faster and more efficient transport of charges from the active layer to the electrodes, which generates more power. Similarly, in organic field-effect transistors, the mobility of the charge carriers determines the device's speed and its ability to switch on and off quickly[22, 23, 24]. In organic light-emitting diodes, mobility determines the brightness of the device, since higher mobility leads to a more efficient transfer of energy from the electrons to the light-emitting molecules. Mobility is also important in the development of new organic electronic materials, as it can guide the design of new molecules that possess higher mobility. Over the past few years, researchers have developed several strategies to improve the mobility of organic semiconductor crystals. These include improving the molecular packing and intermolecular interactions in the crystal, reducing defects and impurities, and using additives to enhance charge transport. By incorporating these strategies, researchers have been able to achieve a significant improvement in the mobility of organic semiconductor crystals, making them more capable of competing with traditional inorganic semiconductors[25, 26, 27].

In conclusion, the mobility of organic semiconductor crystals is a crucial property for their use in electronic devices. Increasing the mobility of these materials leads to improvements in device performance, making them more efficient and reliable. Understanding the factors that affect mobility and developing strategies to enhance it is essential for the development of new and improved organic electronic materials. With these advances, organic semiconductors can provide alternative solutions to traditional inorganic semiconductors and play a significant role in the future of electronics. In this research we tried to investigate some of the computational challenges of OSCs in terms of charge and energy transfer by employing computational efficient method to model these complex problems. We concentrated on studying the charge propagation in Organic Semiconductor Crystals (OSCs) through non-adiabatic molecular dynamic simulation methods. Furthermore, the study investigates the influence of halogen groups on the charge transport properties of n-type Organic Semiconductor Crystals, with a specific focus on halogenated tetraazapentacenes (TAPs). In addition, our study explores

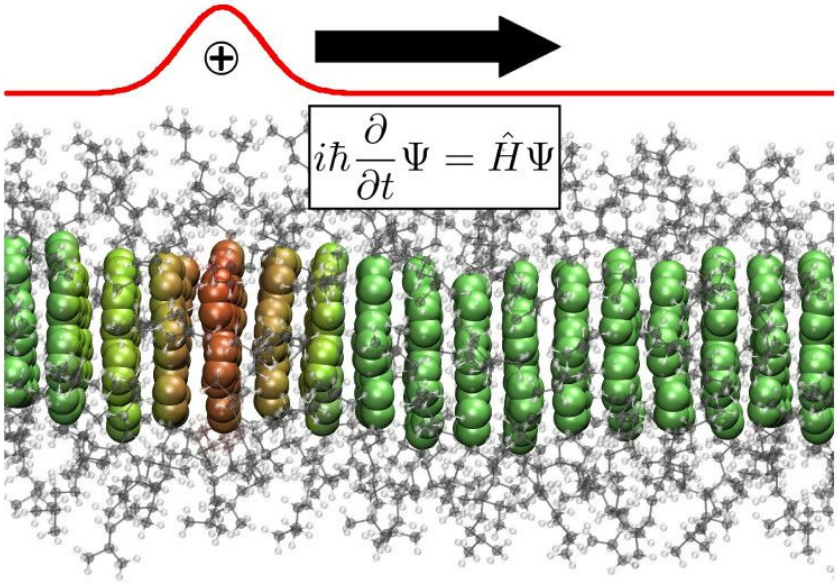

Figure 1.2.: Charge transfer in organic semiconductors[28]

the influence of substituents on hole mobilities in diphenylanthracene. To gain a comprehensive understanding of how various substituents affect charge transport, we commenced our research by examining anthracene (Ant) with dimethyl and dimethoxy as electron-donating groups, and dicyano and dibromo as electron-withdrawing groups. We systematically analyzed the effects of these substituents on reorganization energy, transfer integrals, and charge mobility.

2. Theoretical Background

Electronic structure theory in computational chemistry provides a robust framework, allowing us to comprehend and forecast the behavior of molecules and materials based on their electronic properties. This foundation is invaluable for studying chemical reactions, developing novel compounds, and exploring material properties, all without the need for extensive and costly experiments. By integrating principles from quantum mechanics and computational techniques, electronic structure theory offers deep insights into the distribution and behavior of electrons within a system.

At its core, electronic structure theory seeks to solve the Schrödinger equation, describing the quantum behavior of electrons in a molecular system. However, due to its complexity, direct analytical solutions are usually unattainable, especially for intricate systems. Consequently, computational methods are employed to numerically approximate and solve the equation, enabling the study of progressively complex molecular systems.

The fundamental concept of electronic structure theory centers around the wave function, a mathematical representation of a system's electronic state. This function contains information about electron positions and energies, and its square magnitude signifies the probability density of locating an electron within the system. Nevertheless, due to the high dimensionality of the electronic wave function, exact solutions for large systems remain challenging.

To tackle this complexity, various approximation methods have been developed. One widely used method is the Hartree-Fock approach, which simplifies the problem by assuming electrons move independently within an average field generated by other electrons. This simplification results in a set of coupled one-electron equations, known as the self-consistent field equations, which can be iteratively solved to obtain an approximate electronic structure solution.

Another prevalent technique is density functional theory (DFT), which focuses on electron density rather than the wave function. DFT relates a system's energy to its electron density using the Hohenberg-Kohn theorems, providing an efficient computational framework for studying larger systems. Due to the exchange-correlation functional in DFT calculations, this method offers a superior description of electron correlation interactions compared to HF theory.

Additionally, there are more advanced techniques, such as post-Hartree-Fock methods (e.g., configuration interaction and coupled cluster methods) and sophisticated variants of DFT (e.g., hybrid functionals and time-dependent DFT). These methods aim to enhance accuracy by incorporating higher-order electron correlation effects or addressing time-dependent phenomena.

2.1. Computational quantum mechanical modelling

2.1.1. The electronic structure problem

The fundamental object at the heart of quantum chemistry and condensed-matter physics is the molecular Hamiltonian that describes the interaction of electrons and atomic nuclei. In atomic units, where Planck's constant $\hbar$, and the electron charge e and mass m are set to unity, it reads:

$$H = \sum_i \frac{p_i^2}{2} + \sum_k \frac{P_k^2}{2M_k} + \frac{1}{2}\sum_{i\neq j}\frac{1}{|r_i - r_j|} + \frac{1}{2}\sum_{k\neq l}\frac{Z_k Z_l}{R_k - R_l} - \sum_{i,k}\frac{Z_k}{|r_i - R_k|} \tag{2.1}$$

The r_i and p_i are the electronic positions and momenta, R_k and P_k those of the nuclei, and M_k, Z_k are the nuclear masses and charges. The fundamental commutator relations hold:

$$\left[r_{i\alpha}, r_{j\beta}\right] = \left[p_{i\alpha}, p_j\right] = 0,\ \left[r_{i\alpha}, p_{j\beta}\right] = i\delta_{ij}\delta_{\alpha\beta} \tag{2.2}$$

For electrons, and likewise for nuclei. α, β label Cartesian coordinates, and $\delta_{i,j}$ refers to the Kronecker delta. In the position representation, that is, using a basis of position eigenstates, the momentum operator takes the form $p = -i\nabla r$. From the molecular Hamiltonian one commonly splits off the electronic Hamiltonian H_{elec} describing an electron cloud in an external electrostatic potential created by nuclei at fixed positions.

The eigenvalue spectrum of H_{elec} then yields the electronic energy levels $E_i; i = 0, 1, 2, \ldots$:

$$H_{elec}\,|\psi_i\rangle = E_i\,|\psi_i\rangle \tag{2.3}$$

with the electronic states$|\psi_i\rangle$. This eigenvalue problem is the time-independent electronic Schrödinger equation. The E_i as a function of the nuclear coordinates $E_i(R_1; R_2, \ldots)$ are called potential energy surfaces, as they act as an effective potential for the nuclei. Solids and molecules are stationary points on the lowest energy, or ground-state, surfaces. That is at molecular equilibrium geometries $\nabla_R E_0(R_1, \ldots) = 0$ holds.

The complete wavefunction $|\Psi\rangle$ of electrons and nuclei can be expanded using the electronic eigenstates

$$|\Psi\rangle = \sum_{i=1} |\chi_i\rangle|\psi\rangle_i \tag{2.4}$$

with nuclear wave functions $|\chi_i\rangle$. Applying the Hamiltonian to this form of the wavefunction and projecting out the electronic part results in

$$H|\chi_i\rangle = \left(\sum_k \frac{P_k^2}{2M_k} + E_i(R_1, \ldots) + \left[\sum_{j,k}\left(2\langle\psi_i|P_k|\psi_j\rangle P_k + \langle\psi_i|P_k^2|\psi_j\rangle\right)\right]\right)|\chi_i\rangle \tag{2.5}$$

for the Hamiltonian applied to the nuclear wavefunction. If the terms in square brackets, the socalled non-adiabatic couplings, are disregarded, the potential energy

surfaces E_i act indeed as independent potentials for the nuclei. Such an assumption is known as the Born-Oppenheimer approximation and is valid whenever the energy levels are well separated, as is commonly the case near equilibrium molecular geometries. It breaks down when energy levels cross. The resulting non-adiabatic effects are of crucial importance especially for charge and energy transport processes because they allow transitions between different electronic states. The time evolution of a quantum mechanical system obeys the time-dependent Schrödinger equation:

$$i\partial \left|\Psi_{(t)}\right\rangle = H \left|\Psi_{(t)}\right\rangle \tag{2.6}$$

Much of this thesis is concerned with approximate solutions of eq.2.7.

2.1.2. Density functional theory

Density Functional Theory (DFT) is a prevalent computational technique applied in condensed matter physics, materials science, and chemistry. It operates on the principle that a system's ground-state characteristics can be ascertained by examining its electron density instead of the wavefunction. The electron density is computed using the Kohn-Sham equations, which are derived from the Hohenberg-Kohn theorem and the Kohn-Sham variational principle.

2.1.2.1. The Hohenberg-Kohn theorems

The initial Hohenberg-Kohn theorem asserts that the electron density of a system's ground state uniquely specifies the external potential in a quantum mechanical setup, consequently determining the system's total energy. This implies that the electronic configuration of a molecule or material can be entirely characterized by its electron density, eliminating the need for the complete wave function encompassing all electrons. This simplifies and enhances the efficiency of calculations significantly.

The second Hohenberg-Kohn theorem, on the other hand, states that the true ground state density attains the minimum energy, with all other densities resulting in higher energies.

2.1.2.2. The Kohn-Sham approach

In the Kohn-Sham equations, the many-body problem of interacting electrons is simplified by transforming it into a set of non-interacting electron problems. The central idea is to introduce a set of auxiliary non-interacting electrons, known as the Kohn-Sham orbitals, which mimic the behavior of the real interacting electrons within the system. These orbitals are determined in such a way that they produce the same electron density $E[\rho]$ as the actual interacting electrons. The functional $E[\rho]$ represents the total energy of the system, which includes contributions from electron-electron interactions, electron kinetic energy, and the interaction with an external potential. The Kohn-Sham equations essentially find the non-interacting electron orbitals that minimize this total energy functional. Solving these equations

involves finding the optimal electron density and the corresponding Kohn-Sham orbitals, allowing researchers to explore various properties of molecules and materials without the need for highly complex calculations involving the full many-body wavefunction of all electrons. This approach significantly simplifies and enhances the efficiency of electronic structure calculations in computational chemistry.

We split up the functional $E[\rho]$ as

$$E[\rho] = T[\rho] + E_{\text{xc}}[\rho] + E_{\text{H}}[\rho] + \int d^3r \rho(\mathbf{r}) V_{\text{ext}}(\mathbf{r}), \tag{2.7}$$

where $E_{\text{H}} = \int d^3r d^3r' \frac{\rho(\mathbf{r})\rho(\mathbf{r}')}{|\mathbf{r}-\mathbf{r}'|}$ is the classical Coulomb interaction of the electron density with itself, the final integral is the interaction of the density with the nuclear electrostatic potential, and the functionals $T[\rho]$ and E_{xc} entail all the complicated non-classical physics. $T[\rho]$ yields the electronic kinetic energy, and $E_{\text{xc}}[\rho]$ accounts for exchange and correlation. Now, Kohn and Sham 's approach offers a simple expression for $T[\rho]$. A system of N interacting electrons is mapped to a system of N non-interacting electrons, with orthogonal single electron orbitals $|\phi_i\rangle, i = 1, \ldots, N$. The many-body wavefunction $|\Psi\rangle$ for the non-interacting system is a single Slater determinant formed by the orbitals, and the kinetic energy is given by the expression for non-interacting electrons:

$$T[\phi_1, \ldots] = \sum_i \frac{1}{2} \langle \phi_i | \mathbf{p}_i^2 | \phi_i \rangle. \tag{2.8}$$

In order to maintain the connection to the real, interacting system the density of both systems is set to be the same:

$$\rho(\mathbf{r}) = \sum_i |\langle \phi_i | r \rangle|^2. \tag{2.9}$$

Thus, the whole unknown physics is bundled in the exchange-correlation term $E_{\text{xc}}[\rho]$ that needs to account for the difference between the non-interacting and true kinetic energy, as well. Within this formalism, the variational principle $\frac{\delta E[\rho_0]}{\delta \rho} = 0$ leads to the set of single electron eigenvalue equations

$$\left(\frac{\mathbf{p}^2}{2} + V_{\text{ext}}(\mathbf{r}) + \frac{\delta E_{\text{xc}}[\rho]}{\delta \rho(\mathbf{r})} \right) |\phi_i\rangle = \varepsilon_i |\phi_i\rangle, \tag{2.10}$$

known as Kohn-Sham equation. From the equation, the orbitals can be found, and hence the energy through reinsertion into the functional. The orbital eigenvalues ε_i enter as Lagrangian multipliers for the orthonormality condition, and ε_N can be identified with the ionization potential by Janaka 's theorem [29]. Even though the orbitals $|\phi_i\rangle$ possess no a priori physical meaning, the frontier orbitals are often identified with real single electron wavefunctions, and this has been justified empirically [30].

2.1.2.3. Density functional approximation

The first attempts at a practical approximation of the exchange-correlation functional predate the rigorous foundations of DFT by Hohenberg and Kohn. Thomas and Fermi already put forward a model already in 1927 [31, 32], expressing the kinetic energy of an electron gas in terms of its density. However, their model predicts no stable molecules and is thus unfit for predictive quantum chemical applications. Successive developments have gradually improved the quantitative performance of DFT methods, while remaining computationally efficient, leading to their wide spread adoption, especially also among experimentalists. Two DFT papers are now among the ten most cited scientific works [33]. In the following, we introduce briefly a hierarchy of different functional approximations. Special attention will be payed to long-range corrected functionals that provide the foundation for some of the work in this book and tend to be among the most accurate for many materials occurring in the context of molecular charge and energy transport.

2.1.2.4. Local density approximation

The local density approximation (LDA) goes back to the work of Kohn and Sham [34], and remains popular for solid-state systems, but is usually too inaccurate for molecules. The exchange-correlation energy is expressed as a density weighted integral over an energy density $\varepsilon_{\mathrm{xc}}(\rho)$:

$$E_{\mathrm{xc}}[\rho] = \int d^3r \rho(\mathbf{r}) \varepsilon_{\mathrm{xc}}(\rho(\mathbf{r})). \tag{2.11}$$

$\varepsilon_{\mathrm{xc}}$ is modeled by the expression for the homogeneous electron gas. Then, $\varepsilon_{\mathrm{xc}} = \varepsilon_{\mathrm{x}} + \varepsilon_{\mathrm{c}}$, with the exchange contribution

$$\varepsilon_{\mathrm{x}}(\rho) = -\frac{3}{4}\left(\frac{3}{\pi}\right)^{\frac{1}{3}} \rho(\mathbf{r})^{\frac{1}{3}} \tag{2.12}$$

as derived by Dirac [35]. The correlation contribution ec cannot be derived in closed form, but highly accurate quantum Monte Carlo results are available, to which analytic expressions can be fit[36]. LDA can be generalized to spin polarized systems, then known as local spin density approximation (LSDA), using the spin scaling relation:

$$E_{\mathrm{x}}[\rho_\uparrow, \rho_\downarrow] = \frac{1}{2}(E_{\mathrm{x}}[2\rho_\uparrow] + E_{\mathrm{x}}[2\rho_\downarrow]), \tag{2.13}$$

which is a property of the exact functional. Here, $\rho_{\uparrow,\downarrow}$ are densities for the two different spin polarizations alone, and $E_{\mathrm{x}}[\rho]$ is the exchange functional for an unpolarized system that has been approximated by the Dirac form. The correlation contribution has to be interpolated from the know unpolarized $\rho_\uparrow = \frac{\rho}{2} = \rho_\downarrow$ and fully polarized $\rho = \rho_\uparrow$ cases.

2.1.2.5. Generalized gradient approximation

LDA can only be truly useful for solids, rather than molecules, because its direct adoption from the uniform electron gas requires slowly varying densities. For this reason, corrections have been developed that take into account density fluctuations through inclusion of the density gradient $\nabla\rho(\mathbf{r})$:

$$E_{\mathrm{xc}}[\rho] = \int d^3\rho(\mathbf{r})\varepsilon_{\mathrm{xc}}(\rho(\mathbf{r}), \nabla\rho(\mathbf{r})). \tag{2.14}$$

Such functionals are known as generalized gradient approximations (GGA). There is no unique way to approximate $\varepsilon_{\mathrm{xc}}$ in this way, but many different approaches exist. One popular GGA functional is the Perdew-Burke-Ernzerhof (PBE) functional [37]. It is derived by requiring that certain conditions known to hold for the exact functionals be reproduced by the approximative form. Therefore, it is free of fitted parameters and tends to be accurate for a broad range of systems, while many GGA functionals employ fits to reference data, limiting their applicability. PBE is usually chosen as the underlying functional of the DFTB formalism, to be introduced in a later section, and thus of particular relevance for the work in this thesis. However, introducing the technical details would exceed the scope of a short introduction, and details can be found in the literature.

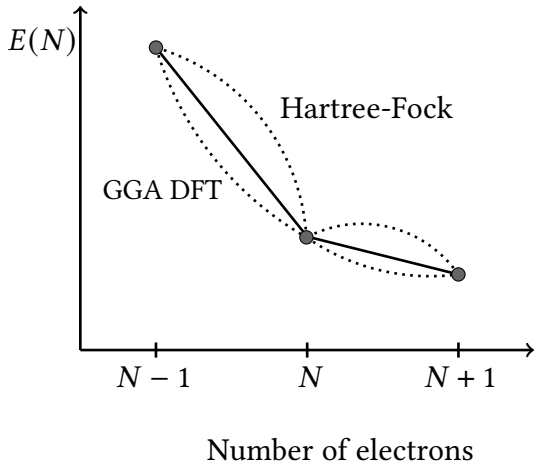

Figure 2.1.: The self-interaction error of DFT functional approximations without Hartree-Fock exchange becomes apparent when the number of electrons deviates from the integers. Such scenarious can be defined in terms of density matrices with densities integrating to arbritary real numbers, and the exact functional predicts that the energy $E(N)$ follows a straight line between integer points[38]. However, due to self-interaction, the approximate functionals predict a smooth, convex form. Hartree-Fock theory is wrong in the opposite direction and predicts a concave dependence on the electron number.

2.1.2.6. Hybrid functionals

Both LDA and GGA functionals suffer from the self-interaction error. They fail to fully remove the interaction of electrons with themselves, or others with the same spin according to the exclusion principle, from the energy contribution. Consequences of this are, for instance, severely underestimated band or HOMO-LUMO gaps, and artificial electron delocalization. LDA and GGA functionals are local in the sense that the energy is the integral over functions of the density at certain points, independent of all other spatial locations. Some minor non-locality is introduced in GGA through the gradient information, but this first order expansion cannot account for interactions over larger distances. The exchange-term in Hartree-Fock theory (HF) on the other hand cancels the self-interaction exactly, but since it is calculated as an integral over two spatial coordinates, it is non-local. Hybrid functionals take the approach to mix HF exchange $E_{\mathrm{x}}^{\mathrm{HF}}$ with GGA exchange-correlation functionals. The energy then reads:

$$E_{\mathrm{xc}}^{\mathrm{Hyb}}[\phi_1, \dots] = \alpha E_{\mathrm{x}}^{\mathrm{HF}}[\phi_1, \dots] + (1-\alpha)E_{\mathrm{x}}[\rho] + E_{\mathrm{c}}[\rho]. \tag{2.15}$$

The amount of HF exchange can be controlled through the parameter α, and different functionals use different values. Performance can also be improved by fine-tuning α for the system under investigation. For example, the PBE0 [39, 40] hybrid functional includes a fraction of $\alpha = 0.25$ HF exchange. The extremely popular B3LYP [41, 42, 43] functionals included $\alpha = 0.2$ of HF exchange, but as two additional mixing parameters.
The HF exchange term

$$E_{\mathrm{x}}^{\mathrm{HF}}[\phi_1, \dots] = -\frac{1}{2}\sum_{i,j}\int d^3r d^3r' \frac{\phi_i^*(\mathbf{r})\phi_j^*(\mathbf{r})\phi_i(\mathbf{r}')\phi_j(\mathbf{r}')}{|\mathbf{r}-\mathbf{r}'|} \tag{2.16}$$

depends explicitly on the individual Kohn-Sham orbitals ϕ_i, not merely on the density ρ. Consequently, the entire functional becomes orbital dependent. Because the evaluation of the HF exchange integral scales quartic with system size, DFT with hybrid functionals scales one order worse than with LDA or GGA functionals. Although in practice distance cut-offs for integrals often allow cubic scaling, hybrid functionals remain somewhat more computationally expensive.

2.1.3. The density functional tight-binding method

Albeit DFT is already computationally very efficient compared to most wavefunction based electronic structure methods, there remain many problems that require quantum treatment, but at much lower computational cost. For instance, such problems include simulations of large nanostructures that can contain many thousands of atoms. Given the large and growing importance of nanotechnology, this is of considerable practical relevance, say in the development process of new integrated circuits or molecular motors. Another field in need of fast computation are all sorts of dynamical simulations, stretching from single molecular electronic dynamics for

spectroscopy to the simulation of chemical reactions at the active sites of proteins in aqueous solution. There, the relevant time scales can be on the order of nanoseconds, requiring millions of quantum calculations, well beyond the scope of DFT. For such purposes, semi-empirical and approximate methods exist that are far less computationally expensive at the cost of some accuracy. Many of those methods rely strongly on fitting of parameters to reference data, severely limiting their transferability. The density functional tight-binding method (DFTB), on the other hand, is derived and largely parametrized from DFT, lending it a certain robustness. It tends to perform particularly well for organic molecules, as the underlying assumptions are usually satisfied, providing a kind of rigorous foundation that many empirical methods lack. As such molecules are the target systems for the studies presented in this work, we opted for DFTB as the underlying method for further development. DFTB does, however, inherit the shortcomings of the applied density functional approximations. This will be addressed in a later chapter. In this section, we derive and explain the basics of DFTB, discuss its time-dependent extension TD-DFTB, and introduce a recent extension to include long-range corrected functionals.

2.1.3.1. Derivation

DFTB [44, 45] can be derived from DFT through a series expansion of the DFT energy functional $E[\rho]$ at a reference density ρ_0. Here we expand up to quadratic order, leading to the so-called SCC-DFTB, or DFTB2, method [45] that is the version most commonly used. Early versions only contained first order terms (DFTB1 [44]), and extensions with third order terms (DFTB3 [46]) exist as well. Starting from the energy expression

$$E[\rho] = \sum_i f_i \langle \phi_i | \nabla^2 + \int d^3r' \frac{\rho(\mathbf{r}')}{|\mathbf{r} - \mathbf{r}'|} + V_{\text{ext}}(\mathbf{r}) | \phi_i \rangle + E_{\text{xc}}[\rho] + E_{\text{nuc}}, \tag{2.17}$$

which is a different way to write eq. 2.10, with Kohn-Sham orbitals $\langle \phi_i |$, orbital occupations f_i, and the internuclear repulsion $E_{\text{nuc}} = \sum_{A,B} \frac{Z_A Z_B}{|\mathbf{R}_A - \mathbf{R}_B|}$, we expand

$$\begin{aligned} E[\rho] = \sum_i f_i \langle \phi_i | \nabla^2 + \int d^3r' \frac{\rho_0(\mathbf{r}')}{|\mathbf{r} - \mathbf{r}'|} + \frac{\delta E_{\text{xc}}[\rho_0]}{\delta \rho(\mathbf{r})} + V_{\text{ext}}(\mathbf{r}) | \phi_i \rangle \\ + \frac{1}{2} \int d^3r d^3r' \left(\frac{1}{|\mathbf{r} - \mathbf{r}'|} + \frac{\delta^2 E_{\text{xc}}[\rho_0]}{\delta \rho(\mathbf{r}) \delta \rho(\mathbf{r}')} \right) \delta\rho(\mathbf{r}) \delta\rho(\mathbf{r}') \\ + E_{\text{xc}}[\rho_0] + E_{\text{nuc}} - \frac{1}{2} \int d^3r d^3r' \frac{\rho_0(\mathbf{r}) \rho_0(\mathbf{r}')}{|\mathbf{r} - \mathbf{r}'|} - \int d^3r \frac{\delta E_{\text{xc}}[\rho_0]}{\delta \rho(\mathbf{r})} \\ + O(\delta\rho^3), \end{aligned} \tag{2.18}$$

with density fluctuations $\delta\rho$ and the reference density ρ_0 such that $\rho = \rho_0 + \delta\rho$. Now, we group together different terms that will then be further approximated.

The first order terms are:

$$\begin{aligned} E^{(1)} &= \sum_i f_i \langle \phi_i | \nabla^2 + \int d^3r' \frac{\rho_0(\mathbf{r}')}{|\mathbf{r}-\mathbf{r}'|} + \frac{\delta E_{\text{xc}}[\rho_0]}{\delta \rho(\mathbf{r})} + V_{\text{ext}}(\mathbf{r}) | \phi_i \rangle \\ &= \sum_i f_i \langle \phi_i | H^{(0)}[\rho_0] | \phi_i \rangle, \end{aligned} \tag{2.19}$$

with the zeroth order Hamiltonian $H^{(0)}$ that depends only on the reference density. The second order terms are given by the Coulomb integral:

$$E^{(2)} = \frac{1}{2} \int d^3r d^3r' \left(\frac{1}{|\mathbf{r}-\mathbf{r}'|} + \frac{\delta^2 E_{\text{xc}}[\rho_0]}{\delta\rho(\mathbf{r})\delta\rho(\mathbf{r}')} \right) \delta\rho(\mathbf{r})\delta\rho(\mathbf{r}'). \tag{2.20}$$

Finally, there are zeroth order terms that depend only on the reference density ρ_0 and the nuclear positions:

$$E^{(3)} = E_{\text{xc}}[\rho_0] + E_{\text{nuc}} - \frac{1}{2} \int d^3r d^3r' \frac{\rho(\mathbf{r})\rho(\mathbf{r}')}{|\mathbf{r}-\mathbf{r}'|} - \int d^3r \frac{\delta E_{\text{xc}}[\rho_0]}{\delta\rho(\mathbf{r}) p_0(\mathbf{r})}. \tag{2.21}$$

All three energy contributions will now be further approximated, after an atom centered basis representation has been introduced:

$$|\phi_i\rangle = \sum_{A,\mu\in A} c_{\mu i} |\chi_\mu\rangle, \tag{2.22}$$

where the upper case Latin index A runs over atoms, Greek index μ over basis functions, and $\mu \in A$ indicates that orbital μ is centered on atom A : $\langle \mathbf{r} | \chi_\mu \rangle = \chi(\mathbf{r} - \mathbf{R}_A)$ for some orbital function χ. The detailed construction of the basis will be discussed later on. Likewise, the reference density ρ_0 is constructed as a sum of atomic densities ρ_A, also centered on the atoms:

$$\rho_0(\mathbf{r}) = \sum_A \rho_A(r). \tag{2.23}$$

It is the fundamental assumption underpinning DFTB that the molecular density ρ is already well described by such a sum of atomic densities, with only modest charge transfer $\delta\rho$. Hence comes the term tight-binding. Within the basis, $E^{(1)}$ can be expanded out as:

$$E^{(1)} = \sum_i \sum_{A,B} \sum_{\mu\in A, \nu\in B} f_i c_{\mu i} c_{\nu i} \langle \chi_m u | H^{(0)}[\rho_0] | \chi_\nu \rangle = \sum_i \sum_{A,B} \sum_{\mu\in A, \nu\in B} f_i c_{\mu i} c_{\nu i} H^{(0)}[\rho_0]_{\mu\nu}. \tag{2.24}$$

In principle, $H^{(0)}[\rho_0]_{\mu\nu}$ depends on the positions of all nuclei. However, the integral is dominated by the density contributions coming from the two atoms on which χ_μ and χ_ν are centered. Hence, we can approximate:

$$H^{(0)}[\rho_0]_{\mu\nu} \approx H^{(0)}[\rho_A + \rho_B]_{\mu\nu} = H^{(0)}_{\mu\nu} \qquad \text{for } \mu \in A \text{ and } \nu \in B, \tag{2.25}$$

where $H_{\mu\nu}^{(0)}$ depends only on the relative positions of atoms A and B, allowing for precalculation. Thus, because $H_{\mu\nu}^{(0)}$ is stored, no integral needs to be evaluated at run-time. As shall be discussed later on, due to symmetry only one rather than three coordinates have to be sampled, reducing memory requirements to a minimum. For $\mu = \nu$ the Hamiltonian element coincides with an orbital eigenvalue of an isolated atom $H_{\mu\nu}^{(0)} = \varepsilon_\mu$. In order to approximate the second order terms $E^{(2)}$, we shall partition the space into disjoint regions V_A of space closest to atom A, such that $\mathbb{R}^3 = \cup_A V_A$, and write the density fluctuations $\delta\rho(\mathbf{r})$ as a sum of atomic density fluctuations $\delta\rho(r) = \sum_A \delta\rho_A(\mathbf{r})$, where $\delta\rho_A$ is non-vanishing only on V_A. Next, we define atomic charge fluctuations as $\Delta q_A = \int_{V_A} d^3r\delta\rho(\mathbf{r}) = \int d^3r\delta\rho_A(\mathbf{r})$, and express charge fluctuations as

$$\delta\rho_A(\mathbf{r}) = \Delta q_A g_A(\mathbf{r}), \tag{2.26}$$

where $g_A(\mathbf{r})$ is a shape function that must integrate to one. We assume a Gaussian shape for g_A:

$$g_a(\mathbf{r}) \frac{1}{\left(2\pi\sigma_A^2\right)^{\frac{3}{2}}} \exp\left(-\frac{\mathbf{r}^2}{2\sigma_A^2}\right). \tag{2.27}$$

In doing so, we impose spherical symmetry on the charge fluctuations, effectively leading to a monopole approximation. Indeed, multipole expansion results in the same form. The width σ_A of the charge distribution is then the only free parameter at second order. The energy expression reads:

$$E^{(2)} = \frac{1}{2}\sum_{A,B} \Delta q_A \Delta q_B \int d^3r d^3r' \left(\frac{1}{|\mathbf{r}-\mathbf{r}'|} + \frac{\delta^2 E_{\mathrm{xc}}[\rho_0]}{\delta\rho(\mathbf{r})\delta\rho(\mathbf{r}')}\right) g_A(\mathbf{r}) G_B(\mathbf{r}'). \tag{2.28}$$

Discarding the exchange correlation term, only the Coulomb integral has to be evaluated, which is possible in closed form [45]:

$$\int d^3r d^3r' \frac{g_A(\mathbf{r})G_B(\mathbf{r}')}{|\mathbf{r}-\mathbf{r}'|} = \frac{\operatorname{erf}\left(C_{Ab}|\mathbf{R}_A - \mathbf{R}_B|\right)}{|\mathbf{R}_A - \mathbf{R}_B|} = \gamma_{AB}(|\mathbf{R}_A - \mathbf{R}_B|), \tag{2.29}$$

with

$$C_{AB} = \sqrt{\frac{1}{2}\frac{1}{\sigma_A^2 + \sigma_B^2}} \tag{2.30}$$

fixed by the charge distribution widths. To fix the width parameters, we consider the expansion of the energy of a free atom A in an excess charge Δq_A:

$$E(\Delta q_A) = E(0) + \frac{dE}{dq}\Delta q_A + \frac{1}{2}\frac{d^2E}{dq^2}\Delta q_A^2 + O(\Delta q_A^3) \tag{2.31}$$

In DFT the second order term is given by the so-called Hubbard parameter U and related to the ionization potential IE and electron affinity EA as

$$\frac{d^2E}{dq^2} = U = \mathrm{IE} - \mathrm{EA} \tag{2.32}$$

The Hubbard parameters can be easily determined from DFT calculations on free atoms. Then, demanding that for free atoms $E^{(2)}$ coincide with $\frac{1}{2}U\Delta q^2$ establishes a connection between the Hubbard parameter U_A of an atom and the width parameter σ_A, hence fixed. In analogy to $\Delta q_A = \int_{V_A} d^3r\delta\rho$, we define atomic charges q_A as

$$q_A = \int_{V_A} d^3r\rho(\mathbf{r}) = \sum_i f_i \int_{V_A} d^3r\phi_i(\mathbf{r})^2 = \sum_i f_i \sum_{\mu,\nu} c_{\mu i}c_{\nu i} \int_{V_A} d^3r\chi_\mu(\mathbf{r})\chi_\nu(\mathbf{r}), \tag{2.33}$$

assuming real orbitals. In the tight-binding spirit, we approximate

$$\int_{V_A} d^3r\chi_\mu(\mathbf{r})\chi_\nu(\mathbf{r}) \approx \frac{1}{2}\int d^3r\chi_\mu(\mathbf{r})\chi_\nu(\mathbf{r}) = \frac{1}{2}S_{\mu\nu}, \tag{2.34}$$

or in other words, the overlap is only non-zero in the atomic regions and can be equally partitioned between both involved atoms. Then q_A simplifies to

$$q_A = \sum_i f_i \sum_{\nu,\mu\in A} c_{\mu i}c_{\nu i}S_{\mu\nu}, \tag{2.35}$$

which is the same as the famous Mulliken charge expression [47]. Δq_A can be computed as $\Delta q_A = q_A - q_A^{(0)}$ with the electronic charge $q_A^{(0)}$ of a neutral atom A. The overlap matrix $S_{\mu\nu}$ can be precalculated, like $H_{\mu\nu}^{(0)}$. Finally, the third order term $E^{(3)}$ remains to be determined. Because $E^{(3)}$ is a function of ρ_0 alone, and in turn ρ_0 is a function of the nuclear positions $\mathbf{R}_A$, $E^{(3)}$ can be written as a function of the $\mathbf{R}_A$. Since most of reference charge interactions happens between atom pairs, with three center contributions smaller, we approximate

$$E^{(3)} = \frac{1}{2}\sum_{A\neq B} V_{AB}(|\mathbf{R}_A - \mathbf{R}_B|), \tag{2.36}$$

The functions V_{AB} are called repulsive potentials. For the functional form of V_{AB} splines or polynomials are employed, where the exact choice does not matter. One function for each pair of elements is used. While in principle V_{AB} could be calculated directly from DFT, usually it is fit to reference data. Hence, empirical corrections to the tight-binding approximation are fit together with the reference as well. Reference data has to be hand-picked to generalize well, and this can be a tedious process, normally the hardest part of the fitting procedure. One part of this work is concerned with a generalization of the repulsive potentials to render the manual selection obsolete by allowing very large data sets to be used. Repulsive potentials will be discussed in more detail at this later point. Eventually, the full DFTB energy reads:

$$E = \sum_i f_i \sum_{\mu,\nu} c_{\mu i}c_{\nu i}H_{\mu\nu}^{(0)} + \frac{1}{2}\sum_{AB} \Delta q_A\Delta q_B\gamma_{AB}(|\mathbf{R}_A - \mathbf{R}_B|) + \frac{1}{2}\sum_{A\neq B} V_{AB}(|\mathbf{R}_A - \mathbf{R}_B|). \tag{2.37}$$

Like in full DFT, Kohn-Sham equations follow from energy minimization, constrained to orthonormal orbitals. Thus, we have:

$$\sum_{\nu}\left(H^{(0)}_{\mu\nu}+\frac{1}{2}S_{\mu\nu}\sum_{C}(\gamma\mu C+\gamma\nu C)\Delta q_C\right)c_{\nu i}=\varepsilon_i\sum_{\nu}S_{\mu\nu}c_{\nu i}, \tag{2.38}$$

where $\gamma_{\mu C}=\gamma_{AC}$ for $\mu\in A$. The equations have to be solved self-consistently in Δq_A to find the Kohn-Sham orbitals ϕ_i and the energy E. Analytic nuclear gradient expressions $\nabla_{\mathbf{R}}E$ are available to calculate forces [45]. Note how the repulsive potentials only appear in the total energy expression, but not in the Kohn-Sham equations. They are important for the description of molecular geometries and absolute energies, but do not affect the electronic structure calculation.

2.1.4. Basis set and reference density

DFTB employs a minimal basis set for the sake of computational efficiency. However, naive minimal basis sets are not usually sufficient for quantum chemical applications because they lead to poor quantitative performance. Therefore, the basis sets used in DFTB are specially optimized. As previously noted, DFTB relies on a tight-binding assumption in which electrons are expected to be largely confined close to the atoms, what is normally the case to a good extent within molecules. In free atoms, on the other hand, electron densities tend to be more diffuse. Accordingly, orbitals coming from free atoms, such as the natural hydrogen s, p, d, ... orbitals, are not a suitable basis set choice. Instead, the basis set is taken from confined free atom orbitals, where a confinement potential $V_{\text{conf}}(\mathbf{r})$ simulates the effect of the molecular environment. More explicitly, the basis functions $\chi_\mu(\mathbf{r})$ centered on atom A are solutions to the modified Kohn-Sham eigenvalue equation

$$\left(\nabla^2+\int d^3r'\frac{\rho_A(\mathbf{r}')}{|\mathbf{r}-\mathbf{r}'|}+\frac{\delta E_{\text{XC}}[\rho_A]}{\delta\rho(\mathbf{r})}-\frac{Z_A}{|\mathbf{r}|}+V_{\text{conf}}(\mathbf{r})\right)\chi_\mu(\mathbf{r})=\varepsilon_\mu\chi_\mu(\mathbf{r}). \tag{2.39}$$

The purpose of V_{conf} is to compress the density, and consequently V_{conf} should grow with the distance from the nucleus. The by far most common choice is a quadratic potential:

$$V_{\text{conf}}(\mathbf{r})=\left(\frac{\mathbf{r}}{r_{\text{wf}}}\right)^2, \tag{2.40}$$

albeit some DFTB parametrization have used other potentials, too [47]. The parameter r_{wf} controls the extend of the confinement. DFTB parametrizations usually fine tune r_{wf} for optimal accuracy. The atomic density ρ_A that appears in the Kohn-Sham potential is likewise determined from a self consistent constraint free atom calculation, but with a different constraint parameter r_{d}. ρ_A also serves as atom A's contribution to the reference density ρ_0. Thus, Hamiltonian elements $H^{(0)}_{\mu\nu}$ for atom pairs A and B are calculated and tabulated as $H^{(0)}_{\mu\nu}=\int d^3r\,\chi_\mu(\mathbf{r})H[\rho_A(\mathbf{r})+\rho_B(\mathbf{r})]\chi_\nu(\mathbf{r})$. Eq. (2.39) is solved in a Slater type orbital basis, that is with exponentially decaying

basis functions. Therefore, the DFTB basis is also effectively of Slater type. Because all integrals are precalculated, there is no associated computational extra cost over, say, Gaussian type functions. While the tabulated integrals $H^{(0)}_{\mu\nu}(\mathbf{R}_A - \mathbf{R}_B)$ and $S_{\mu\nu}(\mathbf{R}_A - \mathbf{R}_B)$ do, in principle, depend on three spatial coordinates, only one dimensional tables for different combinations of orbital symmetry - e.g. $s - s$, $s - p_{x,y,z}$, $p_x - p_y$, etc.- need to be stored, exploiting symmetry and the behavior of the spherical harmonics under rotation. See Fig. 3.2 for a visual explanation.

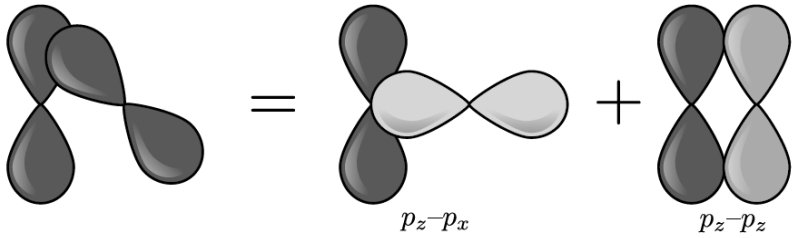

Figure 2.2.: The integral involving two arbitrarily oriented p orbitals can be reduced to the sum of integrals over orbitals of fixed relative orientation by exploiting that p orbitals behave like vectors in $\mathbb{R}^3$ under rotation.

2.1.4.1. Classical Molecular dynamics

Even the fastest empirical quantum mechanical methods are far too slow to simulate truly large systems of ten thousands to millions of atoms, let alone on the nanosecond time scale and beyond. Yet, such large scale problems appear abundantly. Take for example the folding of proteins in solution, which is one of the preeminent subjects of biophysics and chemistry, or the description of large sections of amorphous or crystalline organic semiconducting materials that are studied in this thesis. Therefore, a faster set of methods is required to study them. The gap is filled by so-called force-field methods. The term (force-field) refers to a fit of some mathematical function $V(\mathbf{R}_1, \dots)$ of the nuclear coordinates $\mathbf{R}_i$ to a potential energy surface $E(\mathbf{R}_1, \dots)$, most of the time the ground state, disregarding the other surfaces. Because usually only a small subsection of the potential energy surface is of interest, reasonably simple functions suffice for the fit. In particular, most force-fields do not attempt to describe chemical reactions, only certain molecules. Oftentimes one addresses large scale structural questions, like the secondary structure of proteins that are not overly sensitive to the details of the potential energy surface, so that force-fields are a very adequate manner of description. Indeed, dispersion forces, crucial for the correct description of large scale and intermolecular arrangement, are poorly accounted for by DFT and other fast quantum mechanical methods, which require fitted correction terms akin to force-fields, or else would perform worse.

2.1.4.2. Force-fields

There are many different force-fields in existence that differ in what reference data they employ for fitting, and the precise functional form used. However, most share a number of basic, dominant, and physically inspired terms. Equilibrium molecular geometries are described by way of equilibrium bond lengths R_b, bond angles θ_b, and dihedral angles ω_d. A series expansion to second order for bonds, and a Fourier expansion for the periodic dihedrals then yields the energetic costs of molecular perturbations. The corresponding bonded terms now read:

$$V_{\text{bond}} = \sum_b \frac{1}{2} k_b (|\mathbf{R}^{(b)}| - \mathbf{R}_b)^2, \tag{2.41}$$

$$V_{\text{angle}} = \sum_b \frac{1}{2} k_{\theta b} (\theta^{(b)} - \theta_b)^2, \tag{2.42}$$

and

$$V_{\text{dihedral}} = \sum_d \sum_{n=0}^{N_d} V_{dn} (1 + \cos\left(n\omega_{dn} - \omega^{(d)}\right)), \tag{2.43}$$

where $\mathbf{R}^{(b)}$, $\theta^{(b)}$, and $\omega^{(d)}$ are the bond lengths and angles, and dihedral angles, calculated at the current geometry, respectively. Non-bonded interactions consist of two contributions: electrostatic Coulomb interaction of atom centered charges qi and van-der-Waals interaction. The former accounts for charge transfer within molecules or molecular fragments. The associated potential reads:

$$V_{\text{electrostatic}} = \frac{1}{2} \sum_{i \neq j} \frac{q_i q_j}{|\mathbf{R}_i - \mathbf{R}_j|}, \tag{2.44}$$

where i, j run over all atoms. The later entails short-range Pauli repulsion and dispersion interaction. Usually, the potential is approximated as

$$V_{\text{van-der-Waals}} = \frac{1}{2} \sum_{i \neq j} 4\varepsilon_{ij} \left(\left(\frac{\sigma_{ij}}{R_{ij}} \right)^{12} - \left(\frac{\sigma_{ij}}{R_{ij}} \right)^{6} \right), \tag{2.45}$$

with interatomic distances R_{ij} and parameters $\varepsilon_{ij}, \sigma_{ij}$. The first summand belongs to Pauli repulsion, and its form is purely empirical. An exponential decay would be more accurate, but costly to evaluate numerically, which is why the $1/R^{12}$ form is chosen instead. The second summand belongs to dispersion interaction. The $1/R^6$ form can be derived from perturbation theory as the first correction to mean-field, Hartree-Fock like electronic interaction. Eventually, bonded and non-bonded contributions together yield the complete force-field energy V:

$$\begin{aligned} V(\mathbf{R}_1, \dots) = {} & V_{\text{bond}}(\mathbf{R}_1, \dots) + V_{\text{angle}}(\mathbf{R}_1, \dots) + V_{\text{dihedral}}(\mathbf{R}_1, \dots) + V_{\text{electrostatic}}(\mathbf{R}_1, \dots) \\ & + V_{\text{van-der-Waals}}(\mathbf{R}_1, \dots) \end{aligned} \tag{2.46}$$

The free parameters can be fitted to experimental data or first-principle calculations. The development of good force-fields is difficult. In this thesis, we use different force-field parameters from the literature, except for the bonded parameters k_B and R_b that we fit to equilibrium geometries and normal mode frequencies from first principle calculations. Because there is little interdependence of those and other parameters, such a fit is straightforward and greatly improves the accuracy of the molecular vibrational frequencies that affect intermolecular charge and energy transport.

2.1.5. Molecular dynamics

Most of the time, force-field methods are not used to calculate static properties of single structures, but to sample static and time-dependent properties dependent on the nuclear coordinates and momenta, like thermal expectation values $\langle A(\mathbf{R},\mathbf{P})\rangle$ and time-dependent correlation functions $\langle A(\mathbf{R}(t),\mathbf{P}(t))B(\mathbf{R}(0),\mathbf{P}(0))\rangle$. Here, A and B are classical functions of the positions and momenta, not quantum mechanical operators. Likewise, we consider the positions and momenta as classical phase space variables. Molecular dynamics (MD) considers the time evolution of a classical, many-atom system, described by a Hamiltonian function $H(\mathbf{R}_1,\mathbf{P}_1,\dots) = T(\mathbf{P}_1,\dots) + V(\mathbf{R}_1,\dots)$. $T = \sum_i \frac{\mathbf{P}_i^2}{2M_i}$, with the atomic masses M_i, is the classical kinetic energy; V the potential energy that can come directly from an electronic structure calculation (ab initio MD), but for large systems is usually calculated with a force-field. The system's time evolution follows the classical canonical equations:

$$\frac{\mathrm{d}\mathbf{R}_i}{\mathrm{d}t} = \frac{\partial H}{\partial \mathbf{P}_i} \tag{2.47}$$

and

$$\frac{\mathrm{d}\mathbf{P}_i}{\mathrm{d}t} = -\frac{\partial H}{\partial \mathbf{R}_i} \tag{2.48}$$

In the Cartesian coordinates we use here, eq. (2.48) reduces to $\frac{\mathrm{d}\mathbf{R}_i}{\mathrm{d}t} = \frac{1}{M_i}\mathbf{P}_i$, yielding after insertion into eq. (2.47):

$$M_i \frac{\mathrm{d}^2\mathbf{R}_i}{\mathrm{d}t^2} = -\frac{\partial V(\mathbf{R}_1,\dots)}{\partial \mathbf{R}_i} = \mathbf{F}_i, \tag{2.49}$$

with the forces $\mathbf{F}_i = -\frac{\partial V(\mathbf{R}_1,\dots)}{\partial \mathbf{R}_i}$. This is the classical Newtonian equation of motion. Most MD codes for chemical applications use Cartesian coordinates and, hence, solve Newton's equation. In this thesis, we use the Gromacs code [48] to integrate eq. (2.49) numerically. Gromacs offers several integration algorithms, of which we opt for the leap-frog algorithm [49]. Leap-frog evaluates positions and velocities $V = \frac{\mathrm{d}\mathbf{R}}{\mathrm{d}t}$ at alternating moments in time. First one expands

$$\mathbf{V}_i\left(t + \frac{1}{2}\Delta t\right) \approx \mathbf{V}_i\left(t + \frac{1}{2}\Delta t\right) + \frac{1}{M_i}\mathbf{F}_i(t)\Delta t, \tag{2.50}$$

then

$$\mathbf{R}_i(t+\Delta t) \approx \mathbf{R}_i + \mathbf{V}_i\left(t+\frac{1}{2}\Delta t\right)\Delta t, \tag{2.51}$$

with the time step Δt, usually on the order of 1 fs. With initial conditions $\mathbf{R}_i(0) = \mathbf{R}_0$ and $\mathbf{V}_i\left(-\frac{\Delta t}{2}\right) = \mathbf{V}_0$ these iterative expressions define the time evolution of the system. Locally the expansion error is of $O(\Delta t^3)$ because quadratic terms cancel, so that globally the error is $O(\Delta t^2)$. Crucially, leap-frog conserves energy on average for small enough time steps, leading to stable and physically meaningful dynamics. The peculiar offset of $\Delta t/2$ between position and momentum evaluations avoids the addition of terms of different order in Δt, which is important for the numerical stability of the simulation.

2.1.6. Thermal and pressure equilibration

The canonical equations lead to energy conserving dynamics $E = T(\mathbf{P}) + V(\mathbf{R}) =$ const. Thus, naive molecular dynamics simulations sample a microcanonical ensemble in the sense of statistical mechanics. If N is the number of atoms, and V a volume to which the system is confined, we also speak of an NVE ensemble. However, normally the canonical, or NVT, ensemble, where only the expectation value $\langle E\rangle$ of the energy is fixed, corresponds best to experimental conditions that allow energy exchange with the environment. Then, the probability for the system to attain energy E should be $p(E) = e^{-\beta T}/Z$, with $\beta = 1/(k_B T)$, temperature T, and the partition function $Z = \int d^{3N}Rd^{3N}Pe^{-\beta E(\mathbf{R},\mathbf{P})}$. Canonical energy distribution has to be introduced artificially by suitably altering the dynamics. To this end, there are various ways. One way is to turn Newton's equation into a stochastic differential equation by addition of a random force term, leading to a Langevin equation. In this work, another approach is used. Nos and Hoover showed that there is a unique deterministic way to enforce a canonical ensemble through the addition of a dummy degree of freedom s. This algorithm is known as the Nose-Hoover thermostat [50, 51]. s is linked to the rest of the system in the form of a friction term $-s\mathbf{P}/M$, yielding altered equations of motion:

$$M_i\frac{\mathrm{d}^2\mathbf{R}_i}{\mathrm{d}t^2} = \mathbf{F}_i - s\frac{\mathrm{d}\mathbf{R}_i}{\mathrm{d}t}. \tag{2.52}$$

s obeys its own equation of motion:

$$\frac{\mathrm{d}s}{\mathrm{d}t} = \frac{1}{Q}(T - T_0). \tag{2.53}$$

Q is a parameter controlling how strongly the thermostat alters the dynamics of the system. T_0 is the desired temperature, while T is the estimated current temperature of the system. The equipartition theorem is employed to estimate $T = \frac{2}{3Nk_B}\sum_i \frac{P_i^2}{2M_i}$. Under experimental conditions often the volume of the system may vary, while the pressure P is fixed, leading to an NPT ensemble. In that case, with a second dummy degree of freedom, dynamics can be altered to achieve the correct average

pressure. This Parrinello-Rahman barostat works similarly as the Nose-Hoover thermostat [52, 50]. Some of the dynamical simulations presented in this thesis are in the NVT, some in the NPT ensemble. Usually, there is little difference for solids, but for liquids effects of pressure coupling are more pronounced.

2.2. Charge transport theory

This thesis aims to provide new tools for the study of charge and energy transport processes in molecular materials. There is a wide range of materials than can be considered molecular for the purpose of the methods to be introduced, but, specifically, we will think of bulk materials composed of organic molecules that are semiconductors. Organic semiconductors come as amorphous and crystalline materials. Since the latter tend to be particularly effective conductors, a special focus will be on molecular crystals. Organic semiconductors are of significant and growing industrial interest. They feature prominently in three kinds of devices: as organic field effect transistors (OFETs), as organic photovoltaic devices (OPVs), and as organic light emitting diodes (OLEDs). In the light of their usefulness, much theoretical and modeling research has been undertaken. Theory mostly contributes to development in two ways: through a more thorough understanding of the fundamental driving forces, allowing for educated molecular design, and as a tool for fast screening of potential materials in the huge space of chemically feasible molecules. Most of the commonly used models apply in one of two possible limiting cases in which charge or excitations are spatially either highly localized on individual molecules, or fully delocalized throughout the system. In the following, we will review the origin of both regimes and the fundamental ideas behind the methods dealing with them. As far as energy transport is concerned, in this thesis we confine ourselves to energy transport in the form of Frenkel excitons. A Frenkel exciton is a molecular excitation localized on a single molecule, that is, there is no charge transfer from one molecule to another. One can also think of it as an electron-hole pair bound on a single molecule. While the extend of the excitation itself is confined, excitations on different molecules are coupled, so that excitons can move around via the combined excitation and deexcitation of a pair of molecules. Exciton and charge movement then take on the same form and can often be studied on the same footing, albeit arising parameters have different origins. Therefore, many results about charge transport apply to exciton transport as well, and the following discussion is meant to apply to both of them. To simplify language, we may sometimes refer to only one, but mean both. In chapter 4 the Frenkel exciton model is explained in more detail.
One very important property of interest is how easily charges and excitons can move around. For charge transport the corresponding quantity of interest is the charge carrier mobility μ:

$$\mu = \frac{\langle v \rangle}{E}. \tag{2.54}$$

Here, the expectation value of the velocity $v = \frac{dx}{dt}$ is the drift velocity of the charge under the influence of the external electrical field of strength E. In principle, μ is a 2-rank tensor because in anisotropic materials a field applied in a certain direction can cause charges to move in another, but since μ is positive semidefinite, it can be diagonalized and decomposed into three independent one dimensional mobilities. The conductivity σ of a semiconductor is to μ alongside the charge carrier density ρ as $\sigma = \rho_c \mu$. Because the Fermi level lies above the valence band in semiconductors, charge carriers are either electron excited to the conduction band, or the holes in the valence band, which they leave behind, that behave as effective particles with positive charge. μ can depend on the field E, but is constant in the low field limit $E \longrightarrow \infty$. It is related to the diffusion constant D through a fluctuation-dissipation theorem, the Einstein-Smoluchowski relation:

$$\mu = \frac{D}{K_B T}. \tag{2.55}$$

The relation connects the field induced, directed movement with the random, thermally induced movement, where the average distance traveled in time t is

$$\sqrt{\langle (x(t) - x(0))^2 \rangle} \sim \sqrt{Dt}. \tag{2.56}$$

Obviously, because excitons posses no charge, electrical fields cannot cause them to move, and consequently no mobility μ can be defined. They do, however, diffuse through the material and their proneness to move is still quantifiable by the diffusion constant. For example, exciton diffusion is very important in OPVs because phonons are absorbed in the bulk, but charge separation takes place only at interfaces, which the excitons have to reach.

2.2.1. The Holstein model

In this section we explore the Holstein model[53] , a simple toy model for an organic crystal. While the model, introduced in 1959, simplifies much of the complex physics of molecular materials, it still offers a useful picture that highlights the essential forces shaping transport processes to large degree. The model is visualized in Fig. 3.3. We consider a one dimensional molecular crystal into which we place a single charge or exciton. The nuclear degrees of freedom of each molecule i are described by a single coordinate xi, and the molecular potential energy surface is expanded to second order, so that the nuclear potential energy becomes a parabola $E_{\text{nuc}} = \sum_i \frac{1}{2} M \omega x_i^2$, with the molecular vibrational frequency ω, and nu-clear effective mass M. For the wavefunction of the charge we assume only one state per site is necessary to describe it, with identical site energies, all put to zero, and couplings J to nearest neighbors. The corresponding Hamiltonian then takes on a simple tight-binding form $H_{TB} = J \sum_i (a_i^\dagger a_{i+1} + a_{i+1}^\dagger a_i)$, where the operator $a_i^\dagger$ creates a charge at site i, and its conjugate a_i destroys it. The ionization or excitation energy, as represented by the site energies, depends on the nuclear conformation x_i. To account for this, the change in energy is expanded to linear

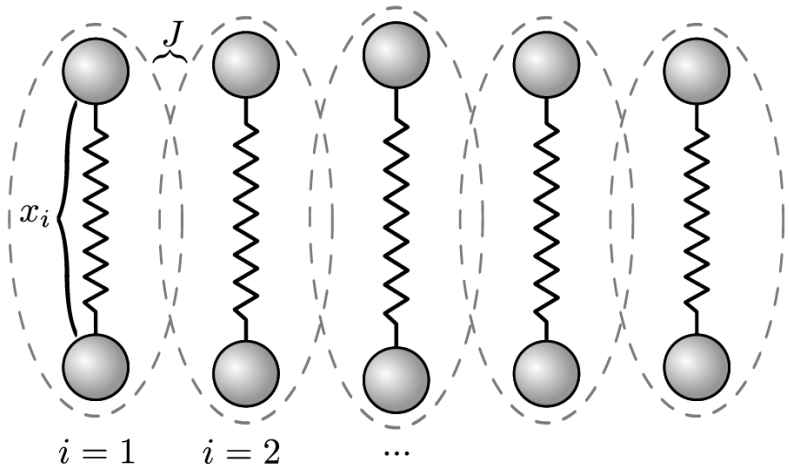

Figure 2.3.: The Holstein model for a one dimensional molecular crystal. Molecules are modeled by one nuclear degree of freedom xi, and one electronic state per site i, coupled to neighboring sites with coupling J.

order, yielding the electron-phonon interaction energy $Eint = \sum_i \alpha x_i a_i^\dagger a_i$, with coupling constant α and the site occupation $a_i^\dagger a_i$. α is related to the strength of the reaction of a molecule to the presence of a charge. Completing the square, we see for a single molecule $E_{\text{nuc}} + E_{\text{int}} = \frac{1}{2}Mx^2 + \alpha x = \frac{1}{2}M\left(x + \frac{\alpha}{M\omega^2}\right)^2 + \frac{1}{2}\frac{\alpha^2}{M\omega^2}$. Therefore, the presence of the charge causes a molecular reorientation, accompanied by an energy change

$$\lambda = \frac{1}{2}\frac{\alpha^2}{M\omega^2}. \tag{2.57}$$

λ is known as the internal reorganization energy of the molecule and has a very strong influence on the transport regime. Eventually, the full electronic Holstein Hamiltonian, as the sum of all terms, reads:

$$H = \sum_i (J(a_i^\dagger a_{i+1} + a_{i+1}^\dagger a_i) + \alpha x_i a_i^\dagger a_i) + \sum_i \frac{1}{2}M\omega^2 x_i^2. \tag{2.58}$$

Let $|i\rangle = a_i^\dagger|0\rangle$ be the state in which the charge is localized on a single site. The localized states form a basis in which to expand electronic wavefunctions:

$$|\Psi\rangle = \sum_i c_i|i\rangle, \tag{2.59}$$

with expansion coefficients ci. In case all nuclear coordinates agree $x_1 = x_2 = \ldots$ the Holstein model is identical to a simple, one dimensional tight-binding model. Then wavefunctions $c_j \infty e^{ikdj}$, with lattice spacing d and wavenumber k are electronic eigenstates, as is easy to verify by insertion. The energy spectrum for $x_1 = x_2 = \cdots = 0$ forms a band with dispersion relation

$$\begin{aligned} E(k) &= -2L\cos(kd) \\ &\approx -2J + Jd^2k^2 \text{ for small } k. \end{aligned} \tag{2.60}$$

The band is, however, not the ground state, but there are bound states with lower energy. Those states require $x_i \neq 0$, coupling the charge and the nuclei, and forming a bound pair of charge and molecular deformation, known as a polaron. Clearly, the presence of bound states with energies below the band can have a huge impact on charge mobility. When $E(x_1, \dots)$ is the minimal energy, then $\frac{\partial}{\partial x_i} E(x_1, \dots) = 0$ for all i. Applying this condition to the electronic eigenvalue problem establishes a connection between the wavefunction and the nuclear coordinates of the polaron:

$$x_i = \frac{\alpha}{M\omega^2}|c_i|^2 = \frac{2\lambda}{\alpha}|c_i|^2. \tag{2.61}$$

Hereupon it is possible to find the minimum in two limiting cases of either very large or small electronic coupling J between sites, relative to the electron-phonon coupling a. In the first case of large J, the wavefunction should still look much like a band solution, and hence be spread out over many sites. Therefore, this limit is known as the large polaron solution. Due to the large extension of the wavefunction, we can assume that i is a continuous index and expand $c_{i+1} = c_i + \frac{\partial c_i}{\partial i} + \frac{1}{2}\frac{\partial^2 c_i}{\partial i^2}$. Substitution into the eigenvalue equation yields the minimum energy

$$E_{lp} = -2J - \frac{1}{48}\frac{1}{J}\left(\frac{\alpha^2}{M\omega^2}\right)^2 = -2J - \frac{1}{48}\frac{\lambda^2}{J}. \tag{2.62}$$

Compared with the minimum energy $E_b = -2J$ of the band, this corresponds to a polaron binding energy of $E_{lp} - E_b = -\frac{1}{48}\frac{\lambda^2}{J}$. Assuming that in the large polaron limit λ is at most on the order of J, and a typical large value of $J \approx 100$meV, the binding energy is on the order of 1meV. At ambient temperature T = 300K the typical thermal energy is about $k_B T = 26$meV, which is much larger. Thus, as the band is easily thermally accessible, the Holstein model suggests transport behavior in the large polaron limit is largely determined by the band structure of the crystal. Next, we tend to the other limit where J is small. At $J = 0$ a possible eigenstate is given by $c_i = \delta i i_0$ for some i_0. From this state perturbation theory in J yields the corrected solution:

$$c_i = \delta_{ii_0} + \frac{JM\omega^2}{\alpha^2}(\delta_{i(i_0+1)} + \delta_{i(i_0-1)}) = \delta_{ii_0} + \frac{J}{2\lambda}(\delta_{i(i_0+1)} + \delta_{i(i_0-1)}) \tag{2.63}$$

Because λ is much bigger than J, the wavefunction is almost completely localized on one side. Therefore, this solution is known as the small polaron solution. The energy of the small polaron is given by

$$E_{sp} = -\frac{\alpha^2}{2M\omega^2} = -\lambda. \tag{2.64}$$

The physical picture behind this is the charge localizing on one molecule and by reorganization it creates a potential well of depth λ. The magnitude of the binding energy $E_{sp} - E_b = -\lambda + 2J$ is much larger than the thermal energy at $T = 300$K. Hence, the small polaron is stable, and in order to move an energy barrier λ has to

be overcome by thermal activation. That is a typical scenario for transition state theory, which is, indeed, commonly used in this limit. In the following section, we will elaborate more on how to deal with the two extreme cases predicted by the Holstein model. Part of this thesis is concerned with the intermediate regime in between the extremes. The Holstein model ignores some effects that become important exactly there, such as the fluctuation of the couplings J here assumed to be constant. The extended Holstein- Peierls model [54], which includes coupling fluctuations, is still used for practical, predictive applications [55].

2.2.2. The hopping regime

In this section, we explore the hopping limit of charge and energy transport. As previously established, if the molecular reorganization energy is much larger than the intermolecular electronic coupling J, the charge or exciton becomes localized on a single site, and in order to move to a neighbor it has to overcome an energy barrier. The barrier is higher than the typical thermal energy in the molecule, so to reach the top of the barrier is a random event, driven by molecular vibration,+ that happens only occasionally. When the barrier is overcome through thermal activation, transport happens swiftly before the charge becomes trapped again on the next site. Essentially, the charge moves around by random hopping events, performing a random walk throughout the material bulk. Because the charge usually stays long enough on each site for it to relax and thermally equilibrate to a Boltzmann energy distribution, the charge's random walk is a Markov process. If $p_i(t)$ is the probability to find the charge on site i at time t, the time evolution of the probabilities, and hence the movement of the charge, obeys the master equation:

$$\frac{\mathrm{d}p_i(t)}{\mathrm{d}t} = \sum_j (p_j(t)k_{ji} - p_i(t)k_{ij}), \tag{2.65}$$

where k_{ij} is the rate of transition from site i to j, i.e. the expected number of hops per time interval. Put into words, the change in probability to be on site i is composed of the chance to be on another site and move to i, reduced by the chance to already be on i but to move away to some other site. When an external field E is applied, the charge is more likely to hop into the direction of field, resulting in a drift. The transition rates k_{ij} determine the drift velocity $\langle v \rangle = \sum_{i,j} d_{ij}k_{ij}$, with the distances d_{ij} between sites. The drift may be anisotropic, but we suppress directional indices here for simplicity. The field induced drift is associated with the mobility

$$\mu = \frac{1}{E}\sum_{i,j} d_{ij}k_{ij}. \tag{2.66}$$

One of the fundamental problems of charge and energy transport in the hopping regime has now become to determine the transition rates k_{ij}. Under various assumptions about the nature and conditions of the intersite transfer, different expressions can be derived [56, 57]. Classical transition state theory assumes that transfer only

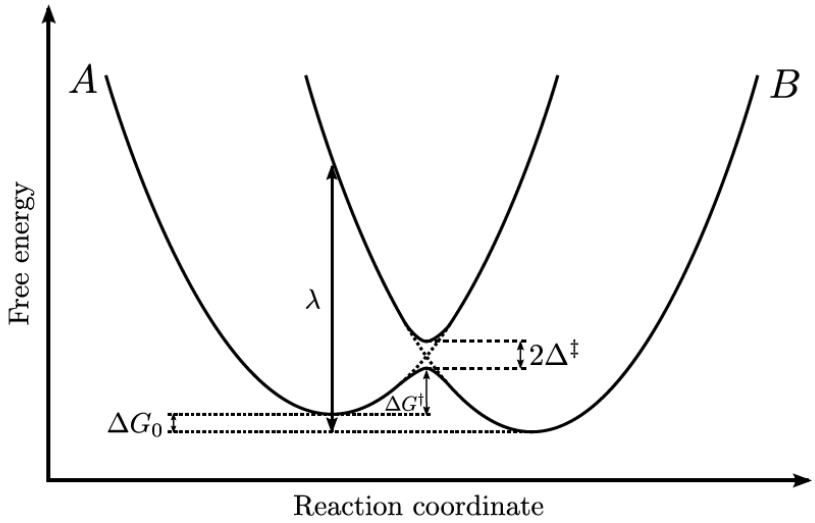

Figure 2.4.: Visualization of free energy surface of the transfer process and the important quantities that appear in the rate equation.

happens in a transition state, which is a well founded approximation if λ is much larger than J. Thus, transition state theory can be applied with the charge localized and relaxed on one site as initial state A, and localized and relaxed on a neighboring site as final state B. After expansion of the initial and final potential energy surfaces to quadratic order the transition state rate equation can be derived as [58]:

$$k_{AB} = \nu_{\text{eff}} \mathcal{K}_{el} e^{-\beta \Delta G^{\dagger}}. \tag{2.67}$$

Here, ν_{eff} is the frequency of the effective mode that drives the transition, i.e. it is related to the curvature of the potential energy surface expanded in the reaction coordinate. A reaction coordinate commonly used for electron transfer processes [59, 60] is the energy gap $\Delta E(\mathbf{R}) = E_B(\mathbf{R}) - E_A(\mathbf{R})$ between the energy of the initial and final state at the nuclear conformation $\mathbf{R}$. $\mathcal{K}_{el}$ is the electronic transmission coefficient, the probability of a transfer to actually happen when the transition state is reached. Assuming a single crossing of energies E_A and EB, the transfer probability may be derived from the Landau-Zener model[61, 62], which exactly calculates the transition probability P_{LZ} in a two state system where the energy gap varies linearly in time $\Delta E \sim t$ from $-\infty$ to $+\infty$. Then[61, 62] ,

$$\mathcal{K}_{el} = \frac{2P_{\text{LZ}}}{1 + P_{\text{LZ}}}, \tag{2.68}$$

with

$$\begin{aligned} P_{\text{LZ}} &= 1 - e^{-2\pi\Gamma}, \\ 2\pi\Gamma &= \frac{\pi^{\frac{3}{2}} \langle |H_{AB}|^2 \rangle_{\text{TS}}}{V_{\text{eff}} \sqrt{\lambda k_B T}}, \end{aligned} \tag{2.69}$$

where $H_{AB} = \langle A|H|B\rangle$ is the electronic coupling of initial and final state. H_{AB} is the same as J in the Holstein model, but since the coupling may actually fluctuate, the

expectation value at the transition state must be taken. The final quantity in the transition state rate expression is the activation free energy $\delta G^{\dagger}$, the height of the reaction barrier. For charge and exciton transfer between small molecules the free energy is mostly identical to the energy because entropic contributions are small. $\delta G^{\dagger}$ can be decomposed into two contributions:

$$\delta G^{\dagger} = \delta G^{\ddagger} - \delta^{\ddagger}. \tag{2.70}$$

$\delta^{\ddagger}$ is the diabatic activation energy, the energy of the initial state at the transition geometry. It is determined by the reorganization energy λ and the driving force ΔG_0, the equilibrium energy difference between final and initial state [63]:

$$\Delta G^{\ddagger} = \frac{(\lambda + \Delta G_0)^2}{4\lambda}. \tag{2.71}$$

In crystals all sites are equivalent, so that DG0 is entirely brought about by the external field: $\Delta G_0 = \pm E d_{AB}$ for charges or $\Delta G_0 = 0$ for excitons. In amorphous materials different environments, including polarizability, need to be taken into account. $\Delta^{\ddagger}$ is the lowering of the barrier due to the energy splitting caused by the interaction of initial and final state [63]:

$$\Delta^{\ddagger} = \left\langle |H_{AB}|^2 \right\rangle_{\mathrm{TS}}^{\frac{1}{2}} - \frac{1}{\lambda} \left\langle |H_{AB}|^2 \right\rangle_{A}. \tag{2.72}$$

The rate expression can be further simplified in the nonadiabatic limit $\Gamma \ll 1$ that assumes very fast transfer at the transition state. Under this assumption $e^{-2\pi\Gamma}$ can be expanded to first order, such that $1 - e{-2\pi\Gamma} \approx -2\pi\Gamma$, and the rate simplifies to

$$k_{AB} = \frac{2\pi}{\sqrt{4\pi\lambda k_B T}} \left\langle |H_{AB}|^2 \right\rangle_{\mathrm{TS}} e^{-\beta \Delta G_{\ddagger}}. \tag{2.73}$$

Eq. (2.73) is the famous Marcus rate expressions that has found ample use in charge transport simulations[64, 65, 66, 67]. It has also been applied to exciton transport [68], although the alternative Forster rate [69] expression is far more popular for energy transport [70].

2.2.3. The band regime

Many high-performance organic semiconductors form crystals. As such they do not differ fundamentally from inorganic semiconductors, except for the usually weaker bond between lattice sites, and the larger electron-phonon coupling due to intramolecular relaxation. As already indicated by the Holstein model, if relaxation is not too strong, the crystalline band structure may prevail. Therefore, the band regime is the second commonly discussed transport regime, on the opposite end from hopping. Note that while band structure is most of the time associated with charge transport, the translational symmetry that leads to electronic bands can also cause excitonic bands to form. The methods for the study of the band

transport regime are largely the tools solid-state physics has developed for inorganic semiconductors. The crystal geometry is invariant under translations $\mathbf{R} \rightarrow \mathbf{R} + \mathbf{a}$, where a is a multiple of the crystal lattice vectors. Because for that reason the Hamiltonian commutes with translation operators, there is a joint basis of eigenvectors, or in other words, electronic wavefunctions take the form of Bloch waves[71] :

$$\Psi(\mathbf{r}) = e^{i\mathbf{kr}} u_{\mathbf{k}}(\mathbf{r}), \tag{2.74}$$

where $u_{\mathbf{k}}(\mathbf{r}+\mathbf{a}) = u_{\mathbf{k}}(\mathbf{r})$ for a multiple a of the lattice vectors, and the wave number $\mathbf{k}$ is the momentum of state Ψ. Bloch states are spatially delocalized across the entire crystal, and hence the exact opposite of the localized states of hopping transport. The electronic spectrum then consists of a discrete set $E_\alpha, \alpha = 1, 2, \ldots$ of continuous energy bands $E_\alpha(\mathbf{k})$. In semiconductors the Fermi levels falls in between bands, so that all bands are either fully occupied or vacated. Some charges are thermally excited from the filled valence band to the empty conduction band, resulting in only partially filled bands for electrons and holes. Excitonic bands are also normally only occupied by a few quasi-particles. Therefore, charge and energy carries can usually be modeled as quasi free particles. For a free particle the relation between its momentum k and kinetic energy T is $E(k) = \frac{k^2}{2m}$, with the particle mass m. Then, one of the classical canonical equations reads $\frac{\mathrm{d}r}{\mathrm{d}t} = \frac{\partial E(k)}{\partial k} = \frac{k}{m}$, relating momentum and velocity. The semiclassical approach to particle dynamics in semiconductors is to assume that the classical canonical equations are valid, but

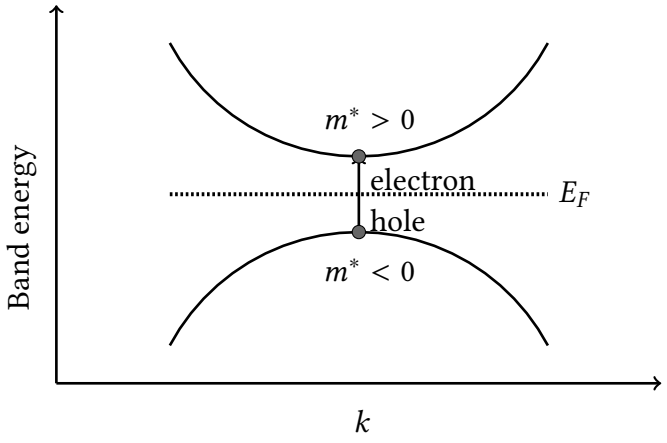

Figure 2.5.: A charge is excited from the the valence to the conduction band, leaving behind a hole. The Fermi level E_F falls in between the two bands. The curvature of the bands is related to their effective mass m^* that can be negative.

the free particle dispersion relation is replaced with the band structure dispersion $E_\alpha(k)$ [72]. The velocity $\frac{\mathrm{d}r}{\mathrm{d}t}$ can in this context be interpreted as the group velocity of the wavefunction. Near the band minima and maxima, where $\frac{\partial E_\alpha(k)}{\partial k} = 0, E_\alpha(k)$ can be expanded $E_\alpha(k) \approx E_0 + \frac{1}{2}\frac{\partial^2 E_\alpha(k)}{\partial k^2} k^2 = E_0 + \frac{k^2}{2m^*}$, resulting in same form as for

the free particle, but with an effective mass m^* given by the band structure:

$$\frac{1}{m^*} = \frac{\partial^2 E_\alpha(k)}{\partial k^2}. \tag{2.75}$$

The effective mass m^* can differ extremely from the real mass of the charge carriers. In fact, m^* can even be negative and is typically anisotropic, although directional indices have been suppressed here for simplicity. Besides the band structure entering into m^*, the interaction of carriers and phonons needs to be accounted for, too. However, in the band limit, we may assume the interaction to take the form of occasional, random scattering events. Let $f(k, r, t)$ be the distribution function of momenta and positions at time t. In thermal equilibrium the time and position independent distribution $f_0(k)$ is given by the Fermi-Dirac or Bose-Einstein distribution:

$$f_0(k, r) = \frac{1}{1 \pm e^{(E_\alpha(k)-\mu)/(k_B T)}}, \tag{2.76}$$

where μ is not the mobility, but the chemical potential, and the sign is positive for fermions like electrons and holes and negative for bosons like singlet and triplet excitons. The time derivative of f excluding interaction with phonons is $\frac{\mathrm{d}f(k,r,t)}{\mathrm{d}t} = (\partial_t + \frac{\mathrm{d}r}{\mathrm{d}t}\partial_r + \frac{\mathrm{d}k}{\mathrm{d}t}\partial_k) f(k, r, t)$ by the chain rule. The derivatives of r and k can be calculated according to the semi-classical equations of motion from above: $\frac{\mathrm{d}r}{\mathrm{d}t} = \frac{k}{m^*}$, and $\frac{\mathrm{d}k}{\mathrm{d}t} = \pm E$, in an external electrical field E. For excitons we set $E = 0$ because they have no charge, and in the following we pick the minus sign of the electron case for simplicity. Hence follows the Boltzmann equation for transport in bands[72] :

$$\left(\partial_t + \frac{k}{m^*}\partial_r - E\partial_k\right) f(k, r, t) = \left(\frac{\partial f}{\partial t}\right)_{\text{coll}} \tag{2.77}$$

The term $\left(\frac{\partial f}{\partial t}\right)_{\text{coll}}$ is called the collision integral and describes scattering on phonons. At only small deviations from the equilibrium distribution the relaxation time approximation is valid. It assumes that the extend of scattering is proportional to the distance from equilibrium:

$$\left(\frac{\partial f}{\partial t}\right)_{\text{coll}} = -\frac{f(k, r, t) - f_0(k)}{\tau(k)}. \tag{2.78}$$

Here, $\tau(k)$ is the relaxation time, which determines how fast the system relaxes back to equilibrium after a perturbation. τ is available from ab initio electronic structure calculations. One condition for the Boltzmann equation based approach to be valid is that τ is significantly larger than the typical transfer time from one site to the other, since otherwise the random scattering assumption breaks down. In the relaxation time formalism the Boltzmann equation is solvable in closed form, and one obtains for the conductivity σ [72]:

$$\sigma = -\frac{1}{3\pi^2} \int dk \frac{\partial f_0(k)}{\partial k} \frac{k^3}{m^*} \tau(k). \tag{2.79}$$

At small temperatures $\frac{\partial f_0(k)}{\partial k}$ is strongly peaked at the Fermi level: $\frac{\partial f_0(k)}{\partial k} \sim -\delta(k - k_F)$, allowing to approximate further $\sigma \approx \frac{\rho\tau}{m^*}$, with the carrier density ρ and the relaxation time τ at the Fermi level. Then, we directly find the mobility $\mu = \sigma/\rho$:

$$\mu = \frac{\tau}{m^*}. \tag{2.80}$$

This approximate expression for the mobility is known as the Drude form. It tells us that in the band limit the mobility is determined by the band structure and electron-phonon scattering. The former enters through the effective mass m^*, related to the curvature of the band, and the later in the from of the scattering time τ. The mobility increases with τ, that is, less scattering leads to higher mobilities. It decreases with $m*$, which means that flat bands lead to lower mobilities.

2.3. Nonadiabatic molecular dynamics

2.3.1. Quantum Mechanics/Molecular Mechanics Scheme

The molecular complex is decomposed into a quantum chemical (QM) region, where the excess charge carrier propagates and the remainder of the complex is treated with molecular mechanics (MM). The energy of the QM region containing no excess charge is approximated with MM, and is included in the total MM energy $E^{\text{tot}}_{\text{MM}}$. The total energy of a molecule in QM zone with a hole can be approximated as

$$E^+ \approx E^{\text{tot}}_{\text{MM}} - \langle\Psi|H[\rho_0]|\Psi\rangle + \Delta E_{\text{QM/MM}}\,, \tag{2.81}$$

where $|\Psi\rangle$ is the hole wave function, $H[\rho_0]$ is the Kohn–Sham Hamiltonian of the neutral system, and $\Delta E_{\text{QM/MM}}$ is the interaction energy between the QM and MM subsystems. Further details may be referred to in Ref. [28].

The molecules in OSCs interact with non-covalent forces, which allows for a concenptually simple coarse-graining of the electronic structure of the QM zone: [28]

The wave function of the hole is expressed as a linear combination of (orthogonalized) molecular orbitals, $|\phi_m\rangle$, of fragment molecules A,

$$\Psi = \sum_A \sum_{m\in A} a_m|\phi_m\rangle\,, \tag{2.82}$$

where ϕ_m are the molecular orbitals of the individual fragments (molecules).

2.3.1.1. Quantum Chemical Calculations and the Fragment Orbital Scheme.

Since low-energy charge transfer typically occurs in a narrow energy window around the Fermi level, any strongly bound electronic states are affected negligibly, and it is sufficient to consider frontier orbitals of the fragments. In the following, the set of ϕ_m will be restricted to the set of such frontier orbitals.

Inserting Eq.2.82 into Eq.2.81, we obtain the total energy expressed in a fragment orbital (FO) basis,

$$E^{+} = E^{0} - \sum_{A,B} \sum_{m\in A} \sum_{n\in B} a_m^* a_n \langle \phi_m | H[\rho_0] | \phi_n \rangle + \Delta E_{\mathrm{QM/MM}} \,, \tag{2.83}$$

where E^0 is the energy of the charge-neutral system and $H^0_{mn} = \langle \phi_m | H[\rho_0] | \phi_n \rangle$ is the Hamilton matrix elements. This approach performs a quantum propagation of an excess charge carrier, thus it differs from traditional MFE/FSSH simulations that typically propagate all the electronic degrees of freedom.

The QM/MM interaction term is given within the DFTB method as

$$\Delta E_{\mathrm{QM/MM}} = \sum_{A} \sum_{m\in A} |a_m|^2 \sum_{K} \sum_{\alpha\in A} \frac{\Delta q_\alpha^m q_K^0}{|R_\alpha - R_K|} \,, \tag{2.84}$$

where q_K^0 is the partial charge on atom K of the neutral environment and Δq_α^m is the change of Mulliken charge on atom α due to a hole located at orbital m.

The Hamilton matrix elements, $H^0_{mn} = \langle \phi_m | H[\rho_0] | \phi_n \rangle$, are computed using the non-self-consistent variant of the density functional tight-binding method (DFTB) as discussed in Ref. [28]. DFTB is derived from DFT by a Taylor expansion of the total energy around a well-defined reference density, and is found to be two to three orders of magnitude faster than DFT-GGA functionals with mid-sized basis sets [73, 74]. DFTB was shown to provide electronic couplings in a good agreement with other DFT approaches, and the application of an uniform scaling factor allows the accuracy comparable to high-level *ab initio* methods [75, 76]. In the present work, the electronic couplings obtained with the DFTB method were scaled by a factor of 1.54 and 1.795 for hole and electron transport to reach the accuracy of the second-order couple cluster (CC2) calculations [76].

2.3.2. Mean-Field Ehrenfest

By inserting Eq.2.82 into time-dependent electronic Schrödinger equation, we obtained the propagation equation for the expansion coefficients

$$\dot{a}_m = -i \sum_{n} H_{mn} a_n - \sum_{n} a_n \langle \phi_m | \dot{\phi}_n \rangle \,, \tag{2.85}$$

where H_{mn} are the DFTB Hamiltonian matrix elements including the QM/MM interactions. The last term is negligible small and thus omitted in the integration of the TDSE. Note a_m can be approximated as the expansion coefficients of the electronic wave function in the diabatic basis set $\{\phi_m\}$.

The classical equation of motion for nuclei is given by

$$m_K \ddot{R}_k = -\frac{\partial E^{\mathrm{tot}}_{\mathrm{MM}}}{\partial R_k} + \sum_{mn} a_m^* a_n \frac{\partial H^0_{mn}}{\partial R_k} - \frac{\partial \Delta E^{\mathrm{QM/MM}}}{\partial R_k} \,, \tag{2.86}$$

where k denotes x, y and z of atom K.

2.3.3. Fewest Switches Surface Hopping

In the FSSH method [77], the electronic wave function is expressed as a linear combination of adiabatic basis functions $\{|\psi_i\rangle\}$

$$\Psi = \sum C_i^{\mathrm{ad}} |\psi_i\rangle \ , \tag{2.87}$$

where C_i^{ad} are the expansion coefficients of the electronic wave function in the adiabatic representation. Inserting Eq.2.87 into the time-dependent Schrödinger equation and projecting onto the adiabatic electronic basis states, we obtain

$$i\hbar \frac{dC_j^{\mathrm{ad}}}{dt} = C_j^{\mathrm{ad}} H_j^{\mathrm{ad}} - i\hbar \sum_k C_k^{\mathrm{ad}} \mathcal{D}_{jk} \ , \tag{2.88}$$

where H_j^{ad} is the potential energy (PE) of adiabatic state j. The diagonalization of the matrix $\boldsymbol{H}$ yields the adiabatic PEs

$$\boldsymbol{H^{ad}} = \boldsymbol{U H^0 U^\dagger} \ , \tag{2.89}$$

where $\boldsymbol{U}$ is the diabatic-to-adiabatic (AtD) transformation matrix.

According to the chain rule, the time derivative coupling between the adiabatic electronic states j and k, $\mathcal{D}_{jk}$, can be written as

$$\mathcal{D}_{jk} = \left\langle \psi_j \middle| \frac{d}{dt} \middle| \psi_k \right\rangle = \dot{\boldsymbol{R}} \boldsymbol{d}_{jk} \ , \tag{2.90}$$

where $\boldsymbol{d}_{jk}$ denotes the nonadiabatic coupling vector (NCV). In the present study, the NCV is approximately given by [78]

$$\boldsymbol{d}_{jk} \approx \frac{\left[\boldsymbol{U}^\dagger \nabla \boldsymbol{H^0 U}\right]_{jk}}{H_k^{ad} - H_j^{ad}} \ . \tag{2.91}$$

For the derivation of NCV, the reader is referred to Ref. [78].

Classical trajectories are propagated on a single electronic state according to Newton's equation of motion

$$\begin{aligned} m_K \ddot{R}_k &= -\frac{\partial E_{\mathrm{MM}}^{\mathrm{tot}}}{\partial R_k} + \frac{\partial H_j^{\mathrm{ad}}}{\partial R_k} - \frac{\partial \Delta E^{\mathrm{QM/MM}}}{\partial R_k} \\ &= -\frac{\partial E_{\mathrm{MM}}^{\mathrm{tot}}}{\partial R_k} + \sum_{mn} U_{am} U_{an} \frac{\partial H_{mn}^0}{\partial R_k} - \frac{\partial \Delta E^{\mathrm{QM/MM}}}{\partial R_k} \ , \end{aligned} \tag{2.92}$$

where H_a^{ad} denotes the adiabatic energy of the current state j. Note that the charge relaxation in FSSH and MFE simulations is governed by the quantum forces, $\sum_{mn} U_{am} U_{an} \frac{\partial H_{mn}^0}{\partial R_k}$ and $\sum_{mn} a_m^* a_n \frac{\partial H_{mn}^0}{\partial R_k}$ in Eq. 2.86, respectively. This treatment is referred to 'explicit relaxation (ER)' in the following sections.

The hopping probability from the current state j to another state k is defined as

$$P_{\mathrm{FSSH}}^{j\to k} = \max\left\{0, 2\mathcal{D}_{jk}\frac{\mathrm{Re}\left(C_k^{\mathrm{ad}*}C_j^{\mathrm{ad}}\right)}{|C_j^{\mathrm{ad}}|^2}\Delta t\right\} . \tag{2.93}$$

A uniform random number ξ between 0 and 1 is generated and a switch from the current state j to another state k takes place, if

$$\sum_{i=1}^{k-1} P_{\mathrm{FSSH}}^{j\to i} < \xi \leq \sum_{i=1}^{k} P_{\mathrm{FSSH}}^{j\to i} . \tag{2.94}$$

To ensure the conservation of total energy for each trajectory, the nuclear momenta are adjusted along the NCV, $\boldsymbol{P}' = \boldsymbol{P} + \alpha \boldsymbol{d}_{jk}$, where the factor α is determined by

$$\tfrac{1}{2}\left|\boldsymbol{P} + \alpha\boldsymbol{d}_{jk}\right|^2 + H_k^{\mathrm{ad}} = \tfrac{1}{2}\left|\boldsymbol{P}\right|^2 + H_j^{\mathrm{ad}} . \tag{2.95}$$

If the adjustment of momentum is not sufficient to compensate the change of the PE by the hopping (which is a so-called 'energy-forbidden hop' or 'frustrated hop'), the trajectory continues running in the original electronic state j, and the momenta along the NCV are reversed.

Due to conceptual simplicity and well-defined algorithm of the FSSH method, this method nowadays has been widely used to gain insights into many nonadiabatic physical and chemical processes. However, it cannot be derived rigorously from quantum mechanics and suffers a few inherent problems. The problems and their corrections used in the present study are discussed in Supporting Information.

2.3.3.1. Approximation I: Boltzmann correction (BC)

Instead of adjusting the velocity to obey detailed balance condition, one can rescale the hopping probability with the Boltzmann factor g_{BC},

$$P_{\mathrm{FSSH}}^{j\to k} \leftrightarrow P_{\mathrm{FSSH}}^{j\to k} g_{BC} , \tag{2.96}$$

where

$$g_{BC} = \begin{cases} \exp\left(-\frac{H_k^{\mathrm{ad}} - H_j^{\mathrm{ad}}}{k_{\mathrm{B}}T}\right), & H_k^{\mathrm{ad}} > H_j^{\mathrm{ad}} (\text{upward hops}) \\ 1, & H_k^{\mathrm{ad}} \leq H_j^{\mathrm{ad}} (\text{downward hops}) . \end{cases} \tag{2.97}$$

The velocity remains unchanged during the hopping event. The BC approximation avoids the time-consuming computation of the muti-component NCV and thus is much more efficient.

2.3.3.2. Approximation II: Implicit charge relaxation (IR)

It is found that the charge relaxation in OSCs is dominated by the high-frequency modes ($\tilde{2}0$ fs) [79, 80], which is, in most cases, faster than charge transfer. On the basis of this speculation, one can assume the charge relaxation is instantaneous and neglect the quantum force in Eq. 2.92, leading to

$$m_K \ddot{R}_k \approx -\frac{\partial E^{\text{tot}}_{\text{MM}}}{\partial R_k} \ . \tag{2.98}$$

This is reminiscent of the classical path approximation (CPA) used in the nonadiabatic dynamics simulations for nanosystems [81, 82]. However, the instantaneous charge relaxation (IR) approximation differs from CPA in that the change of charge population can affect the nuclear dynamics through the classical energy, $E^{\text{tot}}_{\text{MM}}$ in Eq. 2.98, which depends on the nuclear charges.

To consider the effect of charge relaxation on electronic system, the on-site energy, H_{nn} is reduced by a precalculated parameter (usually taken as reorganization energyλ_n) weighted by charge occupation ΔQ_n on site n[83],

$$H^{'}_{nn} = H_{nn} - \lambda_n \Delta Q_n \ . \tag{2.99}$$

Inserting into time-dependent electronic Schrödinger equation Eq. 2.100, we obtain

$$\dot{a}_m = -i \sum_n (H_{mn} - \sum_n \lambda_n \Delta Q_n \delta_{mn}) a_n \ , \tag{2.100}$$

The charge occupation ΔQ_n can be evaluated either by $|a_n|^2$ (henceforth, referred to wave function population) or by $|\boldsymbol{U}_{jn}|^2$ (referred to surface population), where j denotes the current adiabatic surface. We find that the surface population used in IR approximation in the FSSH simulations strongly overestimates the charge mobilities of p-MSB and rubrene (see Fig. SI1), in comparison with the FSSH-ER mobilities. However, the FSSH-IR using wave function population reproduces mobilities well. Therefore, the wave function population approach is employed in the following FSSH simulations with IR approximation.

The IR approximation avoids the evaluation of the quantum force $\frac{\partial H^0_{mn}}{\partial R_k}$ and thus reduces computational cost.More importantly, it allows to remedy the deficiency of DFTB forces by using an accurate reorganization energy as an input parameter for charge relaxation. In the followings, we will first examine the performance of BC and IR in the FSSH simulations (FSSH-BC and FSSH-IR), respectively, in comparison with FSSH simulation with explicit charge relaxation (FSSH-ER), for CT in one-dimensional anthracene chain. Second, the accuracy of the FSSH with the combination of IR and BC approximations (FSSH-IR-BC) will be evaluated in comparison with the FSSH-ER simulations as well as experimental references for CT in ten representative OSCs.

3. Efficient Surface Hopping approach for modeling charge transport in organic semiconductors

Reprinted in parts with permission from
Roosta, S., Ghalami, F., Elstner, M. and Xie, W.
Efficient surface hopping approach for modeling charge transport in organic semiconductors. Journal of Chemical Theory and Computation, 18(3), 1264-1274, (2022). DOI: 10.1149/1945-7111/ad0264

3.1. Introduction

Organic semiconductors (OSCs) have been gained large-area applications in the electronic and optoelectronic devices, such as organic field effect transistors (OFETs), organic photovoltaics (OPV) devices and organic light emitting diodes (OLEDs). Due to the extraordinary properties of low cost and flexibility, OSCs have become promising materials complementing applications of traditional inorganic semiconductors.

Charge carrier mobility is key quantity to measure the performance of OSC devices. While the development of sample and device fabrication techniques has allowed to synthesize organic crystals with mobilities of over 10 $cm^2\ V^{-1}\ s^{-1}$ at room temperature [84], these are still not comparable to that of inorganic semiconductors. In organic solids, molecules are held together by van der Waals interactions, in contrast to the covalent bonding in inorganic semiconductors. This particular characteristics of OSCs is a 'double-edged sword'. It opens the door for the application of OSCs in flexible displays and lighting devices. On the other hand, the weak molecular interactions lead to large thermal fluctuations and comparably smaller electronic couplings, which suppress the charge transfer in OSCs.

Theoretically, several models for the description of charge transport processes in OSCs have been proposed. The band transport model, which is based on the semiclassical Boltzmann theory, considers electrons as Bloch waves and the scattering to the lattice vibrations as a perturbation. The band theory successfully reproduces the charge mobility in inorganic semiconductors; however, it breaks down in OSCs where the mean free path of the charge carrier is on the order of magnitude of the lattice spacing[85, 86, 87]. Another widely used model to compute charge mobility is charge hopping theory, in which a charge carrier is completely localized on a single molecule and hops between nearest-neighbor by thermal activation. While this model has been successfully used in the evaluation of charge mobility in disordered and semi-disordered organic materials [88, 89, 90, 91]. this model is unable to describe charge transport in high-mobility organic crystals, where the electronic coupling is large such that the activation barrier vanishes effectively.

To go beyond the limitations of these models, novel methods based on explicit propagation of the charge carrier have been proposed. Recently, mean-field Ehrenfest (MFE) and surface hopping (SH) methods, which are widely used in nonadiabatic molecular dynamics simulations for photoinduced reactions, have been extended to be applied to model charge and exciton transport in OSCs [92, 93, 94]. In these approaches, nuclear degrees of freedom follows classical trajectories and the electronic wave function is propagated with the time-dependent Schrödinger equation. In the MFE approach, classical trajectories are propagated on a mean PE surface that is averaged over all electronic states and weighted by corresponding state populations. In the SH approach, an stochastic algorithm, based on the comparison of computed hopping probability and a random number, is employed to determine the hopping between PE surfaces. Perhaps the most popularly used formulations of the SH method is Tully's fewest switches surface hopping (FSSH) method[77],

which is designed to minimize the number of the switching events occurring between different electronic states. The hopping probability in the FSSH algorithm is proportional to the flux of state population. The deficiencies and their corrections of the MFE and FSSH methods have been intensively discussed in the literature [93, 95, 96, 97, 98, 99, 100]. The aim of the present study is the systematical exploration of the performance of two approximations – Boltzmann correction and implicit charge relaxation – in the FSSH simulations for charge transport (CT) in OSCs.

In the standard FSSH method, the nuclear velocity is adjusted along the direction of nonadiabatic coupling vector (NACV) to conserve the total energy during surface hopping. NACV is a multicomponent vector with the dimensionality of number of nuclear degrees of freedoms, The numerical evaluation of NACV needs a large number of electronic structure calculations, which is not feasible for large systems. In the Boltzmann correction (BC), the velocity rescaling is replaced by the scaling of the hopping probability with the Boltzmann factor[81]. Therefore, the evaluation of NACV is not required, which provide an addition computational advantage.

In the implicit charge relaxation (IR), the quantum feedback from the change of quantum states to the dynamics of nuclear motion is neglected and the on-site energy is reduced by a precalculated parameter (usually taken to be reorganization energy) weighted by charge population. The computation of quantum force from charge relaxation is not needed, which makes FSSH simulations more efficient for large systems. More importantly, this approximation allows to examine the performance of the different reorganization energies on charge transport in OSCs, which may help to answer the controversy over the computation of the reorganization energy. In 2004, Bredas and co-workers [79, 80] computed the reorganization energies of aromatic hydrocarbons using the parameters obtained by the fitting to the experimental photoelectron spectra. They found the reorganization energies are in good agreements with the reorganization energies computed by B3LYP functional. However, a recent computational study [101] shows the ωB97XD functional gives the least error among various tested functionals, in comparison with the high-level *ab initio* methods. This seemingly conflicting findings will be discussed in the present work.

3.2. System preparation and computational method

The supercells for each OS were constructed based on the experimental crystal structures, containing the following number of molecules along the crystal axes as well as the number of molecules in QM zone: $42 \times 84 \times 2$ (76) for PEN, $4 \times 85 \times 4$ (80) for RUB, $105 \times 5 \times 3$ (105) for TIPS-TAP, $90 \times 6 \times 2$ (80) for DATT, $3 \times 50 \times 3$ (32) for ANT, $\times \times$ () for NAP, $30 \times 15 \times 3$ (26) for TIPS-PEN, $6 \times 25 \times 4$ (20) for p-MSB, $4 \times 6 \times 15$ (12) for PER. The GROMACS 5.0.4 package[102, 103] was used to build the supercells and to perform classical MD simulations. The force field parameters were derived from the general AMBER force field (GAFF)[104, 105], where the atomic charges were generated from restrained fitting on the electrostatic potential (RESP) [106, 107] calculated at HF/6-311G*,[108, 109] using Gaussian09

software.[110] After an initial minimisation, a further NVT simulation of 1 ns at 300K was performed to equilibrate supercell. The Nose-Hoover thermostat [111] was used to obtain a correct cannonical ensemble.

The final structure from the equilibrium MD simulation was taken to start a 1 ns simulation to generate the initial conditions for CT simulations using IR approximation. To create the initial conditions for CT simulations using explicit charge relaxation, we take the final structure from NVT simulation to start 1 ns simulation with a hole placed on the first molecule of the chain, keeping all other molecules charge-neutral. The first 0.5 ns of this simulation were considered as equilibration in the charged state, and the last 0.5 ns MD simulation were used to generate the initial structures and velocities for the individual FSSH/MFE-ER simulation. The hole wave function was initially localized on the first molecule, $\Psi(0) = \phi_1(0)$. For FSSH-ER, the probability, $|U(0)_{j1}|^2$ (i.e., $|\langle\psi_j(0)|\phi_1(0)\rangle|^2$), was used to randomly distribute the trajectories among the manifold of the adiabatic states $\psi_j(0)$. A swarm of 500 trajectories was used to obtain converged charge mobilities.

The charge carrier mobility is computed with the Einstein-Smoluchowski equation

$$\mu = \frac{eD}{k_B T} , \tag{3.1}$$

where k_B is the Boltzmann constant, e is the elementary charge and T denotes temperature. The diffusion coefficient D is calculated by

$$D = \frac{1}{2n} \lim_{t\to\infty} \frac{d\,\mathrm{MSD}(t)}{dt} , \tag{3.2}$$

where n is dimensionality ($n = 1$ for a one-dimensional chain). The mean square displacement (MSD)$\mathrm{MSD}(t)$ of the charge is defined as

$$\mathrm{MSD}(t) = \frac{1}{N_{\mathrm{traj}}} \sum_{l}^{N_{\mathrm{traj}}} \sum_{A} (x_A(t)^{(l)} - x_0^{(l)})^2 P(t)^{(l)}(t) , \tag{3.3}$$

where $x_A(t)^{(l)}$ and $P(t)^{(l)}$ are the center of mass of molecule A and corresponding charge population along the trajectory l, respectively. $x_0^{(l)}$ is the center of charge at $t = 0$. The inverse participation ratio (IPR), which is a measure of the number of molecules over which electronic wave function is delocalized on average, is defined as

$$IPR = \sum_{l=1}^{N_{\mathrm{traj}}} \frac{1}{\sum_k |U_{jk}^{(l)}|^4} \tag{3.4}$$

Master equation (ME) has been widely used, together with kinetic Monte Carlo algorithm, to compute the charge hopping mobility in OSCs. It describes the time evolution of the charge population at each molecule,

$$\dot{P}_i^d = \sum_j \left(k_{ji} P_j^d - k_{ij} P_i^d \right) , \tag{3.5}$$

where P_i^d is the charge population at molecule i and k_{ij} is the charge transfer rate from the molecule i to molecule j. In the present study, the ME was integrated by the fourth-order Runge-Kutta algorithm and the charge transfer rate constants were evaluated according to the semiclassical transition state theory (TST) [94],

$$k_{ij}^{TST} = \nu_{eff}\kappa \exp\left(-\frac{\Delta G^{ad}}{k_B T}\right) , \tag{3.6}$$

where ν_{eff} is the effective frequency (in OSCs, the frequency of the carbon double bond, 1700 cm^{-1} was used). κ is the transmission coefficient which is mainly dependent on the electronic coupling and reorganization energy

$$\kappa = \frac{2P_{LZ}}{1 + P_{LZ}} , \tag{3.7}$$

where Laudau-Zener transition probability for a single crossing through the transition region is given by

$$P_{LZ} = 1.0 - \exp\left(-\frac{\pi^{3/2}\langle H_{ij}^2\rangle}{h\nu_{eff}\sqrt{\lambda k_B T}}\right) . \tag{3.8}$$

ΔG^{ad} in eq. 3.6 is the adiabatic activation energy and can be divided into two contributions

$$\Delta G^{ad} = \Delta G^d + \Delta^* \tag{3.9}$$

$$= \frac{\lambda}{4} + \left(\langle H_{ij}^2\rangle^{1/2} - \frac{\langle H_{ij}^2\rangle}{\lambda}\right) , \tag{3.10}$$

where the first term is diabatic activation energy ΔG^d, the latter ones are adiabatic correction factor Δ^*, λ is the reorganization energy. The reorganization energy computed by B3LYP was used to compute the charge transfer rate if not stated otherwise.

In the low-coupling regime, TST can be approximately reduced to Marcus rate equation,

$$k_{ij}^{Marcus} = \frac{\langle H_{ij}^2}{\hbar}\frac{1}{\sqrt{4\pi\lambda k_B T}} \exp\left(-\frac{\Delta G^d}{k_B T}\right) . \tag{3.11}$$

Recently, transient localization theory (TLT), proposed by Fratini and Ciuchi, has been successfully used to compute the charge mobility for OSCs [112, 113, 114]. This theoretical model is based on the observation that the dynamics disorder caused by thermal molecular motion induces a "transient localization" of charge carrier wave function, suppressing charge diffusion. In the present work, the TLT mobilities are computed using the code adopted from Ref. [114].

3.2.1. Problems and corrections for the fewest switches surface hopping (FSSH) method

Since the TDSE for the electronic wave function is solved using a single trajectory, the original FSSH method tends to overestimate electronic coherence. Here, we employed the an simple empirical correction proposed by Granucci and Persico [99]. with a correction parameter $\alpha = 0.1$ E_h. While such an ad hoc correction may preserve the internal consistency between the fractions of trajectories and averaged adiabatic populations, it tends to quickly collapse the wave function to a wrong electronic state after a surface hop with a very low (but still non-vanishing) probability has taken place. Such an improper surface hop can lead to artificial long-range charge transfer and divergent charge mobilities with respect to system size in OSCs [94]. In this work, we employed a similar correction scheme used by Blumberger and coworkers in a recent study in the surface hopping simulations for charge transport in OSCs [94]. Briefly, we define an active region including 0.999 diabatic populations, set the wave function amplitudes outside this region to zero and then renormalized the wave function amplitudes inside the active region. For more details, readers can be referred to Ref. [94].

Another major problem of the FSSH method is its failure to propagate the correct state in the vicinity of trivial unavoided crossings. In large molecules and molecular complexes, unavoided crossings often occur whenever two spatially separated and thus noninteracting states cross. In such cases, the ordering of these states changes (the states swap), and their nonadiabatic coupling exhibits a sharp peak localized in the proximity of crossing point strongly. To solve this problem, we used an simple state-tracking algorithm based on the wave function overlaps between successive time step. In this algorithm, a threshold (0.9 in their work) of wave function overlap was defined to distinguish between (i) unavoided crossings between interacting states and (ii) trivial unavoided crossings between noninteracting states. If a maximum wave function overlap between the new state i and old state j is greater than the threshold, a trivial unavoided crossing is detected and the new state i is mapped on state j; if otherwise, the hopping probability to a unavoided crossing state is corrected according to [100]

$$P^{j\to k}_{\mathrm{SC-FSSH}} = \frac{|C^{ad}_j(t)|^2 - |C^{ad}_j(t+dt)|^2}{|C^{ad}_j(t)|^2} - \sum_{i\neq k} P^{j\to i}_{\mathrm{FSSH}} \,. \tag{3.12}$$

3.3. Results and discussion

Fig.3.1 presents ten representative OSCs studied in this work. The experimental charge mobilities for theses materials range in three orders of magnitude (see Table 2) and thus allow for a systematic examination of the performance of the Boltzmann correction (BC) and implicit charge relaxation (IR) approximation in the FSSH simulations for charge transport (CT) in OSCs. The reorganization energies and electronic couplings for the studied OSCs are summarized in Table.3.1.

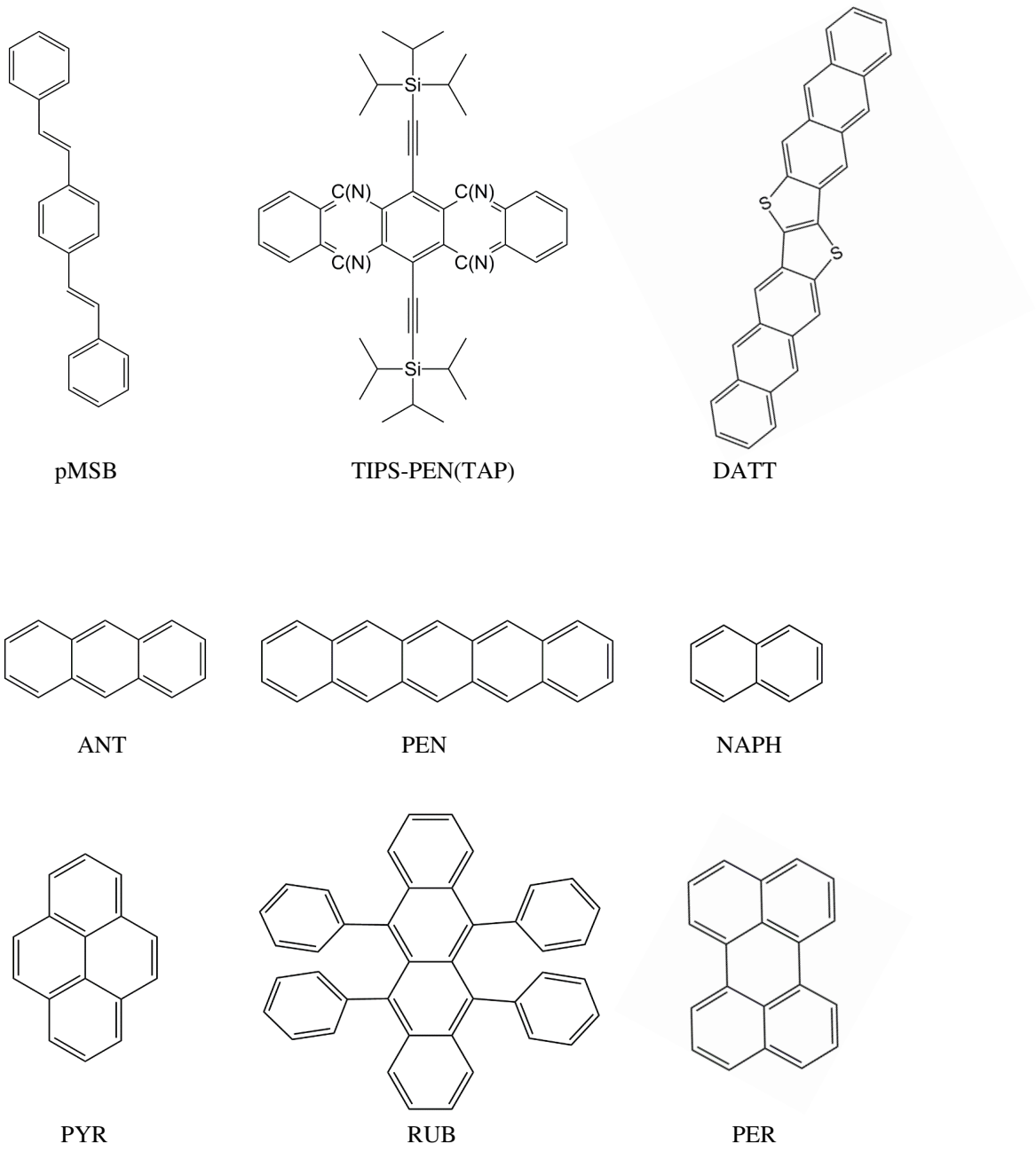

Figure 3.1.: Molecular structures of organic materials studied in the present work.

As a first step, we examine the accuracy of the FSSH and MFE methods using explicit forces for charge relaxation (FSSH-ER and MFE-ER) in comparison with the experiments. Fig.3.2 (a)-(d) shows the hole carrier wave function propagated with the FSSH-ER and MFE-ER methods for two representative OSCs, low-mobility OSC pMSB and high-mobility OSC rubrene. In the MFE-ER simulation (Fig.3.2 (a)), the wave function is initially localized on a single pMSB molecule and starts to hop after 400 fs.
Meanwhile, the hole is gradually delocalized over a few molecules, which is not expected for the low-mobility material. This artificial charge delocalization may be the consequence of the notorious shortcomings of the MFE method, such as the overheating of electronic system and electronic overcoherence. The problem becomes more seriously for the high-mobility materials, such as RUB (Fig.3.2 (b)), where the wave function quickly spreads over the entire system. The situation is strikingly different in the FSSH-ER simulations. For pMSB (Fig.3.2 (c)), the wave function is localized on a single pMSB molecule and hops between neighboring molecules. The charge carrier in RUB (Fig.3.2 (d)) is delocalized over several molecules and propagates across the crystal by diffusive hops over several lattice spacings.

Fig.3.3 (a)-(b) shows the charge mobilities computed by the MFE-ER and FSSH-ER methods for all OSCs studied in this work. As expected, the MFE-ER method (Fig.3.3 (a))overestimates the charge mobilities in comparison with experiments, particularly for high-conductivity materials ($\mu_{Exp} > 10\ cm^2V^{-1}s^{-1}$), where the MFE mobilities are about one order of magnitude higher than the experimental values. A better agreement with experiments is achieved by the FSSH-ER method (Fig.3.3 (b)), with deviations for most OSCs less than a factor of 2. The errors can be attributed to the underestimation of reorganization energy by DFTB, which leads to the overestimation of charge mobilities.

We take pMSB and RUB as two representative OSCs to examine the performance of the IR and BC approximations in the FSSH simulations for low- and high-conductivity materials. In IR approximation, the on-site energy is reduced by a precalculated parameter (usually reorganization energy is used) weighted by diabatic populations. The implicit relaxation approximation neglects two factors: (i) the effects of intermolecular charge relaxation (i.e., the electronic coupling derivatives with respect to nuclear coordinates, see Eq. 2.92); (ii) the feedback from electronic relaxation to the nuclei. To understand the effects of these factors on modeling CT in OSCs, we set the off-diagonal forces, $\frac{\partial H^0_{mn}}{\partial R_k}$, to 0 in the FSSH simulations (henceforth, referred to FSSH-ER(onsite)) for pMSB and RUB. The charge mobility difference between obtained by FSSH-ER(onsite) and FSSH-ER methods for rubrene is much larger than the difference for p-MSB. This is due to the one order of magnitude higher electronic coupling in rubrene (107 meV) than in p-MSB (11 meV). For both materials, the FSSH-IR(W) mobilities are in good agreements with FSSH-ER(onsite) mobilities, which indicates that the back-reaction from electronic relaxation to the nuclei has a minor influence on the CT in OSCs.

In comparison to the velocity rescaling along the NCV in the FSSH simulation for pMSB, the rescaling of transition probability with a Boltzmann factor results in the overestimation of charge mobility. This is consistent with our previous benchmark study that the BC approximation overestimates the charge mobility in low coupling regime[93]. For rubrene, the FSSH-BC mobility agrees well with FSSH-ER mobility. The FSSH simulations with the combination of IR and BC approximations for both OSCs give a reasonably good mobility values in comparison to FSSH-ER.

Fig 3.4. shows the comparison of charge mobilities computed by FSSH-ER and FSSH-BC-IR for the OSCs studied in the present work (the values are shown in Table 3.2). Overall, the FSSH-BC-IR mobilities agree very well with the FSSH-ER mobilities, yet the computational time is reduced to about 50 % of that of FSSH-ER. This indicates that the FSSH-BC-IR is a reliable and efficient method for modeling CT in OSCs.
Two key quantities dominating CT in OSCs are electronic coupling and reorganization energy. We have shown in a previous study [76] that scaling the DFTB electronic coupling with an unform factor can lead to the electronic coupling as accurate as obtained by the high-level *ab initio* method. The computation of the reorganization energy is under debate. Bredas and coworkers [79, 80] found good agreements between the reorganization energies computed by B3LYP functional and the reorganization energies obtained by fitting to experimental photoelectron spectra. On the other hand, a computational benchmark study [101] shows the ωB97XD functional gives accurate reorganization energy in comparison with the high-level *ab initio* methods. Herein, the IR approximation enables the systematic examination of the performance of the reorganization energies computed by different DFT functionals in CT in OSCs.

Fig. 3.5(a)-(c) shows the comparison of the experimental mobilities with the charge mobilities obtained by FSSH-BC-IR with input reorganization energies computed by B3LYP and ωB97XD methods, respectively. The FSSH-BC-IR simulations using ωB97XD reorganization energy (Fig. 3.5(a)) underestimate the measured mobilities for most OSCs. The error is large for the low-mobility materials while become small for high-mobility materials. This is understandable as the effect of reorganization energy tends to vanish due to charge delocalization over several molecules. The relaxation energy can be written as $E^m_{relax} = \frac{1}{2}\lambda Q^2_m$, where Q_m is the charge of site m. The charge is delocalized over a few molecules in high-mobility materials (see Fig. 3.5 (d)), leading to a negligible effect of charge relaxation. We note that ωB97XD functional has been shown to provide reorganization energy in a good agreement with high-level *ab initio* methods [101].
Thereby, the underestimation of the charge mobilities may be due to the lack of nuclear quantum effects in the FSSH simulations. For a variety of OSCs, the charge mobilities computed by FSSH-BC-IR using B3LYP reorganization energy (Fig. 3.5(b)) are in good agreements with experimental values. This is reminiscent of the well-known statement in quantum chemistry community: B3LYP underestimates the barrier height of chemical reaction, while the predicted chemical rate is in a good agreement with the experiment. The reasonable underestimation of the reorganization energy leads to a lower barrier height for charge transfer, resembling an effective correction to cure the shortcoming of the neglect of the nuclear quantum effects in FSSH simulations and, thus resulting in a good agreement with experiment. Fig. 3.5 (c) shows the average size of polaron (defined by inverse participation ratio (IPR) as described in Methods) computed by the FSSH simulations.

Table 3.1.: Computed reorganization energies and electronic couplings (in meV) for OSCs studied in this work.

Crystal	λ_{DFTB}	λ_{B3LYP}	$\lambda_{\omega B97XD}$	<J>	σ_J
PEN-h^+(a)	37	98	170	100.5	28.1
RUB-h^+(b)	51	152	210	106.5	26.0
TIPS-TAP-e^-(a)	110	205	325	158.0	31.2
DATT-h^+(a)	51	88	198	93.3	18.6
ANT-h^+(b)	84	142	202	38.1	20.3
NAP-h^+(b)	130	187	244	38.9	22.0
TIPS-PEN-h^+(a)	34	136	215	20.3	27.2
p-MSB-h^+(b)	140	255	540	10.5	6.0
PYR-e^-(c)	175	222	302	3.2	20.5
PER-e^-(a)	120	177	265	26.6	15.0
PER-e^-(c^*)	120	177	265	8.0	9.5

It can be seen the charge mobility correlates well with polaron size. Fig. 3.5 (d) shows a comparison of charge mobilities computed in this work with a recent work by Blumberger et al [94]. For most OSCs, FSSH-BC-IR mobilities are in good agreements with the their mobilities.

Fig. 3.6(a) shows the charge mobilities obtained by solving the master equation with transition state theory (TST) and Marcus rate equation, respectively. Somewhat unexpectedly, both hopping theories reproduce the experimental mobilities spanning three orders of magnitude well. Marcus theory is derived from the perturbation theory and thus expected to be valid only in the low-coupling regime; however, the results show that the computed mobilities are also in good agreements with experiments for the high-coupling regime, where the charge transfer barrier no longer exists. The accidental agreements can be attributed to the overestimated transition probability for the crossing of charge transfer transition state, which cancels out the effect of the overestimation of the charge transfer barrier height by using diabatic activation energy (ΔG^d), instead of adiabatic activation energy (ΔG^{ad}) in Marcus theory (Eq. 3.11).
This is verified by the underestimated charge mobilities (TST-diab in 3.6(a)) using the corrected transition probability . Fig. 3.6(b) shows the mobilities computed by transient localization theory (TLT) using electronic Hamiltonian with on-site energy fluctuations (pink circles, denoted as 'TLT_0') and the removal of the on-site energy fluctuation by setting the on-site energies to be zeros (blue circles). Overall, both TLT mobilities coincide with the experimental values for high-mobility regime. The TLT_0 fails in the low mobility regime, $\mu < 1\ cm^2V^{-1}s^{-1}$, while the TLT using Hamiltonian including the on-site energy fluctuation qualitatively reproduces the mobilities for low-coupling regime.

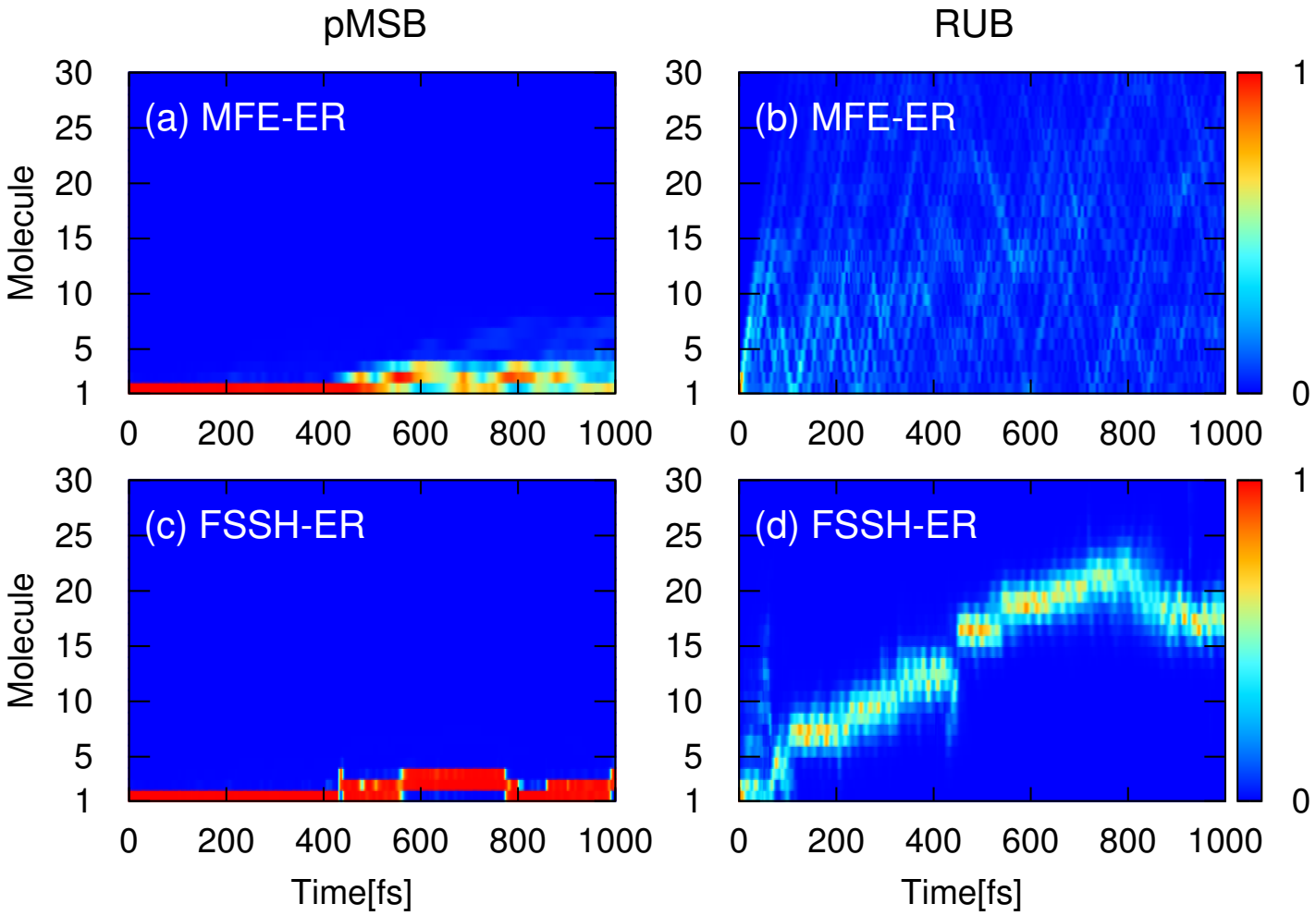

Figure 3.2.: Time-dependent hole carrier populations obtained by (a-b) MFE-ER and (c-d) FSSH-ER for pMSB and RUB.

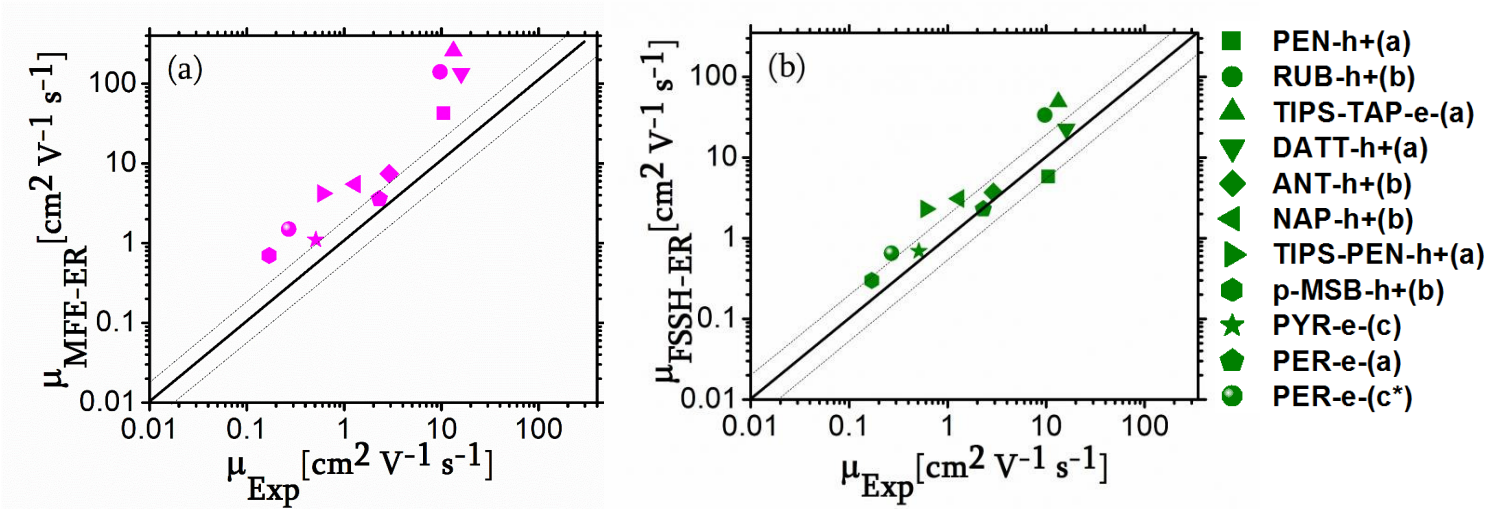

Figure 3.3.: Experimental mobilities versus the mobilities obtained by (a) MFE-ER and (b) FSSH-ER methods.

Table 3.2.: Computed and experimental charge mobilities (in $cm^2V^{-1}s^{-1}$).

Crystal	μ_{ER}	$\mu_{IR(DFTB)}$	$\mu_{IR(B3LYP)}$	$\mu_{IR(\omega B97XD)}$	μ_{MFE}	μ_{Exp}
PEN-h$^+$(a)	5.8	10.1	6.5	5	42.9	10.5
RUB-h$^+$(b)	33.5	52.3	26.2	17.5	114.3	9.7
TIPS-TAP-e$^-$(a)	49.0	71.3	44.8	30.6	257.6	13.3
DATT-h$^+$(a)	22.5	36.5	35.5	15.2	134.9	16.0
ANT-h$^+$(b)	3.7	6.7	3.1	0.71	7.4	2.9
NAP-h$^+$(b)	3.1	4.2	2.2	0.73	5.5	1.3
TIPS-PEN-h$^+$(a)	2.3	5.3	0.72	0.061	4.2	0.6
p-MSB-h$^+$(b)	0.33	0.39	0.016	–	0.7	0.17
PYR-e$^-$(c)	0.69	0.65	0.3	0.089	1.1	0.51
PER-e$^-$(a)	2.3	3.4	1.1	0.15	3.6	2.3
PER-e$^-$(c*)	0.65	0.96	0.24	0.017	1.5	0.27

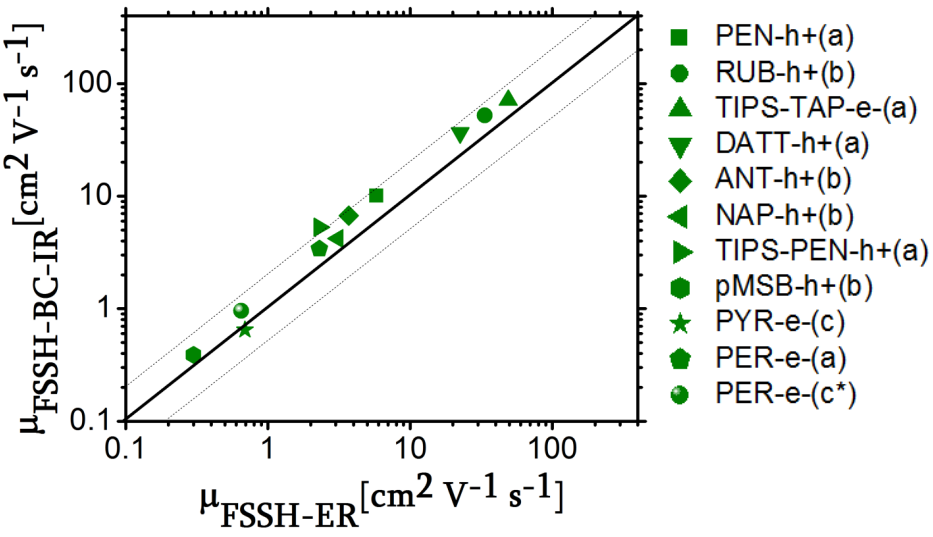

Figure 3.4.: Charge mobilities computed by FSSH-ER versus FSSH-BC-IR. The reorganization energies computed by DFTB is used as an input parameter for IR approximation.

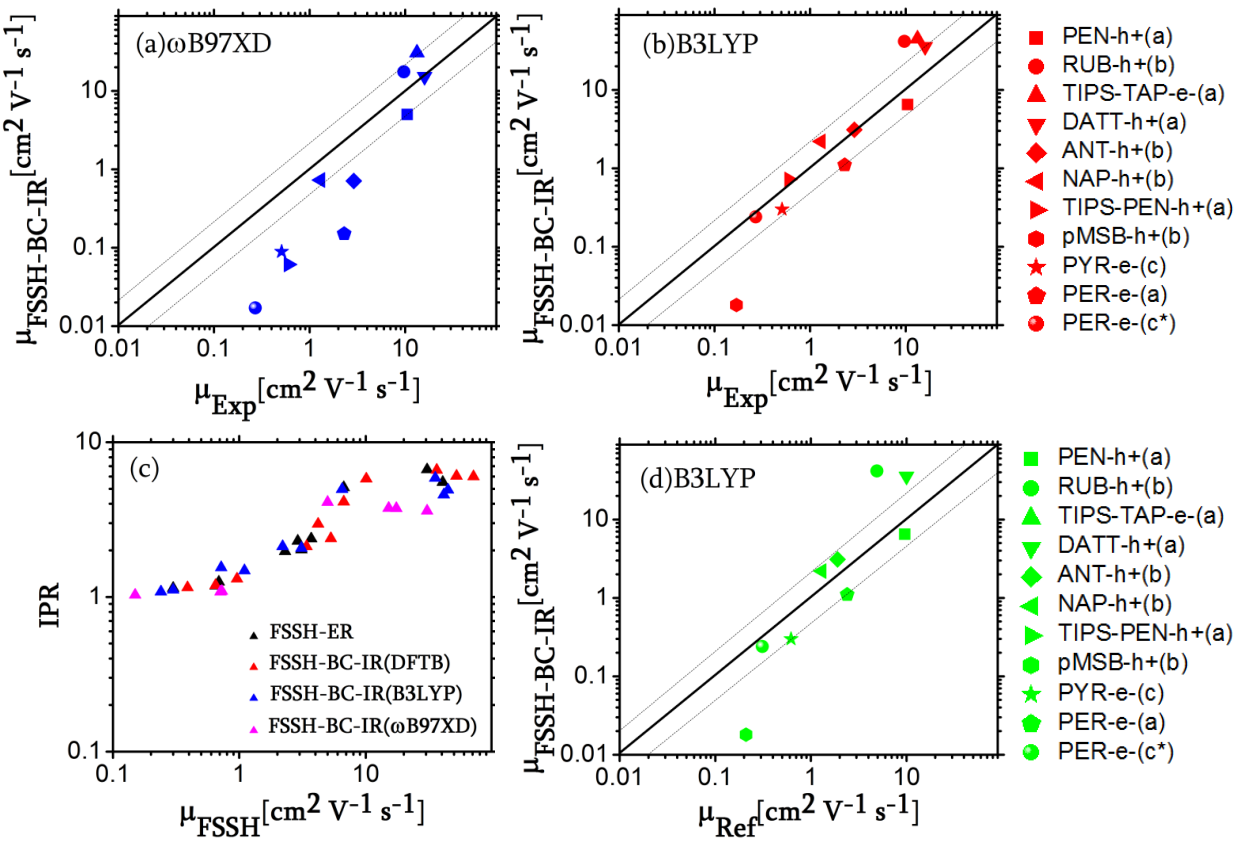

Figure 3.5.: Experimental measured mobilities versus mobilities computed by FSSH-BC-IR using input reorganization energies computed by (a) ωB97XD and (b) B3LYP, respectively. (c) Correlation between IPR and computed mobilities.(d) Comparison of charge mobilities in this work and a recent work by Blumberger et al.

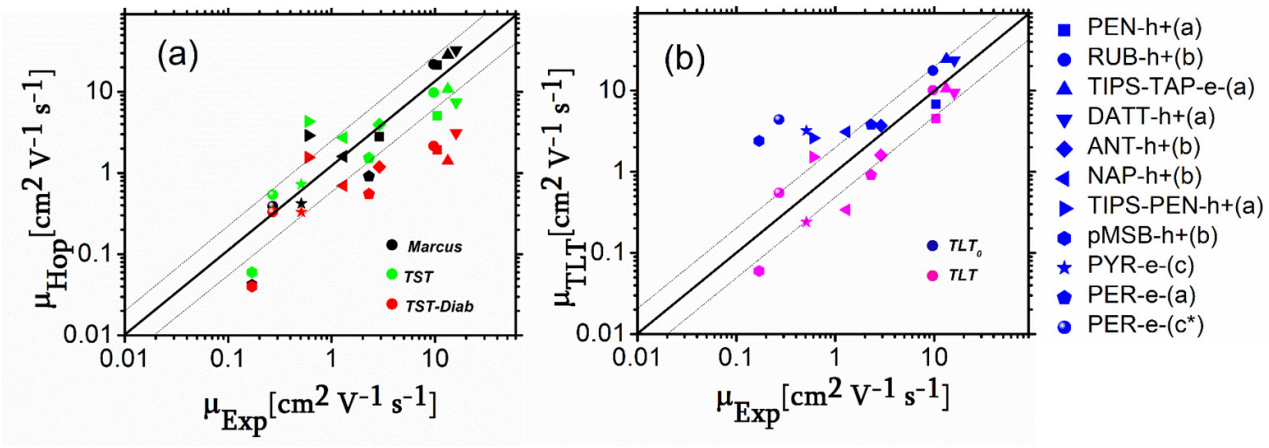

Figure 3.6.: Experimental charge mobilities versus mobilities computed by (a) TLT and (b) Marcus hopping theory.

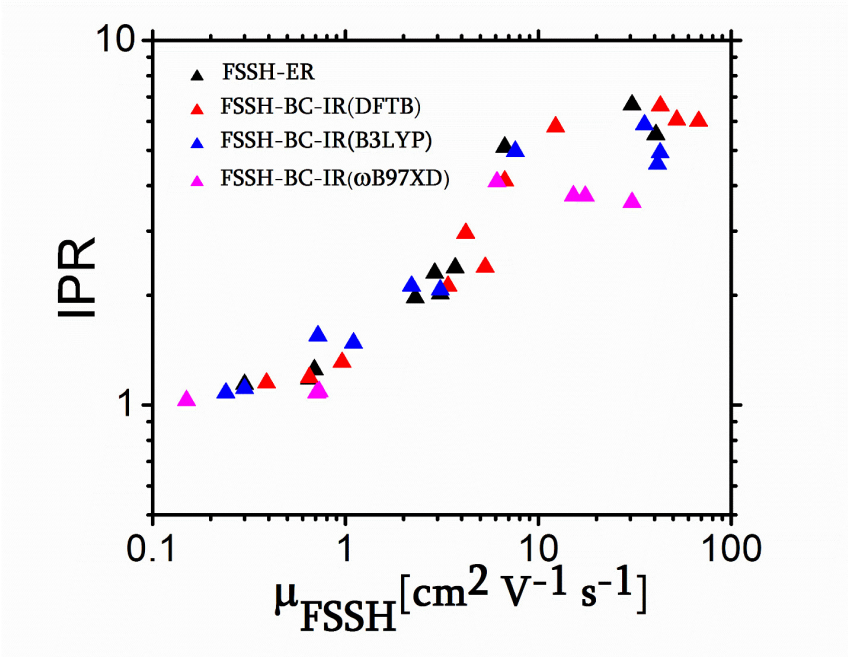

Figure 3.7.: Correlation between IPR and computed mobilities.

3.4. Conclusion

In summary, our study meticulously investigated the efficacy of two approximation methods, namely the Boltzmann correction (BC) and implicit charge relaxation (IR), in FSSH simulations of charge transport processes across various organic materials. Our findings revealed a commendable concordance between FSSH-BC-IR and FSSH with explicit charge relaxation (FSSH-ER) across a broad spectrum of charge mobilities, encompassing three orders of magnitude. However, it became apparent that both techniques tended to overestimate experimental mobilities due to the inherent underestimation of reorganization energy as calculated by DFTB. Notably, the IR approximation emerged as a promising approach, enabling the incorporation of an accurately estimated reorganization energy to address this limitation.

In our simulations, FSSH-BC-IR, utilizing reorganization energies computed by ωB97XD, displayed results consistent with high-level electronic structure methods, indicating a noticeable disparity between experimental data and FSSH-BC-IR mobilities in the low-coupling regime, albeit remaining relatively small (less than a factor of 2) in the high-coupling regime. This observation underscored the potential significance of nuclear zero point energy (ZPE) in the hopping transport regime. Intriguingly, FSSH-BC-IR employing B3LYP reorganization energy demonstrated a remarkable agreement with experimental outcomes across all organic semiconductors (OSCs). We attribute this favorable alignment to the compensatory effect of the underestimated reorganization energy, effectively offsetting the loss incurred by ZPE in our simulations.

In essence, our comprehensive analysis sheds light on the subtle intricacies of charge transport simulations, providing valuable insights for refining computational methodologies and advancing our understanding of organic electronic materials.

4. Effects on charge transport of halogen derivatives of TIPS-TAP

4.1. Introduction

The pursuit of low-power complementary circuits has led to a significant focus on developing efficient p- and n-channel organic field-effect transistors (OFETs)[115]. While p-type organic semiconductors have shown impressive electron mobility, surpassing 40 $cm^2V^{-1}s^{-1}$[116, 117], the progress in enhancing n-type organic semiconductors, a crucial component for complementary circuits, has been limited.
This study focuses on recent developments in a number of classes of *n*-type materials. So far, only four *n*-type organic semiconductors have been reported to exhibit field effect mobility higher than 10 $cm^2V^{-1}s^{-1}$ [118]. One of them is 6,13 bis ((triisopropylsilyl) ethynyl)-5,7,12,14-tetraazapentacene (TIPS-TAP) is the most successful member of the N-heteroacene family for applications in OFETs [119, 120, 121, 122]. Recently, several theoretical and experimental studies have shown that the introduction of electron-withdrawing groups through, for example, halogenation (Br and Cl), is a promising way to transform p-type semiconductors into n-type ones[118]. Hydrogen atoms of TIPS-TAP can be substituted by halogen atoms as shown in fig. 4.1.
The substitution changes the electronic properties of N-heteroacenes and influence their semiconducting capability. With 4Cl-TAP, Miao et al. even set a new record for the electron mobility of n-channel organic field-effect transistors, reaching electron mobilities as high as 27.8 $cm^2V^{-1}s^{-1}$. The subject of this work is the theoretical investigation of possible electron mobilities for the halogenated TIPS-TAP molecules, including fluorine, chlorine and bromine [123, 118, 124]. Understanding the natural mechanism of the charge transport process in these materials is important for the design of better organic materials in term of charge mobility.
In this study, we utilized computational methods such as FSSH-IR(ωB97XD) and (B3LYP) to estimate the electron mobilities of the crystals under investigation. Additionally, we calculated transfer integrals and reorganization energies. Our research delved into a comprehensive analysis of the impact of electron-withdrawing substituents on the geometric structures and electronic properties of these crystals. These theoretical findings offer valuable insights into understanding the influence of substituent groups and structural changes on the charge transport properties of organic semiconductors. This knowledge is essential for enhancing the efficiency of charge transport in organic materials and provides essential information for further advancements in the field.

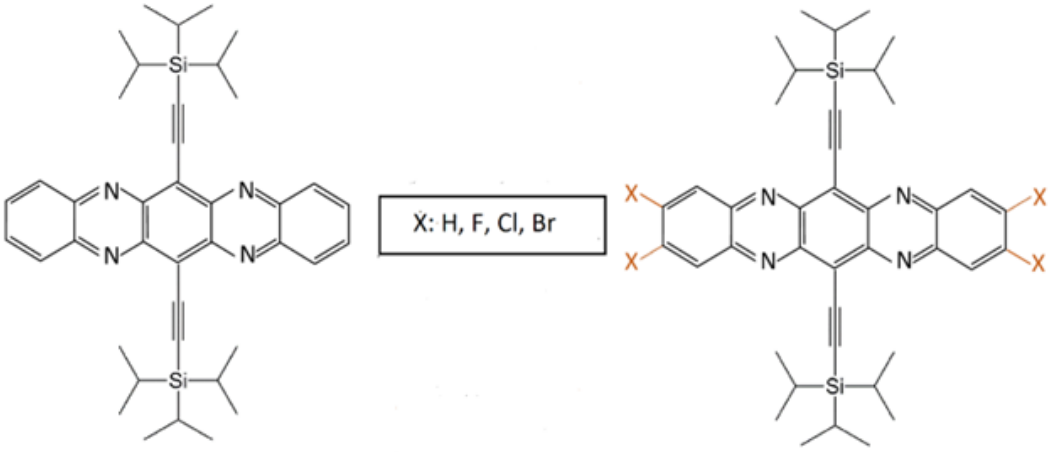

Figure 4.1.: Symmetric halogen derivatives of TIPS-TAP.

4.2. System Preparation

The crystal structures of TIPS-TAP , 4F-TIPS-TAP , 4Cl-TIPS-TAP and 4Br-TIPS-TAP were obtained from the Cambridge Structural Database. The supercells for the studied halogenTAP were constructed based on the experimental crystal structures, containing the following number of molecules along the crystal axis as well as the number of molecules in the QM zone: $100 \times 5 \times 3$ for TIPSTAP, $40 \times 40 \times 3$ for FTAP, $70 \times 70 \times 2$ for ClTAP, $70 \times 70 \times 2$ for BrTAP. The force field parameters were derived from the general AMBER force field (GAFF) [104, 105], where the atomic charges were generated from restrained fitting on the electrostatic potential (RESP) [106, 107] calculated at HF/6-311G* [108, 109] using Gaussian09 software [110]. After an initial minimization, a further NVT simulation of 1 ns at $300K$ was performed to equilibrate the supercell. The Nose-Hoover thermostat was used to obtain a correct canonical ensemble. The GROMACS 2018 package was used to perform classical MD simulations. The final structure from the equilibrium MD simulation was taken to start a 1 ns simulation to generate the initial conditions for CT simulations using IR approximation. To create the initial conditions for CT simulations, we take the final structure from NVT simulation to start 1 ns simulation with a electron placed on the first molecule of the chain, keeping all other molecules charge-neutral. The first 0.5 ns of this simulation were considered as equilibration in the charged state, and the last 0.5 ns MD simulation were used to generate the initial structures and velocities for the FSSH simulation. The wave function was initially localized on the first molecule, $\Psi(0) = \phi_1(0)$. For FSSH-ER, the probability, $|U(0)_{j1}|^2$ (i.e., $|\langle\psi_j(0)|\phi_1(0)\rangle|^2$), was used to randomly distribute the trajectories among the manifold of the adiabatic states $\psi_j(0)$. A swarm of 500 trajectories was used to obtain converged charge mobilities.

4.3. Results and Discussion

Two key quantities dominating charge transfer in OSCs are electronic coupling and reorganization energy. So we have calculated coupling as well as reorganization energy and summarized in Table 4.1 for TipsTap and halogen Tap to investigate the effects of substitution on charge transfer and electronic structure.

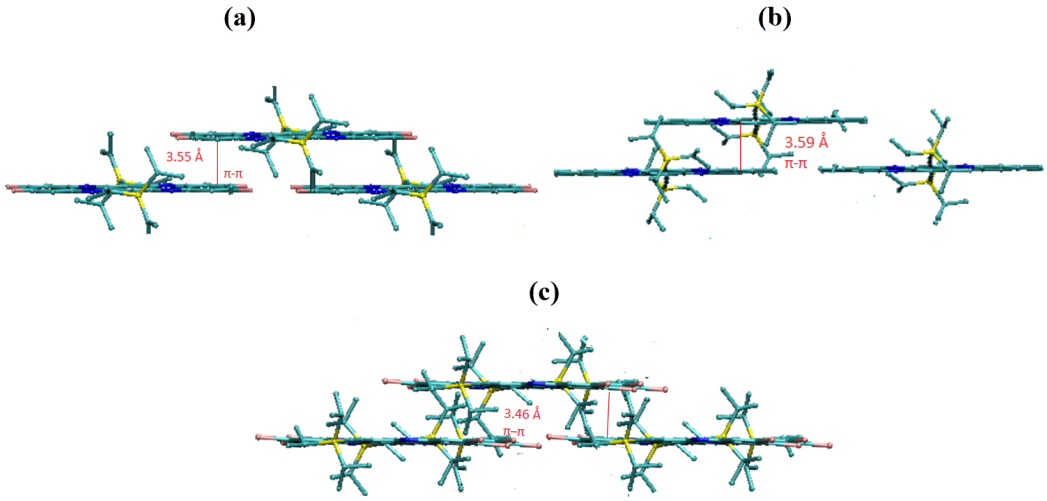

Figure 4.2.: Crystal structure of FTAP, ClTAP and BrTAP.

4.3.1. Electron Coupling

It is found that the electron transfer integral is very sensitive to subtle changes in the 2D π stacking with brickwork arrangement.

This sensitivity is due to the fact that the electronic coupling is not related to the spatial overlap between adjacent molecules but rather to the degree of wavefunction overlap. The electronic coupling can often be estimated by only taking the LUMO (or HOMO) of a dimer into account. In that scenario, the extreme dependence on the π-stacking can be rationalized by imagining the bonding-antibonding pattern. For example, when displacing two dimers along the long axis, minima and maxima of the transfer integral could be reached, while the mean amplitude continuously decreases and reaches zero when there is no more spatial overlap. 4F-TIPS-TAP is an example of the sensitivity of the transfer integral. It has the smallest π-π distance while showing by far the smallest transfer integrals. Since smaller π-π distances should result in larger transfer integrals, the importance of the π-displacements is shown again. These are quite different from all other derivatives and this kind of displacement is likely particularly unfavorable for wavefunction overlap. 4Br-TIPS-TAP and 4Cl-TIPS-TAP both show a slightly larger π-π distances as TIPS-TAP; therefore, the smaller transfer integrals could be expected. However, the π -displacements are different and lead to a greater spatial overlap and in this case, it might be beneficial to enhance the wavefunction overlap for dimers,

especially due to the increased size of transfer integrals. The subtle differences in the 2D π-stacking of halogenated TAPs and TIPS-TAP can be measured in several ways, namely by the distances between Si, π-planes and along the long and short axes of the stacked π-backbones. The results suggest that the modification of TIPS-TAP with different F, Cl, or Br can fine-tune the π-stacking, in particular, the displacements of the π-stacking can strongly affect the intermolecular electronic couplings in a way that is closely related to the phase and nodal properties of the frontier molecular orbitals.

It is well-established that in the organic semiconductors, charge carrier transport occurs along π orbitals. So, the π orbital overlap between neighboring molecules seriously determines the mobility and the molecular packings directly influence the transport properties. The crystal structures of the halogenated TAPs show similar 2D-π stacking of the flat tetraazapentacene backbones in brickwork arrangements, similar to those of TIPS-TAP. It is found that 4Cl-TAP has larger electron transfer integrals than TIPS-TAP, and Br- TAP is approximately the same as TIPs-TAP, while FTAPs have lower electron transfer integrals than TIPS-TAP (Table1).

It is found that halogenated TAPs generally have lower LUMO energy levels than TIPS-TAP and halogen substituents lead to a lower LUMO energy level as expected. Br is found to be more effective than F and Cl in lowering the LUMO energy level although F is more electronegative than Cl and Br. This finding is in agreement with the earlier observations on chlorinated and fluorinated organic semiconductors, and can be attributed to the fact that the empty 3d orbitals in Cl can accept π-electrons from the conjugated core, while no empty orbitals in F are available for such delocalization [118].

Another finding from the crystal structures is that the halogenated TAPs all have intermolecular short contacts with halogen atoms in each layer of the brickwork arrangement. In order to see the role of geometrical and electronic properties in the coupling, we calculated the coupling with and without an Halogen group. For this calculation, we treat the halogen in the MM part, so the coupling is just related to geometrical effect. For BrTAP, ClTAP, when the substitution is considered as the MM part and only core is treated in the QM part, the geometry plays an important role as the coupling does not change dramatically. But in the case of FTAP, when F is in the MM part, the coupling changes significantly and the role of electronic effects can be seen. So It can be concluded that for FTAP electronic properties exhibit an important role in coupling however in the case of Br and Cl TAP structural properties play a significant role in coupling.

4.3.2. Reorganization Energy

In order to calculate the reorganization energy the geometries of the neutral and anionic TIPS-TAP, 4F-, 4Cl-, 4Br- were optimized, and the respective energies were obtained subsequently. Then the energies of the neutral states at the optimized anionic geometries as well as the anionic states at the optimized neutral geometries were computed by computed by ωB97XD and B3LYP, respectively, with the 6-

311g* basis set implemented in the GAUSSIAN 09 package [110]. The results of the calculation is shown in Table 4.1. Reorganization energies follow the trend: 4F-TIPS-TAP > TIPS-TAP ~ 4Cl-TIPS-TAP > 4Br-TIPS-TAP. In Table 4.1, the reorganization energy was initially computed for the entire molecule. However, in Table 4.2, the reorganization was specifically determined for the core, while the silicon component was disregarded due to its minimal impact on mobility. This selected data was then employed as an input for the mobility calculation. For halogenated TAPs it is found that (-Br and -Cl), are more effective than F in lowering the LUMO energy level although F is more electronegative than Cl and Br. In the case of Cl, It and can be attributed to the fact that the empty 3d orbitals in Cl can accept π-electrons from the conjugated core, while no empty orbitals in F are available for such delocalization [118].

The increased reorganization energy of FTAP can be attributed to the enhancement of breathing as well as stretching vibrations of its pentacene bonds framework, and the additional stretching of C-F. On the other hand, Br substituents seem to suppress the breathing and stretching vibration of the pentacene framework. The weaker C-Br and C-Cl bonds further reduce the additional contribution of the halogen C bond to the reorganization energy, leading to a quite similar- TAP reorganization energy as TIPS.

Table 4.1.: Reorganization energies, electronic couplings (in meV) and Distance between Si for Tips and halogenated TAPS.

Crystal	distance(Si-Si)	λ_{DFTB}	λ_{B3LYP}	<J>	σ_J
$TIPS-TAP$(a)	9.96	120	205	62.15	29.84
$TIPS-TAP$(b)	7.94	120	205	158.19	28.81
$FTAP$(a)	10.28	122	240	2.49	32.15
$FTAP$(b)	8.13	122	240	58.79	38.63
$ClTAP$(a)	12.36	113	200	43.35	14.61
$ClTAP$(b)	6.97	113	200	160.97	27.01
$BrTAP$(a)	12.58	111	189	45.81	12.46
$BrTAP$(b)	7.22	111	189	149.22	30.11

4.3.3. Charge Transfer

Next, we calculate electron mobilities for TipsTAP and halogenTap and compare them to experimental values (except BrTAP). The maximum electron mobility of 4Cl-TAP (27.8 cm2 V-1 s-1) [118] is more than twice the reported value of TIPSTAP and is the highest value for all the n-type organic semiconductors as measured from field-effect transistors to the best of our knowledge. As can be seen from Table 4.2, an excellent agreement with experiments is achieved for FTAP. As we discussed before, charge carrier depends on coupling and reorganization energy. In the case of FTAP, we have largest reorganization energy and smallest coupling in comparison with BrTAP and FTAP. The electron mobility of BrTAP is closer to TipTAP and ClTAP has the largest mobility. As the average size of polaron defined by the inverse participation ratio IPR is a common measure for the number of molecules over which the carrier wavefunction is delocalized, it is also calculated.

Table 4.2.: Computed and experimental charge mobilities (in $cm^2V^{-1}s^{-1}$)

Crystal	$\lambda_{\omega B97XD}$	λ_{B3LYP}	λ_{DFTB}	$\mu_{IR(\ B3LYP)}$	$\mu_{IR(\omega B97XD)}$	μ_{Exp}	$IPR_{IR(\ B3LYP)}$	$IPR_{IR(\omega B97XD)}$
TIPSTAP(b)	251	145	105	28.01	22.14	13.3	4.32	4.15
FTAP(b)	302	193	110	6.6	11.56	3.18	2.59	1.91
ClTAP(b)	259	157	106	29.28	25.33	27.8	4.51	4.21
BrTAP(b)	246	142	104	28.59	35.34	...	5.56	4.48

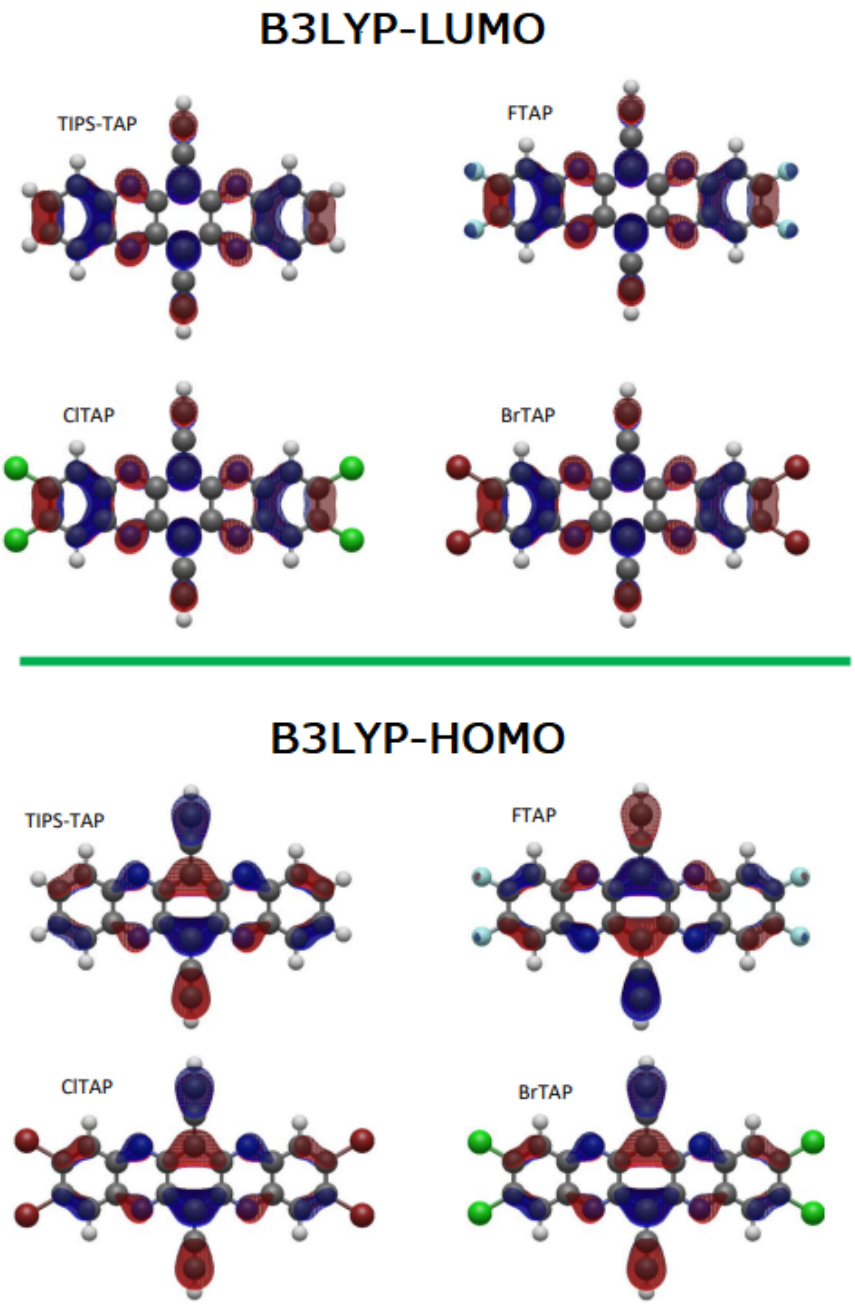

Figure 4.3.: Frontier local molecular orbitals of HalogenTAP calculated at DFT/B3LYP/6-31G* level

4.4. Conclusions

The aim of this work is to examine important electron transfer properties of TIPS-TAP and 4F-, 4Cl-, 4Br- on a theoretical basis. Particular attention was paid to the bromine derivatives since no experimental data is available yet. First of all, transfer integrals and reorganization energies of TIPS-TAP and 4F-, 4Cl-, 4Br-TIPS-TAP, were calculated. The substitution with bromine seems to fine-tune the crystal structure in a similar way as chlorine, since they are, as well as the transfer integrals, very similar. Reorganization energies follow the trend: 4F-TIPSTAP > TIPS-TAP > 4Cl-TIPS-TAP > 4Br-TIPS-TAP , which further indicates that lowering the carbon-halogen bond strength can be used to reduce the reorganization energy. The fact that halogen atoms can fine-tune the crystal structure to increase the electronic coupling and that lowering the C-halogen bond strength decreases the reorganization energy should be considered when designing new semiconductors. The estimated electron mobility of 4Br- and surpasses 4Cl-TIPS-TAP, which shows their potential as semiconductors. However, many approximations were used to calculate the electron mobility. For a better estimation of the electron mobility,

a class of new n-type organic semiconductors based on halogenated tetraazapentacenes, which have their molecular and supramolecular structures fine-tuned by different halogen type of F and Cl and Br substituents. The computational studies on the basis of crystal structures have revealed insights into structure's property relationships. First, Br and Cl substituents slightly decrease the reorganization energy of tetraazapentacene while fluorine substituents increase the reorganization energy. Second, the electron transfer integral is very sensitive to subtle changes in the 2D π-stacking with brickwork arrangement. The unprecedentedly high electron mobility of BrTAP and Cl-TAP is attributed to the reduced reorganization energy and enhanced electron transfer integral as a result of modification of TIPS-TAP with Br and Cl substituents. In oreder to ClTAP we have a good agreement with the experimental values.

since not all effects can be considered in theoretical simulations, the experimental data is also very important. There might be new effects that need to be considered when estimating the electron mobility of 4Br-TIPS-TAP. Although not all the effects were considered in this work, the trend of the electron mobility, as demonstrated above, matches existing experimental values. Therefore, 4Br-TIPS-TAP should definitely be tested since they might show even larger electron mobilities than 4Cl-TIPS-TAP, which sets the current record for charge mobility in n-type semiconductors.

5. Electro-inductive effects on the charge mobilities

5.1. Introduction

With the rapid advancement of compact intelligent organic devices, the demand for novel organic semiconductor materials is on the rise. Aromatic hydrocarbon compounds and their derivatives, such as pentacene, tetracene, and anthracene, have gained significant attention in recent years. This interest stems from their efficient utilization as high-performance organic semiconductors, owing to their rigid structure and extensive planar p-conjugated delocalization [125, 6, 126]. However, using such aromatic compounds as conductive materials presents some issues, such as chemical instability, poor solubility, difficult separation, and vulnerability to oxidation by air. To enhance the efficacy and overcome limitations, it is common to modify chemicals with functional groups. For instance, incorporating alkyl groups into pentacene improves its solubility and stability, while introducing halogen atoms to tetracene reduces its molecular orbital energy levels and alters its stacking patterns [127, 128].

Compared to pentacene and tetracene, anthracene presents several benefits like high optical quantum yield, tunable luminescence, easy preparation, environmental stability, and thermally reversible dimerization properties [129, 130]. Nonetheless, anthracene has a low melting point and limited conductivity. The anthracene single crystals exhibit a mobility of 0.02 $cm^2V^{-1}s^{-1}$ at $170K$ as OFET material, and the hole mobility can reach up to 3.0 $cm^2V^{-1}s^{-1}$ at $300K$ using the time-of-flight photocurrent technique. Consequently, research on anthracene and its derivatives has garnered increased attention, and recent experiments have enabled significant improvements in their mobilities [131, 5, 132]. Studies show that the relationship between the substituent diversity and the molecular stacking motifs is an issue that requires special attention among the factors affecting charge mobility. Meng's team used DFT to study DPA and 2,6-dithienylanthracene (DTAnt) molecules in 2019. DTAnt is a derivative of anthracene that has been substituted at the 2,6 position with bisthiophene. They explained that DPA has a higher mobility by having a reduced reorganization energy during charge transfer due to its more rigid geometric structure and a bigger electronic coupling because of an increase in HOMO overlap [133, 134, 135].

Our interest in learning more about other intrinsic elements that have an impact on charge transport related to anthracene-based materials is sparked by the differences in charge transfer characteristics among organic semiconductor materials

with comparable structures. The main effect of the subtle relationship between the lengths of the acene core and its substituent on the molecular stacking is still under debate. Inspired by these delightful results, our work intends to further investigate the changes caused by substituent as well as different substituted positions [136, 137, 138].

In this part, in order to gain a better understanding of the electro-inductive effects on the charge transport property, we began with calculations for anthracene (Ant) with dimethyl and dimethoxy as electron donor groups and dicyano and dibromo as electron attractor groups (Fig. 5.1). The substituent effect on molecular geometry, reorganization energy, crystal property, transfer integrals and charge mobility was investigated to establish the relationship between crystal arrangements and inductive charging with the charge mobility.

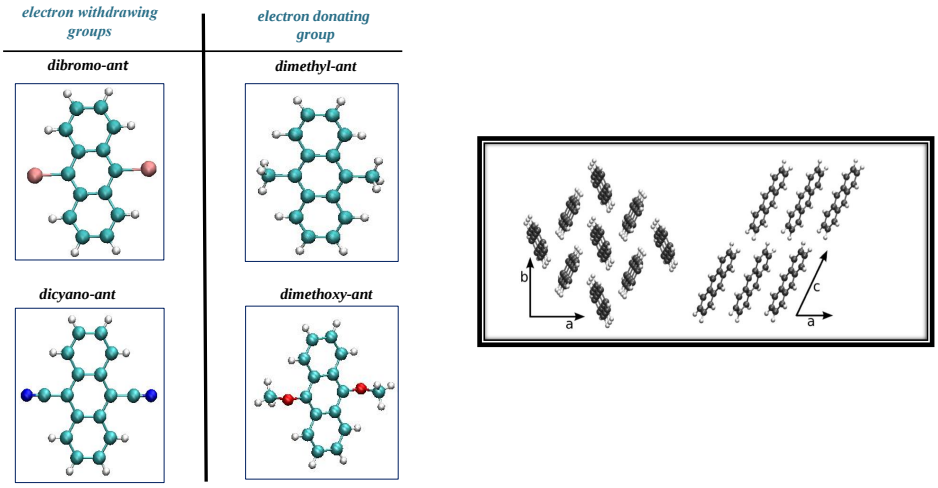

Figure 5.1.: Anthracene with dimethyl and dimethoxy as electron donor groups and dicyano and dibromo.

5.2. Simulation Details

The anthracene single crystal and its derivatives were simulated using a supercell comprising 20 × 20 × 20 unit cells. The starting coordinates were sourced from the crystal structure, and simulation conditions, including charge propagation, calculation of reorganization energy, and coupling methods, remained consistent with those employed in similar systems discussed in previous chapters.

5.3. Result and Discussion

Table 1 shows the results of the hole and electron coupling for the anthracene single crystal and its derivatives. To investigate the influence of both geometric and electronic properties on coupling, we conducted calculations with and without the substituent. In this process, we initially treated the substituent within the quantum mechanical (QM) domain and subsequently integrated it into the molecular mechanical (MM) component for analysis. This step allowed us to assess the coupling effect while considering the interplay between the substituent's electronic structure and its geometry in the system.

It can be seen from Fig. 5.2, and Fig. 5.3 that the coupling does not change dramatically in both electron and hole coupling for dimethyl, dimethoxy, and dicyano anthracene when the substitution is considered as the MM part and only anthracene is treated in the QM part, this means that the electronic effect is disregarded and the geometry plays an important role in the coupling. However, in the case of dibromo-anthracene , when bromine is neglected, the coupling changes significantly, and the role of the electronic effect can be observed.

The results show that the coupling in the b-direction is larger than in the a-direction, so we consider only the b-direction for the calculation of the electron and hole mobility. Table 5.4 and Table 5.5 show the values of mobility obtained with different values of reorganization energy calculated by different methods (DFT: B3LYP and ωB97XD functionals, Table 5.2 and 5.3). Both methods exhibit a consistent trend. It is well-established that minimizing the reorganization energy is imperative to achieve high carrier mobility. This optimization is crucial in enhancing the efficiency of the system's charge transport properties. In the instance of dimethoxy-ant, B3LYP and ωB97XD calculations reveal a substantial reorganization energy and a small coupling. As a result, we anticipate that the extent of charge transfer will be less than in other configurations. The high hole mobility for dicyano-ant can be explained considering the smallest reorganization energy as well as the largest coupling, compared to other structures. The reorganization energy was significantly reduced upon substitution of the CN group in anthracene, especially in the case of positive doping (hole hopping). The lowest reorganization energy of dicyano-anthracene can be attributed to the fact that the electrons were more localized at the CN group, especially at the nitrogen atom. Thus, the delocalized π-electrons in the aromatic backbone of dicyano-anthracene were relatively smaller than those in others. In the case of electron transfer, bromine increases the coupling in comparison with other structures and therefore, charge transfer is increased. It is shown that attaching the electron-withdrawing substituent at the proper position could improve the stability of the materials, enhance the electronic coupling and facilitate the hopping motions, efficiently. Adding bromine to this structure considerably alters the coupling, as observed when incorporating it within both the electron and hole MM components. This suggests that the halogen effect is crucial in comparing various structures and their impact on mobility.

Table 5.1.: Coupling for hole and electron transfer

(Hole)				(Electron)			
Material	Direction	Coupling (meV)	Site energy (eV)	Material	Direction	Coupling (meV)	Site energy (eV)
Anthracene	b	-66.00 ± 28.46	-3.22 ± 0.066	Anthracene	b	-19.64 ± 28.88	5.36.±0.047
	a	34.17 ± 23.64			a	38.15 ± 20.33	
Dimethyl-ant	b	-62.34 ± 34.07	-3.64 ± 0.065	Dimethyl-ant	b	-17.26 ± 40.38	5.68 ±0.051
	a	-4.82 ± 4.27			a	4.54 ± 2.83	
Dimethyl-mm	b	-89.00 ± 41.71	-3.74 ± 0.070	Dimethyl-mm	b	-19.59 ± 38.20	5.86 ±0.048
	a	-4.99 ± 4.30			a	5.25 ±3.28	
Dimethoxy-ant	b	22.57 ± 15.31	-3.45 ± 0.065	Dimethoxy-ant	b	-20.93 ± 7.09	5.44 ±0.068
	a	-6.15 ± 3.42			a	3.73 ± 2.83	
Dimethoxy-mm	b	-30.63±16.96	-3.73 ± 0.065	Dimethoxy-mm	b	-23.87 ± 12.91	5.86 ±0.047
	a	-6.03 ±3.52			a	-5.73 ± 2.80	
Dicyano-ant	b	-106.61 ± 109.83	-4.04 ± 0.110	Dicyano-ant	b	-39.17 ± 70.36	5.93 ±0.042
	a	8.92 ± 8.61			a	-9.95 ± 4.22	
Dicyano-mm	b	-113.08 ± 127.94	-3.75 ± 0.095	Dicyano-mm	b	-32.71 ±74.72	5.85 ±0.080
	a	1.51 ± 92.56			a	-9.86 ±3.84	
Dibromo-ant	b	-165.59 ± 56.30	-3.58 ± 0.067	Dibromo-ant	b	-39.24± 34.07	5.57 ±0.055
	a	7.14 ± 3.60			a	10.64 ± 6.54	
Dibromo-mm	b	-214.98 ± 62.82	-3.73 ± 0.069	Dibromo-ant	b	6.04 ± 49.98	5.86±0.054
	a	2.81 ±2.56			a	-2.63 ± 5.50	

Table 5.2.: Reorganization energies (in meV) for the electron transfer

Material	Direction	$\lambda_{\omega B97XD}$	λ_{B3LYP}
anthracene	b	215	198
dimethyl-ant	b	272	215
dimethoxy-ant	b	300	239
dicyano-ant	b	268	201
dibromo-ant	b	257	209

Table 5.3.: Reorganization energies (in meV) for the hole transfer

Material	Direction	$\lambda_{\omega B97XD}$	λ_{B3LYP}
anthracene	b	183	137
dimethyl-ant	b	211	149
dimethoxy-ant	b	371	366
dicyano-ant	b	163	106
dibromo-ant	b	239	176

Table 5.4.: Hole transfer calculation (in $cm^2V^{-1}s^{-1}$)

Material	Direction	FSSH	BCFSSH implicit DFT lambda (B3LYP)	BCFSSH implicit DFT lambda (ωB97XD)	IPR-BCFSSH implicit lambda (ωB97XD)	IPR-BCFSSH implicit lambda (B3LYP)
anthracene	b	4.48	2.27	1.35	1.28	1.63
dimethyl-ant	b	2.92	1.15	1.02	1.31	1.66
dimethoxy-ant	b	0.994	0.121	0.113	1.01	1.02
dicyano-ant	b	6.53	4.50	4.16	1.80	1.91
dibromo-ant	b	3.40	1.6	0.64	1.35	1.60

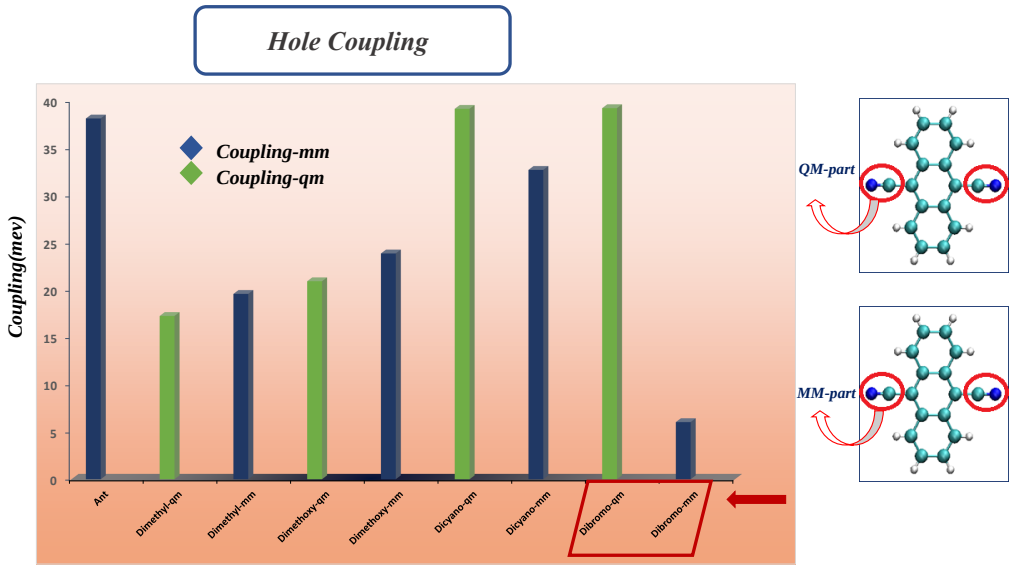

Figure 5.2.: Comparison between hole coupling in anthracene with dimethyl and dimethoxy as electron donor groups and dicyano and dibromo.

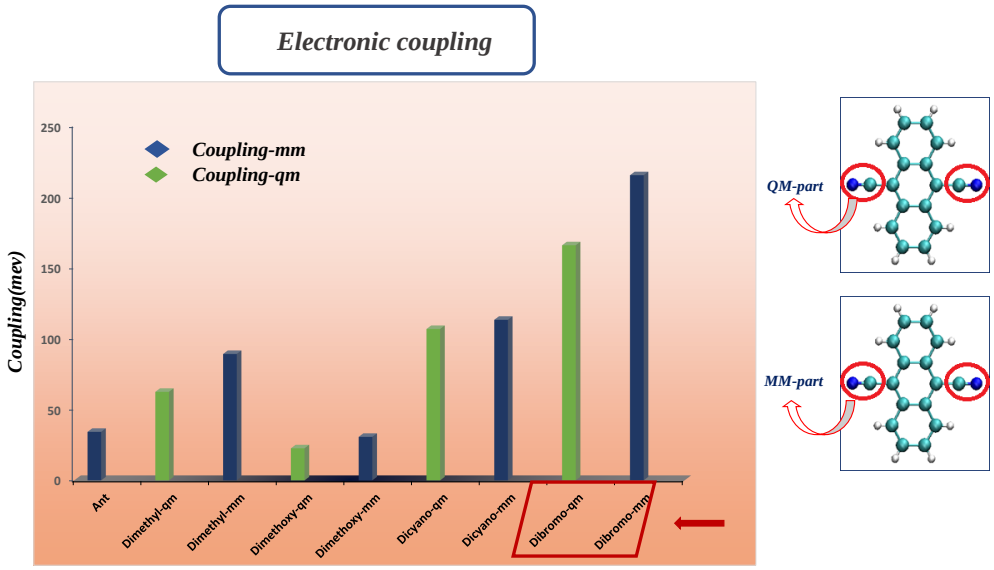

Figure 5.3.: Comparison between electron coupling in anthracene with dimethyl and dimethoxy as electron donor groups and dicyano and dibromo.

Table 5.5.: Electron transfer calculation (in $cm^2V^{-1}s^{-1}$)

Material	Direction	FSSH	BCFSSH implicit DFT lambda (B3LYP)	BCFSSH implicit DFT lambda (ωB97XD)	IPR-BCFSSH implicit lambda (ωB97XD)	IPR-BCFSSH implicit lambda (B3LYP)
anthracene	b	1.6	1.38	1.11	1.43	1.65
dimethyl-ant	b	4.03	3.38	2.45	1.50	1.8
dimethoxy-ant	b	3.64	1.10	0.977	1.04	1.13
dicyano-ant	b	6.30	4.55	3.82	2.18	2.60
dibromo-ant	b	8.87	6.41	4.86	3.23	3.71

5.4. Conclusion

In summary, we investigated the anthracene derivatives with and without electron-withdrawing and electron donating substituent theoretically.
In the results section of this part, the study delved into the significance of molecular conformation and electro-inductive effects using the QM-MM theory. The findings revealed that the presence of dibromo substituents led to electro-inductive effects, while other substituents influenced the molecular packing arrangement. Specifically, the research illustrated how electron-withdrawing or donating substituents could alter both reorganization energy and electronic coupling, thereby impacting charge transfer dynamics.

Notably, the analysis spotlighted Br-anthracene, distinguished by its two bromine substituents, as a standout example. This compound demonstrates proficient electron transport capabilities, boasting an impressive mobility value of $6.41 cm^2 V^{-1} s^{-1}$. This observation highlighted the profound influence that specific substituents wielded over electronic properties. It emphasized the potential for tailored designs, indicating a promising avenue for significantly enhancing charge carrier mobility in organic electronic devices.

Upon replacing the CN group in anthracene, a significant reduction in reorganization energy was observed. This effect was particularly prominent in the case of positive doping (hole hopping). Dicyano-anthracene exhibited the lowest reorganization energy due to enhanced electron localization at the CN group, specifically at the nitrogen atom. Consequently, the delocalization of π-electrons in the aromatic backbone of dicyano-anthracene was comparatively diminished when compared to other molecules. This suggests a distinctive electronic behavior in dicyano-anthracene, indicating potential applications in electronic devices.

6. Summary and Outlook

In this thesis, innovative tools have been introduced to delve into the intricate world of transport processes within molecular materials. These newly developed methods not only provide a fresh perspective on the study of transport but also offer practical applications. Some of these methodologies are specifically tailored to address challenges within the realm of transport processes.
The core focus of our research centers around the rigorous testing and validation of these methods on organic semiconducting materials, with a particular emphasis on organic crystals. Through systematic analysis, this study has paved the way for a deeper understanding of transport phenomena in these materials, opening doors to potential advancements in the field.
The thesis initiates by offering a comprehensive examination of the theoretical underpinnings, delving into the fundamental concepts of charge and energy transport. Within this framework, we explore the complexities of high and low mobility regimes, elucidating the methodologies employed to confront these distinct states. As the research unfolds, we meticulously assess the effectiveness of two different approximations utilized in simulating the charge transport process within representative organic materials. Remarkably, the mobilities predicted by our novel method align closely with experimental values, showcasing its potential for future research endeavors. This alignment not only validates the accuracy of our approach but also signals a promising avenue for advancing the field, underscoring the significance of our findings in the context of organic material science.
Additionally, our research delved deeply into the intricate relationship between substituents and their impact on electronic and charge transport properties. To unravel this complex interplay, we initiated our inquiry by examining the influence of halogen groups on the charge transport characteristics of n-type halogenated tetraazapentacenes (TAPs). Utilizing sophisticated molecular dynamics simulations, we meticulously calculated charge mobilities and rigorously compared them with experimental data.

Our meticulous analysis yielded significant revelations: while TAPs substituted with chlorine and bromine exhibited properties closely resembling those of their unaltered counterparts, the introduction of fluorine led to a marked reduction in charge mobility. This noteworthy disparity was attributed to the potent electron-withdrawing effect of fluoride, causing a decrease in electron transfer integrals and an increase in reorganization energy. These findings illuminate the intricate dynamics between specific substituents and charge mobility, enhancing our comprehension of the underlying mechanisms governing electronic transport in organic materials. The insights garnered from this investigation not only advance our

fundamental understanding of these processes but also offer crucial guidelines for the strategic design and optimization of organic semiconductors for diverse applications in the realm of materials science.
Moreover, we turned our attention to understanding the impact of substituents on charge mobilities in diphenylanthracene. To gain deeper insights into this phenomenon, we conducted meticulous calculations on anthracene, varying the electron donor and attractor groups. This detailed investigation extended to assessing their influence on reorganization energy, transfer integrals, and charge mobility. The objective was to establish a definitive relationship between the structural configurations and their resulting properties.

In our pursuit to discern the role of both geometrical and electronic properties in the coupling process, we conducted comprehensive analyses, considering the coupling with and without specific substituents. For anthracene derivatives like dimethyl, dimethoxy, and dicyano anthracene, where the substitution was treated as the molecular mechanics (MM) component and only anthracene was handled in the quantum mechanics (QM) portion, the geometric factors emerged as crucial determinants. In these instances, changes in geometry played a significant role, yet the coupling remained relatively stable.
However, a striking contrast emerged in the case of dibromo-anthracene. Here, when the influence of bromine was overlooked, the coupling exhibited significant alterations. This observation underscored the pivotal role of electronic effects, particularly the halogen effect, in comparing various structural configurations and their impact on mobility. These findings highlight the nuanced complexities of molecular interactions and emphasize the indispensable role of halogen substituents in shaping the mobility of organic materials. This revelation not only enriches our understanding of structure-property relationships but also offers valuable insights for the design and optimization of organic semiconductors tailored for specific applications. The discoveries presented in this study represent a significant step towards a more profound comprehension of charge transfer phenomena in organic semiconductor crystals (OSCs), with promising implications for future research endeavors. In essence, this comprehensive exploration of charge transfer mechanisms within OSCs has significantly deepened our understanding of their fundamental properties and behaviors. Our innovative blend of theoretical analyses and computational simulations, coupled with the development of novel methodologies, establishes a trajectory for future advancements in the realm of organic electronics. This progress not only opens doors for the creation of efficient and optimized materials but also offers a promising avenue for diverse applications within the field. As we conclude this study, we are poised at the forefront of groundbreaking discoveries, ready to usher in a new era of advancements in organic electronic technology.

Bibliography

[1] A. Kalaria and A Kumar. “Organic materials in electronics: recent achievements in energy transport and charge carrier mobility. Journal of Materials Chemistry”. In: *Journal of Materials Chemistry C, 5(48), 12531-12549.* (2017).

[2] J. Gao et al. “Molecular design of organic materials for high-performance organic field-effect transistors and solar cells.” In: *Physical Chemistry Chemical Physics, 23(13), 7594-7604* (2021).

[3] L. Chi et al. “From molecular design to electronic structure engineering: towards efficient organic solar cells.” In: *Journal of Materials Chemistry A, 7(1), 263-291* (2019).

[4] S. R. Forrest. “Recent Advances in Organic Semiconductor Materials for Optoelectronics and Energy Conversion.” In: *The path to ubiquitous and low-cost organic electronic appliances on plastic.* (2004).

[5] J. Wang et al. “Recent Advances in Organic Semiconductor Materials for Optoelectronics and Energy Conversion.” In: *Small Methods, 2(5), 1700394.* (2018).

[6] Neupane M et al. “Observation of the spin-polarized surface state in a noncentrosymmetric superconductor BiPd.” In: *Nature communications. 7and7(1):13315.* (2016).

[7] J. Rawson and H. Jang. “Molecular Structure-Property Relationships in Organic Electronic Materials.” In: *Chemical Reviews, 119(10), 6994-7044* (2019).

[8] M. Liu, S. Jin, and F Zhang. “Conjugated Organic Materials for Optoelectronic Applications: Design, Synthesis and Devices”. In: *Chemical Society Reviews, 49(15), 5474-5499.* (2020).

[9] V. A. Volkov, T. S. Perova, and A. P Demchenko. “Organic Semiconductors for Optoelectronics: Advances in Molecular Design, Crystallization, and Processing.” In: *Advanced Optical Materials, 7(20), 1900504.* ().

[10] M. Tadaccini et al. “. Organic Semiconductor Crystals: A Versatile Class of Materials for Optoelectronic”. In: *s. Advanced Materials, 30(39), 1707034.* (2018).

[11] T. Kato. “Crystal Growth of Organic Semiconductors: Progress to Date and Future Perspectives”. In: *Journal of Physical Chemistry Letters, 10(14), 4111-4121* (2019).

[12] Ziyi Han et al. “Recent advances in the controlled chemical vapor deposition growth of bilayer 2D single crystals”. In: *Materials Chemistry C, 10(37), 13324-13350* (2022).

[13] Q. Zhang, Sirringhaus Hu W., and K H. Müllen. “Recent progress in emerging organic semiconductors”. In: *Advanced materials (Deerfield Beach, Fla.), 34(22), e2108701* (2022).

[14] J. Yoo, T. Lee, and J. Lee. “Recent Advances in Organic Semiconductor Crystals for High-Performance Electronic and Optoelectronic Devices.” In: *Advanced Materials, 33(29), 2005622* (2021).

[15] X. Zhang, J. Wang, and H Yan. “Recent advances in enhancing charge carrier mobility in organic semiconductor crystals.” In: *Advanced Materials,31(24), 1807032* (2019).

[16] H. Ishii et al. “Charge mobility calculation of organic semiconductors without use of experimental single-crystal data”. In: *Scientific Reports, 10(1), 2524.* (2020).

[17] S. Ghosh, T. Chakraborty, and D. K. Palit. “Organic Semiconductor Materials for Electronic Devices:” in: *A Review. International Journal of Electronics, 107(9), 1509-1529.* (2020).

[18] L. Vila-Nadal, J. López-Andarias, and L. Echegoyen. “Advances in Organic Electronic Materials and Devices: Towards Sustainable, Intelligent, and Flexible Solutions.” In: *Chemical Society Reviews, 45(23), 6659-6727* (2016).

[19] H. Lin, J. Zheng, and H. Yan. “High mobility organic semiconductor crystals: Synthesis, characterization, and applications.” In: *Journal of Materials Chemistry C, 8(42), 14603-14620.* (2020).

[20] R. Ameloot and M. E. Gershenson. “Organic semiconductor crystals: From fundamental understanding to device applications.” In: *Chemical Society Reviews, 48(17), 4646-4664.* (2019).

[21] L. K. Pandey, H. Kim, and S. Park. “Recent advances in organic semiconductor crystals for high-performance field-effect transistors.” In: *Journal of Materials Chemistry C, 6(31), 8295-8320.* (2018).

[22] Yingfeng Wang et al. “High-performance organic field-effect transistors based on single-crystalline microribbons of a two-dimensional fused heteroarene semiconductor”. In: *Chemical Communications, 51(60), 11961-11963.* (2015).

[23] E. M. Kester, F. C. Grozema, and R. W. Havenith. “Mobility measurements on organic semiconductor thin films: Impact of interpretation methods.” In: *Organic Electronics, 55, 242-249* (2018).

[24] S. Park et al. “Mobility of organic semiconductor crystals and its impact on electronic devices.” In: *Journal of Materials Chemistry C, 7(19), 5533-5552.* (2019).

[25] E. Fabiano and M. Berggren. "Organic electronics and organics-based sensors: Overview and developments." In: *Journal of Materials Chemistry C, 6(43), 11557-11579* (2015).

[26] Y. H. Lee, J. Y. Lee, and S. H. Park. "Recent progress in the development of high-performance organic light-emitting diodes.conductors. ." In: *Journal of Materials Chemistry C, 6(6), 1203-1224.* (2018).

[27] D. P. Singh, R. K. Singh, and S. P. Singh. "Organic semiconductors: Development and perspective towards electronic devices." In: *Journal of Materials Chemistry C, 4(14), 2820-2833* (2016).

[28] A. Heck et al. "Multi-scale approach to non-adiabatic charge transport in high-mobility organic semiconductors." In: *Journal of chemical theory and computation. 10and11(11):5068-82* (2015).

[29] J. F. Janak. "Proof that Eni= in density-functional theory". In: *Phys. Rev. B, 18(12):7165,* (1978).

[30] R. Stowasser and R. Hoffmann. "What do the kohn-sham orbitals and eigenvalues mean?J." In: *Am. Chem. Soc., 121(14):3414–3420,* (1999).

[31] L. H. Thomas. "The calculation of atomic fields. I". In: *n Math. Proc. Cambridge Philos. Soc.,volume 23, pages 542–548. Cambridge University Press,* (1927).

[32] E. Fermi. "Un metodo statistico per la determinazione di alcune priorieta dell'atome." In: *Red. Accad. Naz. Lincei, 6(602-607):32, 1927* (1927).

[33] R. Van Noorden, B. Maher., and R. Nuzzo. "The top 100 papers." In: *Nature, 514(7524):550,* (2014).

[34] W. Kohn and L. J. Sham. "Self-consistent equations including exchange and correlationeffects". In: *Phys. Rev., 140(4A):A1133* (1965).

[35] P. A. M. Dirac. "Note on exchange phenomena in the thomas atom". In: *MathematicalProceedings of the Cambridge Philosophical Society, volume 26, pages 376–385. Cambridge University Press,* (1930).

[36] D. M. Ceperley and B. J. Alder. "Ground state of the electron gas by a stochastic method". In: *Phys. Rev. Lett., 45(7):566,* (1980).

[37] J. P. Perdew, K. Burke, and M. Ernzerhof. "Generalized gradient approximation madesimple." In: *Phys. Rev. Lett., 77(18):3865,* (1996).

[38] J. P. Perdew, M. Levy R. G. Parr, and J. L. Balduz Jr. "Density-functional theory forfractional particle number: derivative discontinuities of the energy." In: *Phys. Rev. Lett., 49(23):1691, 1982.* (1982).

[39] J. P. Perdew, M. Ernzerhof, and K. Burke. J. "Rationale for mixing exact exchange withdensity functional approximations." In: *Chem. Phys., 105(22):9982–9985,* (1996).

[40] C. Adamo and V. Barone. "Toward reliable density functional methods without adjustableparameters: The pbe0 model." In: *Chem. Phys., 110:6158,* (1999).

[41] A. c. Becke. "Density-functional exchange-energy approximation with correct asymptotic behavior." In: *Phys. Rev. A, 38(6):3098,* (1988).

[42] C. Lee, W. Yang, and R. G. Parr. "Development of the colle-salvetti correlation-energyformula into a functional of the electron density." In: *Phys. Rev. B, 37(2):785,* (1988).

[43] P. J. Stephens et al. "Ab initio calculationof vibrational absorption and circular dichroism spectra using density functional forcefields." In: *Phys. Chem., 98(45):11623–11627,* (1994).

[44] D. Porezag et al. "Construction oftight-binding-like potentials on the basis of density-functional theory: Application tocarbon." In: *Phys. Rev. B, 51(19):12947,* (1995).

[45] M. Elstner et al. "Self-consistent-charge density-functional tight-binding method for simulations of complex materials properties." In: *Phys. Rev. B, 58(11):7260,* (1998).

[46] Q. Cui M. Gaus and M. Elstner. "Dftb3: extension of the self-consistent-charge densityfunctional tight-binding method (scc-dftb)." In: *Chem. Theory Comput., 7(4):931–948,* (2011).

[47] R. S. Mulliken. "Electronic population analysis on lcao–mo molecular wave functions." In: *Chem. Phys., 23(10):1833–1840,* (1955).

[48] B. Hess et al. "Gromacs 4: algorithms for highlyefficient, load-balanced, and scalable molecular simulation." In: *Chem. Theory Comput., 4(3):435–447,* (2008).

[49] S. P. Goel R. W. Hockney and J. W. "Eastwood. Quiet high-resolution computer modelsof a plasma." In: *Comput. Phys., 14(2):148–158,* (1974).

[50] S. Nose and M. L. Klein. "Constant pressure molecular dynamics for molecular systems". In: *.Mol. Phys., 50(5):1055–1076,* (1983).

[51] W. G. Hoover. "Canonical dynamics: equilibrium phase-space distributions." In: *Phys. Rev.A, 31(3):1695,* (1985).

[52] M. Parrinello and A. Rahman. "Polymorphic transitions in single crystals: A new molecular dynamics method." In: *Appl. Phys., 52(12):7182–7190,* (1981).

[53]] T. Holstein. "Studies of polaron motion: Part i. the molecular-crystal model." In: *.Ann. Phys.,8(3):325–342,* (1959).

[54] K. Hannewald et al. "Theory of polaron bandwidth narrowing in organic molecular crystals." In: *Phys.Rev. B, 69(7):075211,* (2004).

[55] A. Troisi. . "Prediction of the absolute charge mobility of molecular semiconductors: thecase of rubrene". In: *Adv. Mat., 19(15):2000–2004,* (2007).

[56] R. P. Fornari, J. Arago, and A. Troisi. "A very general rate expression for charge hoppingin semiconducting polymers." In: *Chem. Phys., 142(18):184105,* (2015).

[57] B. S. Brunschwig, M. D. Newton J. Logan, and N. Sutin. "A semiclassical treatmentof electron-exchange reactions. application to the hexaaquoiron (ii)-hexaaquoiron (iii)system." In: *Am. Chem. Soc., 102(18):5798–5809,* (1980).

[58] M. D. Newton and N. Sutin. "Electron transfer reactions in condensed phases." In: *Rev.Phys. Chem., 35(1):437–480,* (1984).

[59] A. Warshel. "Dynamics of reactions in polar solvents. semiclassical trajectory studies ofelectron-transfer and proton-transfer reactions." In: *Phys. Chem., 86(12):2218–2224, 1982* (1982).

[60] L. D. Zusman. "Outer-sphere electron transfer in polar solvents." In: *Chem. Phys., 49(2):295–304,* (1980).

[61] L. D. Landau. Zur. "theorie der energieubertragung." In: *Phys. Z. Sowjetunion, 2(46):1–13,1932.* (1932).

[62] C. Zener. "Non-adiabatic crossing of energy levels. In Proc." In: *Royal Soc. London A, volume137, pages 696–702.* (1932).

[63] A. Carof J. Spencer L. Scalfi and J. Blumberger. "Confronting surface hopping molecular dynamics with marcus theory for a molecular donor–acceptor system." In: *Faraday disc.,195:215–236,* (2017).

[64] J. J. Kwiatkowski et al. "Simulatingcharge transport in tris (8-hydroxyquinoline) aluminium (alq 3)." In: *Phys. Chem. Chem.Phys., 10(14):1852–1858,* (2008).

[65] P. Friederich et al. "Molecular origin of the charge carrier mobility in small molecule organic semiconductors." In: *Adv. Mat., 26(31):5757–5763* (2016).

[66] P. Kordt et al. "Modeling of organic light emitting diodes: From molecular to device properties." In: *Adv. Mat., 25(13):1955–1971,* (2015).

[67] V. Ruhle et al. "Microscopic simulations of charge transport in disordered organicsemiconductors." In: *Chem. Theory Comput., 7(10):3335* (2011).

[68] V. Stehr et al. "Singlet exciton diffusion inorganic crystals based on marcus transfer rates." In: *Chem. Theory Comput., 10(3):1242–1255,* (2014).

[69] T. Foerster. "Zwischenmolekulare energiewanderung und fluoreszenz." In: *Phys., 437(1-2):55–75, 1948.* (1984).

[70] Mikhnenko et al. "Exciton diffusion in organic semiconductors." In: *Energy Environ. Sci., 8(7):1867–1888,* (2015).

[71] F. Bloch. "Über die quantenmechanik der elektronen in kristallgittern." In: *Phys. A, 52(7):555–600,* (1929).

[72] C. Kittel. "Introduction to solid state physics." In: *Wiley* (2005).

[73] M. Elstner and G. Seifert. "Density functional tight binding. Philos. Trans." In: *R. Soc., A, 372, 20120483* (2014).

[74] M. Gaus, Q. Cui, and M. Elstner. "Density functional tight binding: application to organicand biological molecules." In: *WIREs Comput. Mol. Sci. 4, 49–61* (2014).

[75] A. Kubas et al. "Electronic couplings for molecular charge transfer: Benchmarking CDFT, FODFT, andFODFTB against high-level ab initio calculations." In: *J. Chem. Phys. 140, 104105* (2014).

[76] A. Kubas et al. "Electronic couplings for molecular charge transfer: benchmarking CDFT, FODFT and FODFTBagainst high-level ab initio calculations. II." In: *Phys. Chem. Chem. Phys. 17, 14342–14354,* (2015).

[77] J. C. Tully. "Molecular dynamics with electronic transitions." In: *J. Chem. Phys. 93,1061–1071* (1990).

[78] A. Carof, S. Giannini, and Blumberger. "Detailed balance, internal consistency, andenergy conservation in fragment orbital-based surface hopping." In: *J. Chem. Phys.. ,147, 214113.* (2017).

[79] M. Malagoli et al. "L. A multimode analysisof the gas-phase photoelectron spectra in oligoacenes." In: *J. Chem. Phys 120, 7490–7496* (2004).

[80] J. Brédas et al. "Charge-transfer and energytransfer processes in -conjugated oligomers and polymers: a molecular picture". In: *Chem.Rev. 104, 4971–5004* (2004).

[81] A. V. Akimov and O. V. Prezhdo. "The PYXAID program for non-adiabatic moleculardynamics in condensed matter systems." In: *J. Chem. Theory Comput. 9, 4959–4972* (2013).

[82] W. Li et al. "Influence of Defects on Excited-State Dynamics in Lead Halide Perovskites: Time-Domain ab Initio Studies." In: *Phys. Chem.Lett. 10, 3788–3804* (2019).

[83] T. Kubar and M. Elstner. "Coarse-grained time-dependent density functional simulationof charge transfer in complex systems: application to hole transfer in DNA." In: *J. Phys.Chem. B 114, 11221–11240.* (2010).

[84] N. A. Minder et al. "Band-Like Electron Transport in Organic Transistors and Implication of the Molecular Structure forPerformance Optimization." In: *Adv. Mater. 24, 503–508* (2012).

[85] A. Troisi. "Charge transport in high mobility molecular semiconductors: classical modelsand new theories." In: *Chem. Soc. Rev. 40, 2347–2358.* (2011).

[86] F. C. Grozema and L. D. Siebbeles. "Mechanism of charge transport in self-organizingorganic materials." In: *Int.Rev. Phys. Chem. 27, 87–138* (2008).

[87] M. Gershenson, V. Podzorov, and A. Morpurgo. "Colloquium: Electronic transport insingle-crystal organic transistors." In: *Rev. Mod. Phys. 78, 973* (2006).

[88] C. Poelking et al. "Characterization of charge-carrier transport in semicrystalline polymers:electronic couplings, site energies, and charge-carrier dynamics in poly (bithiophenealt-thienothiophene)[PBTTT]." In: *J. Phys. Chem. C , 117, 1633–1640.* (2013).

[89] P. Friederich et al. "Ab initio treatmentof disorder effects in amorphous organic materials: Toward parameter free materialsimulation.s". In: *J. Chem. Theory Comput. 10, 3720–3725* (2014).

[90] V. Rühle, J. Kirkpatrick, and D. Andrienko. "A multiscale description of charge transportin conjugated oligomers." In: *J. Chem. Phys. 2010, 132, 134103.* (2010).

[91] V. Marcon et al. "Understanding structure- mobility relations for perylenetetracarboxydiimide derivatives." In: *J. Am. Chem. Soc. 2009, 131, 11426–11432.* (2009).

[92] A. Heck, J. J. Kranz, and M. Elstner. "Simulation of temperature-dependent charge transport in organic semiconductors with various degrees of disorder." In: *J. Chem. Theory Comput. 12, 3087–3096.* (2016).

[93] W. Xie et al. "Performance of Mixed Quantum-ClassicalApproaches on Modeling the Crossover from Hopping to Bandlike Charge Transport inOrganic Semiconductors". In: *J. Chem. Theory Comput., 16, 2071–2084* (2020).

[94] S. Giannini et al. "Quantum localization and delocalization of charge carriers in organic semiconductingcrystals." In: *Nat. Commun. 10, 1–12.* (2019).

[95] O. V. Prezhdo. "Mean field approximation for the stochastic Schrödinger equation." In: *J.Chem. Phys. 111, 8366–8377* (1999).

[96] A. V. Akimov, R. Long, and O. V. Prezhdo. "Coherence penalty functional". In: *Chem. Phys, 140,194107* (2014).

[97] A. Bastida et al. "A modified Ehrenfest methodthat achieves Boltzmann quantum state populations." In: *Chem. Phys. Lett. 417, 53–57* (2006).

[98] U. Müller and G. Stock. "Surface-hopping modeling of photoinduced relaxation dynamicson coupled potential-energy surfaces." In: *J. Chem. Phys. 107, 6230–6245* (1997).

[99] G. Granucci and M. Persico. "Critical appraisal of the fewest switches algorithm for surfacehopping." In: *J. Chem. Phys. 126, 134114* (2007).

[100] L. Wang and O. V. Prezhdo. "A simple solution to the trivial crossing problem in surfacehopping." In: *J. Phys. Chem. Lett. 5, 713–719* (2014).

[101] C. Brueckner and B. Engels. "A theoretical description of charge reorganization energies inmolecular organic P-type semiconductors." In: *J. Comput. Chem. 37, 1335–1344.* (2016).

[102] M. J. Abraham et al. ".GROMACS: High performance molecular simulations through multi-level parallelismfrom laptops to supercomputers." In: *SoftwareX 2015, 1–2, 19–25* (2015).

[103] H. J. C. Berendsen, D. van der Spoel, and R. van Drunen. “GROMACS:A message-passingparallel molecular dynamics implementation.” In: *Comput. Phys. Commun. 1995, 91, 43–56* (2015).

[104] J. Wang et al. “Automatic atom type and bond typeperception in molecular mechanical calculations.” In: *J. Mol. Graphics Modell. 25,247 – 260* (2006).

[105] J. Wang et al. “Development andtesting of a general amber force field.” In: *Comput. Chem. 25, 1157–1174* (2004).

[106] U. C. Singh and P. A. Kollman. “An approach to computing electrostatic charges formolecules”. In: *J. Comput. Chem. 5, 129–145* (1984).

[107] B. H. Besler, K. M. Merz, and P. A Kollman. “Atomic charges derived from semiempiricalmethods”. In: *.J. Comput. Chem. 11, 431–439* (1990).

[108] G. A. Petersson et al. “A complete basis set model chemistry. I. The total energies of close-shellatoms and hydrides of the first-row elements.” In: *J. Chem. Phys 89, 2193–2218* (1988).

[109] G. A. Petersson and M. A. Al-laham. “A complete basis set model chemistry. II. Openshell systems and the total energies of the first-row atoms.” In: *J. Chem. Phys, 94,6081–6090* (1991).

[110] M. J. Frisch et al. “Gaussian 09and Gaussian,” in: *nc.: Wallingford, CT, USA,* (2009).

[111] D. J. Evans and B. L. Holian. “The Nose-Hoover thermostat.” In: *Chem. Phys. 83,4069* (1985).

[112] S. Ciuchi, S. Fratini, and D. Mayou. “Transient localization in crystalline organic semiconductors.” In: *Phys. Rev. B, 83, 081202.* (2011).

[113] S. Fratini et al. “A map of highmobility molecular semiconductors.” In: *A. Nat. Mater. 16, 998–1002* (2017).

[114] T. Nematiaram et al. “A. Practical computation ofthe charge mobility in molecular semiconductors using transient localization theory.” In: *J.Phys. Chem. C , 123, 6989–6997.* (2019).

[115] B. Shan and Q. Miao. “"Molecular design of n-type organic semiconductors for high-performance thin film transistors"”. In: *Tetrahedron Letters, 58(20), 1903-1911* (2017).

[116] Y. Yuan et al. “"Ultra-high mobility transparent organic thin film transistors grown by an off-centre spin-coating method"”. In: *Nature communications, 5(1), 3005* (2014).

[117] B. H. Lee et al. “Flexible organic transistors with controlled nanomorphology”. In: *Nano letters* (2016).

[118] Ming Chu et al. “Halogenated Tetraazapentacenes with Electron Mobility as High as 27.8 cm2 V- 1 s- 1 in Solution-Processed n-Channel Organic Thin-Film Transistors”. In: *Advanced Materials* 30.38 (2018), p. 1803467.

[119] Uwe HF Bunz et al. "Large N-Heteroacenes: New Tricks for Very Old Dogs?" In: *Angewandte Chemie International Edition* 52.14 (2013), pp. 3810–3821.

[120] Qian Miao. "Ten Years of N-Heteropentacenes as Semiconductors for Organic Thin-Film Transistors". In: *Advanced Materials* 26.31 (2014), pp. 5541–5549.

[121] Guobiao Xue et al. "Boosting the electron mobility of solution-grown organic single crystals via reducing the amount of polar solvent residues". In: *Materials Horizons* 3.2 (2016), pp. 119–123.

[122] Xiaomin Xu et al. "Electron mobility exceeding 10 cm2 V- 1 s- 1 and band-like charge transport in solution-processed n-channel organic thin-film transistors". In: *Advanced Materials* 28.26 (2016), pp. 5276–5283.

[123] Jens U Engelhart et al. "Halogenated symmetrical tetraazapentacenes: Synthesis, structures, and properties". In: *The Journal of organic chemistry* 81.3 (2016), pp. 1198–1205.

[124] Hilmar Reiss et al. "Bromination improves the electron mobility of tetraazapentacene". In: *Angewandte Chemie International Edition* 57.30 (2018), pp. 9543–9547.

[125] Bhat Vinayak, Connor P. Callaway, and Chad Risko. "Computational Approaches for Organic Semiconductors: From Chemical and Physical Understanding to Predicting New Materials." In: *Chemical Reviews* (2023).

[126] Cowen and Lewis Matthew. "N-type organic semiconductors and conductors for plastic electronics." In: *Diss. UCL (University College London),* (2021).

[127] C. Li et al. "Rational design of donor–acceptor conjugated polymers for organic solar cells". In: *Journal of Materials Chemistry A, 8(7), 3514-3529.* (2020).

[128] L. Wang et al. "upramolecular doping of organic semiconductors with aromatic amino acids for high-performance organic field-effect transistors." In: *Journal of Materials Chemistry C, 7(34), 10538-10545.* (2019).

[129] L. Chen et al. "Anthracene-Based Nanocomposite for High-Performance Sodium-Ion Batteries." In: *Advanced Materials, 24(16), 2034-2039.* (2012).

[130] N. Tansu and S. Y. Karpov. "Anthracene–based materials for optoelectronic applications." In: *Journal of Physics D.Applied Physics, 51(48), 483001.* (2018).

[131] S. Chai, S. H. Wen, and K. L. Han. "Understanding electron-withdrawing substituent effect on structural, electronic and charge transport properties of perylene bisimide derivatives." In: *Organic electronics, 12(11), 1806-1814.* (2011).

[132] W. Xie et al. "Enhancing the Field-Effect Mobility of Anthracene-Based Semiconductors by Incorporating a Nitrogen-Containing Heteroaromatic Unit." In: *Chemistry -A European Journal, 25(50), 11880-11885* (2019).

[133] J. W. Park et al. “Emergence of a new molecular design strategy for organic semiconductors: The effect of peripheral substitution on the charge mobility.” In: *Journal of Materials Chemistry C, 9(7), 2315-2320* (2021).

[134] B. Koo, H. Kim, and D. 2021 Kim. “Molecular Design of Organic Semiconductors for High-Performance Solution-Processed Thin-Film Transistors.” In: *Advanced Science, 8(6), 2002271* (2021).

[135] G. Rambabu, S. K. Maity, and A. Karim. “Impact of substituent diversity on the electrochemical properties of triptycene-based molecular systems.” In: *Journal of Molecular Structure, 1203, 127398* (2020).

[136] S. Tanaka et al. “Effect of Anthracene Core Substituent on the Optical and Electrical Properties of Organic Semiconductors.” In: *The Journal of Physical Chemistry C, vol. 122, no. 49,, pp. 28054-28061* (2018).

[137] P. Naumov et al. “Crystal engineering of anthracene derivatives: from columnar structures to carbon dots.” In: *Chemical Communications, vol. 56, no. 9,, pp. 1361-1374.* (2020).

[138] T. Miyamoto and H. Yamamoto. “"Tuning the molecular packing structure of anthracene-based organic semiconductors for boosting charge mobility."” In: *Chemical Society Reviews, vol. 47, no. 17, pp. 6514-6526.* (2018).

[139] E. Martín-Martínez, J. E. Ortega, and H. Míguez. “Advances in characterization methods for the determination of charge carrier mobility in organic semiconductors.” In: *Advanced Materials, 28(33), 6806-6843* ().

[140] P. Hohenberg and W. Kohn. “Inhomogeneous electron gas”. In: *Phys. Rev., 136(3B):B864,* (1964).

[141] E. H. Lieb. “Density functionals for coulomb systems.” In: *Quant. Chem., 24(3):243–277,* (1983).

[142] B. Aradi V. Lutsker and T. A. Niehaus. “Implementation and benchmark of a longrange corrected functional in the density functional based tight-binding method.” In: *Chem.Phys., 143(18):184107,* (2015).

[143] L. Wilk S. H. Vosko and M. Nusair. “Accurate spin-dependent electron liquid correlationenergies for local spin density calculations: a critical analysis. Canadian”. In: *Phys., 58(8):1200–1211,* (1980).

[144] J. P.Perdew and A. Zunger. P. “Self-interaction correction to density-functional approximations for many-electron systems.” In: *Phys. Rev. B, 23(10):5048,* (1981).

[145] J. P. Perdew and Y. Wang. A. “ccurate and simple analytic representation of the electron-gascorrelation energy.” In: *Phys. Rev. B, 45(23):13244, 1992.* (1992).

[146] Y. Maeda H. Sekino and M. Kamiya. . “Influence of the long-range exchange effect ondynamic polarizability”. In: *Mol. Phys., 103(15-16):2183–2189,* (2005).

[147] M. E. Casida and M. Huix-Rotllant. ". Progress in time-dependent density-functional theory." In: *Annu. Rev. Phys. Chem., 63:287,* (2012).

[148] M. E. Casida. "Recent Advances in Density Functional Methods, Part I, chapter Timedependent Density Functional Response Theory for Molecules," in: *WorldScientific, Singapore, pages 155–192.* (1995).

[149] . Furche and R. Ahlrichs. "Adiabatic time-dependent density functional methods forexcited state properties". In: *Chem. Phys., 117(16):7433–7447,* (2002).

[150] T. A. Niehaus and F. Della Sala. "Range separated functionals in the density functionalbased tight-binding method: Formalism". In: *Phys. Status Solidi B, 249:237,* (2012).

[151] R. Baer and D. Neuhauser. "Density functional theory with correct long-range asymptoticbehavior." In: *Phys. Rev. Lett., 94:043002,* (2005).

[152] E. Livshits and R. Baer. "A well-tempered density functional theory of electrons inmolecules." In: *Phys. Chem. Chem. Phys., 9:2932–2941,* (2007).

[153] S. Nose. . "A molecular dynamics method for simulations in the canonical ensemble". In: *Mol.Phys., 52(2):255–268, 14* (1984).

[154] T. Kubař and M. Elstner. "A hybrid approach to simulation of electron transfer in complexmolecular systems." In: *R. Soc., Interface. 10, 20130415* (2013).

[155] H. Oberhofer, K. Reuter, and J. Blumberger. "Charge transport in molecular materials: Anassessment of computational methods." In: *Chem. Rev. , 117, 10319–10357* (2017).

[156] Q. Liu, S. E. Bottle, and P. Sonar. "Developments of diketopyrrolopyrrole-dye-based organic semiconductors for a wide range of applications in electronics". In: *Advanced Materials, 32(4), 1903882.* (2020).

[157] Dezhi Yang and Dongge Ma. "Development of organic semiconductor photodetectors: from mechanism to applications". In: *Advanced optical materials* 7.1 (2019), p. 1800522.

[158] Chengliang Wang et al. "Organic semiconductor crystals". In: *Chemical Society Reviews* 47.2 (2018), pp. 422–500.

[159] Xike Gao and Zheng Zhao. "High mobility organic semiconductors for field-effect transistors". In: *Science China Chemistry* 58 (2015), pp. 947–968.

[160] Ran Ding et al. "Organic Single-Crystalline Semiconductors for Light-Emitting Applications: Recent Advances and Developments". In: *Laser Photonics Reviews* 13.10 (2019), p. 1900009.

[161] Chi Y Cheng, Josh E Campbell, and Graeme M Day. "Evolutionary chemical space exploration for functional materials: computational organic semiconductor discovery". In: *Chemical science* 11.19 (2020), pp. 4922–4933.

[162] Yingjian Yu et al. "An n-type all-fused-ring molecule with narrow bandgap". In: *CCS Chemistry* 5.2 (2023), pp. 486–496.

[163] Daniel William Davies et al. "Radically Tunable n-Type Organic Semiconductor via Polymorph Control". In: *Chemistry of Materials* 33.7 (2021), pp. 2466–2477.

[164] Jesse TE Quinn et al. "Recent progress in the development of n-type organic semiconductors for organic field effect transistors". In: *Journal of Materials Chemistry C* 5.34 (2017), pp. 8654–8681.

[165] Alexander Heck, Julian J Kranz, and Marcus Elstner. "Simulation of temperature-dependent charge transport in organic semiconductors with various degrees of disorder". In: *Journal of Chemical Theory and Computation* 12.7 (2016), pp. 3087–3096.

[166] Julian J Kranz and Marcus Elstner. "Simulation of singlet exciton diffusion in bulk organic materials". In: *Journal of chemical theory and computation* 12.9 (2016), pp. 4209–4221.

[167] Weiwei Xie et al. "Performance of Mixed Quantum-Classical Approaches on Modeling the Crossover from Hopping to Bandlike Charge Transport in Organic Semiconductors". In: *Journal of Chemical Theory and Computation* 16.4 (2020), pp. 2071–2084.

[168] Alessandro Troisi. "Dynamic disorder in molecular semiconductors: Charge transport in two dimensions". In: *The Journal of chemical physics* 134.3 (2011), p. 034702.

[169] Samuele Giannini et al. "Quantum localization and delocalization of charge carriers in organic semiconducting crystals". In: *Nature Communications* 10.1 (2019), p. 3843.

[170] Oliver Schalk et al. "Competition between ring-puckering and ring-opening excited state reactions exemplified on 5H-furan-2-one and derivatives". In: *The Journal of Chemical Physics* 152.6 (2020), p. 064301.

[171] Sara Roosta et al. "Efficient surface hopping approach for modeling charge transport in organic semiconductors". In: *Journal of Chemical Theory and Computation* 18.3 (2022), pp. 1264–1274.

[172] Junmei Wang et al. "Development and testing of a general amber force field". In: *Journal of computational chemistry* 25.9 (2004), pp. 1157–1174.

[173] Junmei Wang et al. "Automatic atom type and bond type perception in molecular mechanical calculations". In: *Journal of molecular graphics and modelling* 25.2 (2006), pp. 247–260.

[174] U Chandra Singh and Peter A Kollman. "An approach to computing electrostatic charges for molecules". In: *Journal of computational chemistry* 5.2 (1984), pp. 129–145.

[175] Brent H Besler, Kenneth M Merz Jr, and Peter A Kollman. "Atomic charges derived from semiempirical methods". In: *Journal of computational chemistry* 11.4 (1990), pp. 431–439.

[176] aGA Petersson et al. "A complete basis set model chemistry. I. The total energies of closed-shell atoms and hydrides of the first-row elements". In: *The Journal of chemical physics* 89.4 (1988), pp. 2193–2218.

[177] A Frisch et al. "gaussian 09W Reference". In: *Wallingford, USA, 25p* 470 (2009).

[178] Denis J Evans and Brad Lee Holian. "The nose–hoover thermostat". In: *The Journal of chemical physics* 83.8 (1985), pp. 4069–4074.

[179] Herman JC Berendsen, David van der Spoel, and Rudi van Drunen. "GROMACS: A message-passing parallel molecular dynamics implementation". In: *Computer physics communications* 91.1-3 (1995), pp. 43–56.

[180] Mark James Abraham et al. "GROMACS: High performance molecular simulations through multi-level parallelism from laptops to supercomputers". In: *SoftwareX* 1 (2015), pp. 19–25.

[181] Ke. Pei. "Recent Advances in Molecular Doping of Organic Semiconductors". In: *Surfaces and Interfaces : 101887.* (2022).

[182] Ali R. "Dithieno [3, 2-b: 2, 3-d] thiophene (DTT): an emerging heterocyclic building block for future organic electronic materials and functional supramolecular chemistry." In: *RSC advances12(55):36073-102.* (2022).

[183] Gang. Cheng. "High-efficiency solution-processed organic light-emitting diodes with tetradentate platinum (II) emitters." In: *ACS applied materials and interfaces 11.48: 45161-45170.* (2019).

[184] Neupane. "2D organic semiconductors, the future of green nanotechnology." In: *Nano Materials Science 1.4 : 246-259.* (2019).

[185] et al. Ren Mingzhu. "The structure-activity relationship of aromatic compounds in advanced oxidation processes: a review." In: *Chemosphere : 134071.* (2022).

[186] A. Kumar. "Strategies for enhancing the performance of organic electronic devices using functionalized molecules." In: *Journal of Materials Chemistry C, 8(28), 9360-9384* (2020).

A. Appendix

A.1. Test

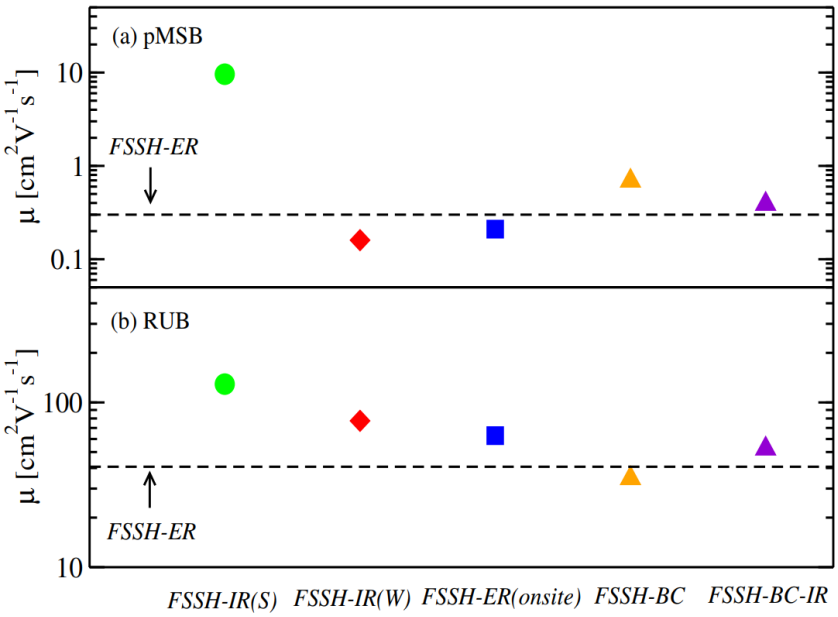

Figure A.1.: Comparison of the charge mobilities computed by fewest switches surface hopping (FSSH) method with different approximations for (a) p-MSB and (b) rubrene. The hole mobilities computed by the FSSH with explicit charge relaxation (FSSH-ER, dashed lines) are used as reference. Green circle and red diamond: FSSH with implicit charge relaxation using surface populations and wave function coefficients to evaluate the weights (FSSH-IR(S) and FSSH-IR(W)); blue square: FSSH with explicit on-site charge relaxation (FSSH-ER(onsite)); orange triangle: FSSH with Boltzmann correction (BC) for hopping probability (FSSH-BC); blue triangle: FSSH-BC-IR. The reorganization energies computed by DFTB are used as the input parameters for IR.